MOLECULAR STRUCTURES –

PREDICTION, DETERMINATION, AND REFINEMENT

by

VERONIKA KASALOVÁ

(Under Direction the of Henry F. Schaefer III)

ABSTRACT

Molecular structures of various molecules were examined. First, a systematic investigation of the As_2F_n / $As_2F_n^-$ systems was carried out using Density Functional Theory. From the first four studied species (As_2F_n, n = 1-4), all neutral molecules and their anions are shown to be stable with respect to As-As bond breaking. The global minima of the neutral As_2F_n species, n = 5-8, are weakly bound complexes, held together by dipole-dipole interactions. All such structures have the AsF_m-AsF_n form, where (m,n) is (2,3) for As_2F_5, (3,3) for As_2F_6, (4,3) for As_2F_7 and (5,3) for As_2F_8. The anions $As_2F_n^-$, n = 5-8, are shown to be stable with respect to the As-As bond breaking, and we predict that all of them have fluorine-bridged or fluorine-linked structures.

Next, in support of mass-selected infrared photodissociation (IRPD) spectroscopy experiments, coupled cluster methods have been used to study the $V^+(H_2O)$ and $ArV^+(H_2O)$ complexes. Four lowest-lying quintet states ($^5A_1$, $^5A_2$, $^5B_1$ and $^5B_2$), all of which appear within a 6 kcal mol^{-1} energy range, were examined. Our computations show an opening of 2°-3º in the equilibrium bond angle of H_2O due to its interaction with the metal ion. Zero-point vibrational averaging increases the *effective* bond angle further by 2.0°-2.5º, mostly due to off-axis motion of the heavy vanadium atom rather than changes in the water bending potential. The total theoretical shift in the bond angle of about +4° is significantly less than the widening near 9º deduced from IRPD experiments.

Last, the equilibrium molecular structures of the two lowest-energy conformers of glycine, Gly-**Ip** and Gly-**IIn**, have been characterized by high-level *ab initio* electronic structure computations. Based on experimentally measured vibrationally averaged effective rotational constant sets of several isotopologues and our *ab initio* data for structural constraints and zero-point vibrational shifts, least-squares structural refinements were performed to determine improved Born–Oppenheimer equilibrium structures of Gly-**Ip** and Gly-**IIn**. The barrier to planarity separating Gly-**IIp** and Gly-**IIn** has been determined to be 20.5 cm^{-1}. The equilibrium torsional angle τ(NCCO) of Gly-**IIn**, characterizing the deviation of its heavy-atom framework from planarity, is 11º.

INDEX WORDS: equilibrium structure, DFT, *ab initio*, quartic force field, di-arsenic fluorides, vanadium-cation/water complex, glycine

MOLECULAR STRUCTURES –

PREDICTION, DETERMINATION, AND REFINEMENT

by

VERONIKA KASALOVÁ

MSc, Comenius University, Slovakia, 2002

A Dissertation Submitted to the Graduate Faculty of The University of Georgia in Partial Fulfillment of the Requirements for the Degree

DOCTOR OF PHILOSOPHY

ATHENS, GEORGIA

2006

MOLECULAR STRUCTURES –

PREDICTION, DETERMINATION, AND REFINEMENT

by

VERONIKA KASALOVÁ

Major Professor:	Henry F. Schaefer III
Committee:	Geoffrey D. Smith
	Nigel G. Adams

Electronic Version Approved:

Maureen Grasso
Dean of the Graduate School
The University of Georgia
May 2006

ACKNOWLEDGEMENTS

First and foremost, I would like to thank my parents for their support and encouragement. They helped me become the person I am today and their constant belief in me was what I needed most to start and continue an academic career. I will be forever grateful for this.

Over the years, many of my friends had a huge impact on my academic life. The moral support they were continuously offering over the years will never be forgotten. Among these people are my best friends from college Lenka Barteková, Marína Blahová, Lýdia Kovaříková, Karol Kovařík, Juraj Štefánik, Juraj Húska, Jozef Vadkerti, and many others. I would like to also thank Zuzana Slavkovská, Petra Lukešová, Katarína Danielčáková, and Jana Lindbloom for being great friends from childhood until now.

During the four years at the Center for Computational Chemistry, many graduate students helped me become a better scientist and a better person. Special thanks goes to Michael Schuurman, my mentor, who introduced me to the basics computational chemistry. I am very grateful for having a chance to know and work with my fellow graduate students: Suyun Wang, Justin Turney, Partha Berra, and Steven Wheeler. Nancy Richardson and Maria Lind were amazing office mates through the years here.

I would like to thank my high school physics and chemistry teacher Gabriela Pástorová for showing me the beauty of the subjects which became so important to me over the years. As an undergraduate student, I was very lucky to have teachers that

influenced my in many good ways. Special thanks goes to Dr. Babinec, my undergraduate advisor, and Drs Hubač, Urban, and Mach.

The senior members of our research group at the Center of Computational Chemistry helped me in many ways. I thank Dr. Yamaguchi and Dr. Xie for very helpful suggestions concerning my research. I especially thank Dr. Allen for his patience, his great ability to motivate, and for being a great mentor. Working with such an enthusiastic person was an awesome experience I will always remember.

I had a chance to work with a research group in Budapest, Hungary, on several projects. I thank Dr. Császár for many motivating conversations in Budapest and here, in Athens. I also thank Eszter Czinki for being a wonderful host in Budapest.

Dr. Schaefer, my major advisor, was the best advisor one can imagine. I am deeply in debt to him for his help with all my projects and continuous encouragement. I also thank him for the opportunity to talk to the visiting professors from all over the world, and for giving me a chance to present my research at various conferences.

I am very grateful for the research staff here, at the Center for Computational Chemistry. I thank Linda Rowe, Amy Peterson, and Karen Branch for taking care of all my paperwork, which has sometimes proven to be a difficult task because I am an international student.

Last, but not least, I would like to thank my husband and fellow graduate student Brian Papas for his love, patience, understanding, and help with my research projects.

TABLE OF CONTENTS

Page

LIST OF TABLES

Page

LIST OF FIGURES

Page

CHAPTER 1

INTRODUCTION AND BACKGROUND MATERIAL

1.1 INTRODUCTION

Everything on the Earth consists of molecules and everything is surrounded by molecules. To understand processes that are happening around us, it is important to know the properties these individual molecules. The properties are determined by atomic arrangements in molecules, and therefore knowing the molecular structure of various molecules is one of the focuses of current chemistry research.

One of the biggest advantages of computational chemistry is determining molecular structures with high degree of accuracy. Computational chemistry, as opposed to experimental chemistry, is not restricted by the ability to synthesize and purify molecular samples, and both well known molecules and "new" molecular species can be studied.

1.2 STRUCTURES OF NOT YET STUDIED MOLECULES

Predicting the arrangement of atoms in molecules that were not studied previously is a difficult task. Many molecular structures have to be considered and therefore a significant number of calculations has to be performed. For this reason, computational methods that are not very time consuming are the best option for such studies. Because of a very large quality of computations to computer time ratio, density functional theory is a good choice when predicting molecular structures of not yet experimentally known molecules.

The basis for density functional theory (DFT) is the proof presented in 1964 by Hohenberg and Kohn[1] which states that the ground-state electronic energy is determined completely by the electron density ρ. The advantage of using electron density rather than

a standers wave function is the following: while a wave function for an N-electron system contains 3N coordinates, three for each atom, the electron density only depends on three coordinates regardless of the number of electrons in the studied molecule. This reduces computational cost significantly. However, there is a "small" problem associated with the use of density functional theory. It was proven that each different density yields different ground state energy, as the functional connecting these two quantities is not known. Therefore the objective of various DFT methods it to design a functional connecting electron density with energy.

Energy functional can be divided in three parts: the kinetic energy under the assumption of non-interacting electrons $T_S[\rho]$, the nucleus-electron attraction $E_{ne}[\rho]$, and the electron correlation that includes the Coulomb term ($J[\rho]$) and the exchange-correlation term ($K[\rho]$). The major problem in DFT is the lack of analytic expression for the exchange-correlation term $K[\rho]$. Various empirically fit expressions have been evaluated for the $K[\rho]$ term. Even though the expressions for the $K[\rho]$ term are not mathematically rigorously derived, DFT methods perform very well when predicting molecular structures to a certain degree of precision. Due to the small computational cost, that is similar to the cost of Hartree-Fock computations, DFT methods are the methods of choice for structure prediction, especially for large molecules for which high level *ab initio* methods can not be used.

1.3 MOLECULAR STRUCTURES FROM AB INITIO METHODS

Theoretical determination of atomic arrangements in molecules can be very helpful for explaining experimental data. In such cases, density functional theory

methods may not be sufficient, and high level ab initio computations, often in conjunction with anharmonic force field computations, are necessary to obtain high accuracy r_e and r_0 structures.

Exact electronic wave function $|\Psi_0\rangle$ for and N electron system can be written as:

$$|\Psi_0\rangle = |\Phi_0\rangle + \sum_{i,a} c_i^a |\Phi_i^a\rangle + \sum_{i<j,a<b} c_{ij}^{ab} |\Phi_{ij}^{ab}\rangle + \ldots, \quad (1.1)$$

where $|\Phi_0\rangle$ is the ground state wave function and $|\Phi_i^a\rangle$ represents Slater determinant where electron is excited from an occupied orbital *a* into a virtual orbital *r* with respect to the ground state determinant.

For the simplest ab initio method, the Hartree-Fock (HF) method,[2,3] the series in 1.1 is truncated immediately after the first term, so $|\Psi_0\rangle = |\Phi_0\rangle$. The HF method describes behavior of each electron in an average electric field of all the other electrons. It does not contain electron correlation effects and therefore is not very accurate. There are three main methods for calculating electron correlation: configuration interaction, coupled cluster, and many body perturbation theory.

In case of configuration interaction (CI) method,[4,5] the coefficients for excited Slated determinants are of a linear form. For actual computations, the series 1.1 has to be truncated at a certain point for systems containing many electrons. If for example the series is truncated so that only single (S) and double (D) excitations are allowed, we get the CISD method.

For coupled cluster methods (CC),[6-8] a more complicated exponential form of coefficients in 1.1 is chosen. The truncation of series leads to CCSD,[9] CCSDT,[10-12] and higher excitation methods. The CC methods containing triple and higher excitations

explicitly are very time and computer power consuming, and often can not be performed for large systems. To improve the performance of CCSD, various approaches for estimating triple contributions have been developed, using perturbative [CCSD(T)[13,14]] or iterative [CCSDT-3,[15] CC3[16]] approaches.

Other type of electronic structure method is based on a perturbative treatment of molecules, where the true molecular electronic Hamiltonian is separated into two parts: the unperturbed part $\hat{H}_0$, that can be solved easily, and a perturbation $\hat{H}'$. In case of the Møller-Plesset (MP) perturbation theory,[17] the unperturbed Hamiltonian is taken as the sum of the one-electron Fock operators. The most commonly used are the second- and fourth-order MP perturbation theories, MP2 and MP4, respectively.

1.4 REFINEMENT OF MOLECULAR STRUCTURES

Other possibility for determining highly accurate equilibrium structures of molecules is combining experimental and theoretical data. In such studies high level ab initio equilibrium structures (r_e) are employed in conjunction with experimental rotational constants (A_0, B_0, C_0) in a least square fit. High level *ab initio* structures are obtained for a given molecule at the highest level of theory allowed by current computational power, and either second order Møller-Plesset perturbation theory (MP2) or coupled-cluster theory with single, double, and perturbative triple excitations [CCSD(T)] with at least triple-zeta quality basis set are usually used at this time. Vibrational effects on rotational constants ($A_e - A_0$, $B_e - B_0$, $C_e - C_0$,) are evaluated at highest possible level of theory, and are used to correct experimentally obtained rotational constants A_0, B_0, and C_0. The "new" equilibrium rotational constants A_e, B_e, and

C_e for various isotopologs and are used in a least square structural refinement fit with the equilibrium structure from theory, and a very accurate refined equilibrium structure for the studied molecule is obtained. For a structural refinement, highly flexible *Mathematica* program MolStruct[18] developed recently in our group is used.

Such method, where high level *ab initio* results are combined with precise experimental data, is a very powerful tool for molecular structure refinement. Gas phase microwave spectra provide information about rotational constants with high accuracy. This given, equilibrium structures of larger molecules, which can not currently be studied with extremely accurate theoretical methods and large basis sets, can be determined with high precision. Also, if no experimental rotational constants are available, or in cases where such rotational constants need to be re-examined, molecular refinement performed in MolStruct can be used to predict vibrationally averaged r_0 structures, rather than the equilibrium r_e structures. In such cases, the theoretically obtained r_e structure and theoretically obtained vibrationaly averaged rotational constants A_0, B_0, and C_0 rotational constants are used for molecular refinement.

1.5 PROSPECTUS

In this work, three ways for obtaining molecular structures are employed.

First, DFT methods are used to predict structures and properties of the di-arsenic fluorides (As_2F_n) and their anions. Many of these molecules were not studied previously, and DFT methods are a good choice for such pioneer studies.

Second, equilibrium structures of the $V^+(H_2O)$ and $ArV^+(H_2O)$ complexes are examined. Because these molecules serve in our work as model systems for probing

metal cation hydration, high-level *ab initio* methods and large basis sets are used to determine all bond lengths and bond angles with high precision. Vibrational anharmonicity effects on the molecular structure of $V^+(H_2O)$ and $ArV^+(H_2O)$ are explored, and vibrationally averaged structures for both molecules are obtained.

Finally, two minima (Gly-**Ip** and Gly-**IIn**) and one transition state (Gly-**IIp**) of the most simple aminoacid glycine are studied with high level *ab initio* methods. Experimental microwave data are used to refine the structures of all three conformers and to explain discrepancy between theory and experiment encountered previously due to low barrier to planarity of the Gly-**IIn** conformer.

1.6 REFERENCES

1 P. Hohenberg and W. Kohn, Phys. Rev. **136**, B864 (1964).

2 W. J. Hehre, L. Radom, P. v. R. Schleyer, and J. A. Pople, Ab initio Molecular Orbital Theory (Wiley-Interscience, New York, 1986).

3 A. Szabo and N. S. Ostlund, Modern Quantum Chemistry: Introduction to Advanced Electronic Structure Theory, 1st ed. revised (McGraw-Hill, New York, 1989).

4 I. Shavitt, in *Methods of Electronic Structure Theory*, H. F. Schaefer, Ed., Plenum Press, New York, 1977, pp. 189-275.

5 C. D. Sherrill and H. F. Schaefer, Adv. Quantum Chem. **34**, 143 (1999).

6 J. Čížek, J. Chem. Phys. **45**, 4256 (1966).

7 J. Čížek, Adv. Chem. Phys. **14**, 35 (1969).

8 J. Čížek and J. Paldus, Int. J. Quantum Chem. **5**, 359 (1971).

[9] G. D. Purvis and R. J. Bartlett, J. Chem. Phys. **76**, 1910 (1982).

[10] J. Noga and R. J. Bartlett, J. Chem. Phys. **86**, 7041 (1987).

[11] G. E. Scuseria and H. F. Schaefer, Chem. Phys. Lett. **152**, 382 (1988).

[12] J. D. Watts and R. J. Bartlett, J. Chem. Phys. **93**, 6104 (1990).

[13] K. Raghavachari, G. W. Trucks, J. A. Pople, and M. Head-Gordon, Chem. Phys. Lett. **157**, 479 (1989).

[14] G. E. Scuseria and T. J. Lee, J. Chem. Phys. **93**, 5851 (1990).

[15] J. Noga, R. J. Bartlett, and M. Urban, Chem. Phys. Lett. **134**, 126 (1987).

[16] H. Koch, O. Christiansen, P. Jørgensen, A. M. S. de Maras, and T. Helgaker, J. Chem. Phys. **106**, 1808 (1997).

[17] C. Møller and M. S. Plesset, Phys. Rev. **46**, 618 (1934).

[18] MolStruct is an abstract program developed by Wesley D. Allen for use within Mathematica (Wolfram Research Inc., Champaign, Illinois) to perform diverse fits of molecular structures to sets of isotopologic rotational constants.

CHAPTER 2

STRUCTURES AND ELECTRON AFFINITIES OF THE DI-ARSENIC FLUORIDES As_2F_N / $As_2F_N^-$ ($_N$=1-8)*

* V. Kasalová and H. F. Schaefer III. 2005. *Journal of Computational Chemistry*, 26: 411-435. Reprinted here with permission of publisher.

2.1 ABSTRACT

Developments in the preparation of new materials for microelectronics are focusing new attention on molecular systems incorporating several arsenic atoms. A systematic investigation of the As_2F_n / $As_2F_n^-$ systems was carried out using Density Functional Theory methods and a DZP++ quality basis set. Global and low-lying local geometric minima and relative energies are discussed and compared. The three types of neutral-anion separations reported in this work are: the adiabatic electron affinity (EA_{ad}), the vertical electron affinity (EA_{vert}) and the vertical detachment energy (VDE). Harmonic vibrational frequencies pertaining to the global minimum for each compound are reported. From the first four studied species (As_2F_n, n = 1-4), all neutral molecules and their anions are shown to be stable with respect to As-As bond breaking. The neutral As_2F molecule and its anion are predicted to have C_s symmetry. We find the *trans* F-As-As-F isomer of C_{2h} symmetry and a pyramidalized vinylidene-like As-As-F_2^- isomer of C_s symmetry to be the global minima for the As_2F_2 and $As_2F_2^-$ species, respectively. The lowest lying minima of As_2F_3 and $As_2F_3^-$ are vinyl radical-like structures F-As-As-F_2 of C_s symmetry. The neutral As_2F_4 global minimum is a *trans*-bent (like Si_2H_4) F_2-As-As-F_2 isomer of C_2 symmetry, while its anion is predicted to have an unusual fluorine-bridged (C_1) structure. The global minima of the neutral As_2F_n species, n = 5-8, are weakly bound complexes, held together by dipole-dipole interactions. All such structures have the AsF_m-AsF_n form, where (m,n) is (2,3) for As_2F_5, (3,3) for As_2F_6, (4,3) for As_2F_7 and (5,3) for As_2F_8. For As_2F_8 the beautiful pentavalent F_4As-AsF_4 structure (analogous to the stable AsF_5 molecule) lies about 30 kcal/mol above the $AsF_3 \cdots AsF_5$ complex. The stability of AsF_5 depends crucially on the strong As-F bonds, and replacing one of these

with an As-As bond (in $F_4As\text{-}AsF_4$) has a very negative impact on the molecule's stability. The anions $As_2F_n^-$, n = 5-8, are shown to be stable with respect to the As-As bond breaking, and we predict that all of them have fluorine-bridged or fluorine-linked structures. The zero-point vibrational energy corrected adiabatic electron affinities are predicted to be 2.28 eV (As_2F), 1.95 eV (As_2F_2), 2.39 eV (As_2F_3), 1.71 eV (As_2F_4), 2.72 eV (As_2F_5), 1.79 eV (As_2F_6), 5.26 eV (As_2F_7) and 3.40 eV (As_2F_8) from the BHLYP method. Vertical detachment energies are rather large, especially for species with fluorine-bridged global minima, having values up to 6.45 eV (As_2F_7, BHLYP).

2.2 INTRODUCTION

Molecular systems exhibiting extreme characteristics, specifically systems with very large electron affinity (EA) values, are of special interest to experimental and theoretical chemists. The $As_2F_{11}^-$ anion is well known due to its extraordinarily high vertical detachment energy of 11.4 eV.[1] The existence of this molecule was first suggested in 1969 on the basis of low-temperature IR[2] and NMR[3] observations. The $As_2F_{11}^-$ anion has the structure of a bi-octahedron with a common apex and it has been extensively studied since 1969.[4-11] Also some of the di-arsenic bromides, chlorides, and iodides, as well as the di-antimony fluorides, were observed previously, in particular $As_2Br_8^{2-}$,[12] As_2Br_6,[13] As_2Cl_6,[13] As_2I_4,[14-17] and As_2I_6.[18] However, the di-arsenic fluorides (As_2F_n) and their anions with number of fluorines, n, smaller than 11 have been studied relatively little. Based on an NMR study in 1970 Davies and Moss stated that it is likely the $As_2F_5^+$ ion was formed in solution in their research (in addition to $Sb_2F_{11}^-$).[19] In 1980 Doiron and McMahon observed the presence of the $As_2F_5^+$ ion using ion cyclotron

resonance spectrometry. They suggested the ion to have either a fluorine-bridged structure, or an intermediate between two possible tautomeric forms of As-As bonded $As_2F_5^+$.[20] In 1991 the heat of formation of As_2F was measured by gas-phase charge-transfer reactions with an upper limit established to be 205 kcal mol^{-1}.[21]

SiF_n (n =1-5), GeF_n (n =1-5), AsF_n (n =1-6) and also Si_2F_n and Ge_2F_n (n =1-6) play an important role in semiconductor materials chemistry, and several experimental and theoretical studies have been performed on these molecules.[22-36] Comparing with the SiF_n - Si_2F_n and GeF_n - Ge_2F_n systems implies that As_2F_n molecules may also play a role in chemical vapor deposition.

In the present study the geometric structures (global and low-lying local minima) and thermochemical properties, including the electron affinities, of the As_2F_n / $As_2F_n^-$ (n =1-8) molecules have been investigated. This study has been limited to species with eight or less fluorines due to the fact that the number of minima on the potential energy surface increases rapidly with successive addition of atoms to the molecule. There are many theoretical approaches for determining molecular structures and energies. With the large number of modest size molecules the inexpensive gradient corrected density functional methods (DFT) were considered adequate. DFT has been shown to be effective for predicting molecular structures for many related inorganic species, such as AsF_n,[22,23,29,31,34,35] BrF_n,[37] SF_n,[38] PF_n,[39] ClF_n,[40] GeF_n,[27] SeF_n,[41] SiF_n,[25,30,32,33] SiH_n,[42] C_2F_n,[43] Si_2F_n[26] and Ge_2F_n.[24,28,36] Several different DFT methods are compared in the present study.

2.3 THEORETICAL METHODS

Five different density functional methods and hybrid Hartree - Fock/density functionals were used in this study:

(a) Becke's 1988 exchange functional (B)[44] with Lee, Yang, and Parr's correlation functional (LYP)[45], BLYP;

(b) Becke's three-parameter exchange functional (B3)[46] with the LYP correlation functional, B3LYP;

(c) Becke's half - and - half exchange functional (BH)[47] with the LYP correlation functional, BHLYP. This method has proven quite effective in describing the structures and electron affinities of related simple systems, such as SiF_4, PF_5, and SF_6.

(d) The B exchange functional with Perdew's correlation functional (P86),[48,49] BP86;

(e) The B3 exchange functional with the P86 correlation functional, B3P86.

Restricted methods were used for closed shell systems and unrestricted methods for open shell system. All computations have been evaluated using the Gaussian 94 suite of programs.[50] The default numerical integration grid (75, 302) was used for As_2F_n (n=1-6) and larger integration grid (99,590) for As_2F_7 and As_2F_8.

A standard double zeta plus polarization (DZP) basis set with the addition of s- and p- diffuse functions (denoted as DZP++) was used in this study. The DZ portion of the basis set was constructed from the Huzinaga – Dunning[51,52] set of contracted Gaussian functions for fluorine and from the Schäfer - Horn – Ahlrichs[53] set of contracted Gaussian functions for arsenic. To construct the DZP basis set, five pure d-type polarization functions have been added on each atom.[51-53] The diffuse function orbital

exponents were determined in even tempered sense as a mathematical extension of the primitive set, according to the formula of Lee and Schaefer:[54] $\alpha_s(F)=0.1409$, $\alpha_p(F)=0.0826$, $\alpha_s(As)=0.031455$, $\alpha_p(As)=0.031639$. The final contraction scheme is (10s5p1d/5s3p1d) for fluorine and (14s11p6d/8s6p3d) for arsenic.

All geometries were found to be minima after determining the harmonic vibrational frequencies at the corresponding stationary points for each functional. Zero-point vibrational energies evaluated at each level of theory (listed in Tables 2.20 and 2.21 for all global minima) were used to correct the adiabatic electron affinities.

The electron affinities are evaluated as the differences of total energies in the following manner: the adiabatic electron affinity

$$EA_{ad} = E \text{ (optimized neutral)} - E \text{ (optimized anion)} \quad (2.1)$$

the vertical electron affinity

$$EA_{vert} = E \text{ (optimized neutral)} - E \text{ (anion at optimized neutral geometry)} \quad (2.2)$$

and the vertical detachment energy

$$VDE = E \text{ (neutral at optimized anion geometry)} - E \text{ (optimized anion)}. \quad (2.3)$$

The reliability of the present prediction is best judge from comparisons between theory and experiment for the simpler AsF_n systems. For diatomic AsF, the predicted dissociation energies are 4.22 eV (B3LYP), 4.52 eV (BP86), and 4.50 eV (BLYP), compared to the experimental value 4.2 ± 0.2 eV. For $AsF_3 \rightarrow AsF_2 + F$, the theoretical results are 4.76 eV (B3LYP), 5.03 eV (BP86), and 4.92 eV (BLYP), all in reasonable agreement with the experimental value 5.03 eV. Thus the thermodynamic predictions with these three methods should be reliable.

For electron affinities, the experimental results for the mono-arsenic systems are limited but supportive of the theoretical methods used here. For the As atom, the EA is known rather precisely to be 0.81 ± 0.01 eV. This is why for the present $As_2F_n^-$ systems, dissociation to As^- is never favored. The methods used here predict EA(As) = 0.74 eV (BHLYP), 0.96 eV (B3LYP), 1.04 eV (BP86), and 0.90 eV (BLYP). The electron affinities of AsF and AsF_2 are known from experiment to within a few tenths of an eV, and all four DFT methods give acceptable agreement. Thus we expect the theoretical predictions of the electron affinities of the larger As_2F_n systems to be reasonable.

2.4 GEOMETRIES AND ENERGIES

2.4.1 As_2F / As_2F^-

Four types of geometrical structures have been investigated for the neutral As_2F molecule - the bent structure with C_s symmetry, the fluorine-bridged structure with C_{2v} symmetry, and a linear structure with $C_{\infty v}$ symmetry. All three optimized geometric neutral minima of the As_2F are shown in Figure 2.1, structures **1na** – **1nc**, and the corresponding relative energies are reported in Table 2.1. Two of the minima have doublet electronic states, $^2A'$ with C_s symmetry (**1na**) and $^2A_2$ with C_{2v} symmetry (**1nc**), and one is predicted to be a $^4A'$ with C_s symmetry (**1nb**). The linear As-As-F structure is also shown to be a stationary point with a doublet electronic state, having a degenerate imaginary vibrational frequency (170i cm^{-1} with B3LYP) leading to the bent **1na** structure. The linear As-F-As isomer is a second order stationary point with highest imaginary frequency (60i cm^{-1} for doublet and quartet with B3LYP) leading to structure **1nc** for the doublet electronic state and structure **1nb** for the quartet. Energetic

comparisons show that the bent $^2A'$ structure (**1na**) is the global minimum for all five functionals. The structures **1nb** ($^4A'$, C_s) and **1nc** ($^2A_2$, C_{2v}) lie 22 kcal mol^{-1} and 38 kcal mol-1 (BHLYP), respectively, above the **1na** minimum. All three minima on the potential energy surface are stable with respect to As-As bond breaking (Table 2.1).

The predicted BHLYP bond lengths and bond angle for the global minimum (**1na**) are 2.241 Å (As-As), 1.764 Å (As-F) and 101.2º (As-As-F). All functionals that contain Hartree-Fock exchange (B3P86, B3LYP, BHLYP) predicted bond distances within 0.017 Å of each other. The BLYP distances are the longest and they are at least 0.03 Å longer than the bond lengths obtained using BHLYP functional. A similar trend can be seen in the angle comparison, where the As-As-F angle for BHLYP functional is much smaller (by at least one degree) than for the other functionals.

The same geometrical structures have been investigated for the As_2F^- anion. All three optimized geometries of the As_2F^- anion are shown in Figure 2.2, structures **1aa**-**1ac**, and their relative energies are presented in Table 2.2. The global minimum is, for all five functionals, the bent (C_s) structure with its closed shell $^1A'$ electronic state (**1aa**), which lies 19 kcal mol^{-1} and 67 kcal mol^{-1} (BHLYP) below the bent $^3A''$ structure (**1ab**) and the bridged $^1A_1$ (C_{2v}) structure (**1ac**), respectively. The As-As-F linear structure with singlet electronic state has a degenerate imaginary frequency, 145i cm^{-1} (B3LYP), leading to the bent (C_s) structure. The linear As-As-F $^3\Pi$ structure has one imaginary (174i cm^{-1}) and one low real (69 cm^{-1}) vibrational frequency, suggesting it is a Renner-Teller stationary point, type C.[55]

The As-As bond distance for the As_2F^- global minimum is shorter than the corresponding bond length for the neutral As_2F global minimum by 0.08 Å (BHLYP).

The As-F distance is, however, longer for the anion than for the neutral molecule. This can be explained by looking at the HOMOs of structure **1aa** (Figure 2.17), which is bonding along the As-As axis but antibonding with respect to the As-F axis. The bonding character of the HOMO also causes an increase of the As-As-F angle.

2.4.2 As_2F_2 / $As_2F_2^-$

The optimized geometries for five geometric minima of As_2F_2 are shown in Figure 2.3 and their relative energies are presented in Table 2.3. Three geometrical minima have been located for the As_2F_2 singlet electronic state species: two F-As-As-F isomers (with C_{2h} and C_{2v} symmetry) and an fluorine-bridged isomer with C_1 symmetry, and two isomers were found for the triplet electronic state species (the As-As-F_2 structure of C_s symmetry and the F-As-As-F structure of C_2 symmetry). The electronic ground state is an F-As-As-F isomer of C_{2h} symmetry and ^1A_g electronic state (structure **2na**). The isomer of C_{2v} symmetry ($^1A_1$, structure **2nb**) is slightly higher in energy (by 3.0 kcal mol^{-1} for the BHLYP). Energetically highest is the fluorine-bridged ^1A isomer (**2ne**) which is 35 kcal mol^{-1} (BHLYP) higher in energy than **2na** and is not a minimum for the BP86 and BLYP functionals.

Two dibridged transition states have been found while looking for the geometrical minima. The non-planar dibridged singlet electronic state isomer (C_{2v}, $^1A_1$) has one imaginary vibrational frequency (330i cm^{-1} with B3LYP) which leads to the ground state C_{2h} isomer (**2na**) when followed. The analogous triplet electronic state isomer ($^3B_2$) has one imaginary frequency (933i cm^{-1} with B3LYP) which leads to structure **2nd**.

The BHLYP As-As distance for the geometry minimum (**2na**) is 2.248 Å. The As-As bonds are longer for the As_2F_2 ground state species than for the As_2F species by 0.007-0.047 Å. The BHLYP As-F distance for the As_2F_2 global minimum is 1.763 Å, which is comparable to the corresponding distance in As_2F (1.764 Å). Addition of the second fluorine to the fluorine-bridged $^2A_2$ structure of As_2F (**1nc**) resulted in a longer As-As bond distance (2.349 Å) and a larger angle between the two arsenics and the bridging fluorine (104º).

All seven distinct geometric minima found for $As_2F_2^-$ are presented in Figure 2.4 (structures **2aa**-**2ag**) and their relative energies are listed in Table 2.4. None of the minima are bridged and the dibridged structures with D_{2h} and C_{2v} symmetries are predicted to be second order stationary points. Among the stable geometric minima, the lowest in energy for the BHLYP, B3P86 and B3LYP functionals is the As-As-F_2 isomer with C_s symmetry and a $^2A'$ electronic state (**2aa**). The F-As-As-F isomer (**2ab**) with C_2 symmetry and ^2A electronic state is the minimum with the BP86 and BLYP functionals. The previous DFT studies of C_2F_2, Si_2F_2 and Ge_2F_2 have shown that methods with pure DFT exchange (BLYP and BP86) have a tendency to favor structures with F atoms distributed among the C, Si or Ge atoms.[4-12,25,30,32,33] Our results for As_2F_2 show the same trend, since structure **2na**, which has an As-As-F_2 form, is favored by functionals that include Hartree-Fock exchange (BHLYP, B3P86 and B3LYP), while the F-As-As-F structure is preferred by the BP86 and BLYP functionals. The As-As and the As-F bond distances for the ground state **2aa** are 2.305 Å and 1.802 Å, respectively, and the As-As-F and F-As-F angles are 106.6º and 88.3º, respectively (BHLYP).

Structure **2ac** (C_2, ^2B) is a *trans* F-As-As-F isomer that lies above **2aa** for all functionals except BLYP, where **2ac** was computed to be 0.8 kcal mol^{-1} below **2aa**. The BP86 functional predicts that **2ac** lies only 0.2 kcal mol^{-1} above **2aa**. Structure **2nc** can be obtained from **2ab** by rotation about the As-As bond by approximately 80º, and the energy difference between **2ab** and **2ac** is less than 1.7 kcal mol^{-1} for all functionals.

Structure **2ad** is predicted to be the lowest lying quartet state (C_{2v}, $^4B_2$) for the $As_2F_2^-$ anion and it lies 32 kcal mol^{-1} higher than **2aa** (BHLYP). The local minima **2ae** (C_{2h}, ^4A_g), **2af** (C_s, $^4A'$) and **2ag** (C_s, $^4A''$) are all predicted to lie at least 38 kcal mol^{-1} above **2aa**. For each functional the relative energies of **2ae**-**2ag** are within 4 kcal mol^{-1} and the relative ordering depends upon the functional. We note that for loosely bound complexes such as **2ag**, the theoretical dissociation energies will not be quantitatively reliable.

2.4.3 As_2F_3 / $As_2F_3^-$

Four geometrical minima were found for the doublet electronic state of As_2F_3 and are presented in Figure 2.5 (**3na**-**3nd**), with the relative energies listed in Table 2.5. The global minimum is predicted to be the vinyl radical-like F_2-As-As-F isomer with C_s symmetry and $^2A''$ electronic state (**3na**). Energetically closest to **3na** is the **3nb** isomer ($^2A''$, C_s), which differs from the global minimum only by rotation about the As-As axis by 180 º and is less than 3.4 kcal mol^{-1} higher in energy. Energetically very close to **2nb** is the F_2-As-As-F isomer of C_1 symmetry and ^2A electronic state (**3nc**), which can be obtained from **2na** or **2nb** by rotation about the As-As bond by approximately 85º and 95º, respectively. Highest in energy is the F_3-As-As isomer of C_s symmetry and $^2A''$

electronic state (**3nd**), which is 26 kcal mol^{-1} above the **3na** global minimum (BHLYP). The tribridged isomer of C_{3v} symmetry (not shown in Figure 2.5) is a fourth order stationary point. A tribridged isomer of C_{2v} symmetry was predicted to have two imaginary frequencies, the highest of which leads to a dibridged transition state of C_s symmetry. Following the imaginary frequency of the dibridged transition state leads to structure **3nc**.

With the addition of an extra fluorine atom to the As_2F_2 ground state minimum (**2na**) the As-As bond length increases by 0.235 Å (BHLYP). However, the As-As bond length increases by only 0.021 Å when an extra fluorine is added structure **2nc** (As-As-F_2). Further comparison of **3na** (As_2F_3, Figure 2.6) and **2nc** (As_2F_2, Figure 2.4) shows that the As-F bond increases by 0.002 Å and the As-As-F angle decreases by 0.1º (BHLYP).

Figure 2.6 (**3aa-3af**) includes the structures for all six distinct geometric minima that have been found for the $As_2F_3^-$ anion and Table 2.6 presents their relative energies. The lowest in energy is the vinyl radical-like F_2-As-As-F isomer with C_s symmetry and $^1A'$ electronic state (**3aa**). The global minimum **3aa** lies 53 kcal mol^{-1} (BHLYP) below the dissociation limit As + AsF_3^-, showing the higher stability of $As_2F_3^-$ compared to the As_2F_3 neutral molecule **3na**, for which the dissociation energy into As + AsF_3 was only 16 kcal mol^{-1} (BHLYP). Energetically closest to structure **3aa** is the *cis* F_2-As-As-F isomer **3ab** (C_s , $^1A'$) which is 1.5 kcal mol^{-1} higher in energy (BHLYP) than **3aa** and may be obtained from **3aa** by rotation about the As-As bond by 180º. The As-As-F bond angles in **3ab** are larger than in **3aa** (by about 5º-15º) due to electrostatic repulsion of the partially negatively charged fluorine atoms. The As-As-F_3 isomer **3ac** (C_{3v}, $^1A_1$) lies 13.1

kcal mol^{-1} (BHLYP) above the global minimum **3aa**. The three triplet electronic state species **3ad** (C_s , $^3A''$), **3ae** (C_s , $^3A''$) and **3af** (C_1 , ^3A) are predicted to be 16 kcal mol^{-1}, 24 kcal mol^{-1} and 31 kcal mol^{-1} higher in energy than **3aa**, respectively. The relative energy of **3af** (F_2As-AsF) is lower than the relative energy of **3ae** (F_3As-As) for the BP86 (by 2.6 kcal mol^{-1}) and BLYP (by 3.0 kcal mol^{-1}) functionals, supporting the idea that the BP86 and BLYP functionals have a tendency to favor structures with fluorine atoms more evenly distributed on the two As atoms.

The predicted As-As bond distance for **3aa** is 2.345 Å, which is shorter than the corresponding distance in the neutral As_2F_3 global minimum (**3na**) by 0.183 Å. The reason for this unusual neutral-anion bond shortening is that the "last" electron was added to an orbital which has bonding character along the As-As bond (Figure 2.17). The As-F bond distances of the anion **3aa** are longer than those of **3na** by at least 0.053 Å due to the HOMO of the $As_2F_3^-$ having some antibonding character along the As-F bonds.

2.4.4 As_2F_4 / $As_2F_4^-$

Figure 2.7 (structures **4na**-**4ne**) shows the geometric minima found for the neutral As_2F_4 species, and Table 2.7 lists their relative energies. We predict the global minimum to be an F_2-As-As-F_2 isomer with C_{2h} symmetry and ^1A_g electronic state (**4na**).This *trans* bent structure is qualitatively similar to that for Si_2H_4.[56] The As-As bond length for the global minimum is 2.503 Å and the As-F bond distances are 1.741 Å (BHLYP). With the default integration grid (75, 302), structure **4na** has a small imaginary vibrational frequency (49i cm^{-1} with BHLYP), which is related to the internal rotation about the As-As bond. This structure falls into a minimum with C_2 symmetry when the imaginary

frequency is followed. Reoptimizing the structure with the larger integration grid (99, 590) yields only positive imaginary frequencies. Therefore, we consider structure **4na** to be a real geometrical minimum.

A skewed F_2-As-As-F_2 isomer (**4nb**) with C_2 symmetry and ^1A electronic state lies only 2.1-2.8 kcal mol^{-1} above **4na** (BLYP-BHLYP), and it can be obtained from **4na** by rotation about the As-As bond by approximately 80º. The next geometric minimum, the F_3-As-As-F isomer **4nc** (C_s, $^1A'$), is 40 kcal mol^{-1} above **4na**. The lowest lying triplet state is predicted to be a pentavalent F_4-As-As isomer of C_{2v} symmetry (**4nd**) and is computed to lie 43 kcal mol^{-1} above the global minimum (**4na**). The dibridged structure (**4ne**) lies 81 kcal mol^{-1} (BHLYP) higher then the global minimum, indicating the low stability of **4ne**.

Figure 2.8 depicts five low lying $As_2F_4^-$ geometric minima and Table 2.8 lists their relative energies. The global minimum is shown to be an interesting C_1 symmetry fluorine-bridged F-As-F-As-F_2 structure with ^2A electronic state (**4aa**). This is the first bridged structure predicted to be a global minimum in the present study. The As-F distance for the bridging fluorine and the As-As distance are predicted to be 2.491 Å and 2.444 Å, respectively (BHLYP). Dissociation into As + AsF_4^- requires 20 kcal mol^{-1}, indicating that the global minimum (**4aa**) is stable with respect to As-As bond breaking, or As-F bond breaking, for that matter.

There are four states above **4aa** that are close in energy, namely the *trans* F_3-As-As-F isomer **4ab** (C_s, $^2A''$), the *cis* F_2-As-As-F_2 isomer **4ac** (C_2, ^2B), the *cis* F_3-As-As-F isomer **4ad** (C_s, $^2A''$) and the pentavalent F_4-As-As isomer **4ae** (C_{2v}, $^2B_1$). Different functionals give somewhat different energy orderings of structures **4ab**-**4ae**, showing that

the BP86 and BLYP functionals favor structures with distributed F atoms (F_2-As-As-F_2 isomer **4ac**). In this case we cannot conclude that functionals that include Hartree-Fock exchange (BHLYP, B3P86 and B3LYP) favor structures of F_3-As-As-F or F_4-As-As form, since the energy difference between **4ab** (F_3-As-As-F) and **4ac** (F_2-As-As-F_2) is less than 0.7 kcal mol^{-1} for B3P86 and B3LYP. The energy difference between **4ac** (F_2-As-As-F_2) and **4ad** (F_3-As-As-F) indicates that the F_2-As-As-F_2 isomer (**4ac**) is preferred by the B3P86 and B3LYP functionals. Structure **4ae** (F_4-As-As) is predicted to lie slightly below **4ab** with the BHLYP functional (by 0.1 kcal mol^{-1}), while B3LYP, BP86 and BLYP predict **4ea** to be above **4ab**, **4ac** and **4ad**.

The lowest lying quartet electronic state of $As_2F_4^-$ is an F_4-As-As isomer of C_s symmetry (**4af**) with a very long As-As separation (3.80 Å with BHLYP), lying 19 kcal mol^{-1} (BHLYP) to 31 kcal mol^{-1} (BP86) above the global minimum. This structure is best described as a loose complex between AsF_4^- and As. As anticipated from the stability of the valence isoelectronic SF_4 molecule, AsF_4^- is found to be favored energetically throughout this work.

2.4.5 As_2F_5 / $As_2F_5^-$

Three geometric minima located for As_2F_5 are presented in Figure 2.9, structures **5na** - **5nc**, and their relative energies are listed in Table 2.9. The global minimum **5na** (C_1, ^2A) is predicted to be a weakly bound complex of AsF_3 and AsF_2. This complex, bound by dipole – dipole interactions, lies only 2.1 – 4.2 kcal mol^{-1} (BP86 and BHLYP) lower than separated AsF_3 and AsF_2 molecules. The pentavalent F_4-As-As-F isomers of C_s symmetry and $^2A''$ electronic state (**5nb** and **5nc**) are shown to be more than

30 kcal mol^{-1} above the global minimum. The conformer highest in energy (**5nc**) can be obtained from conformer **5nb** by rotation about the As-As bond by approximately 90º. The predicted energy difference between **5nb** and **5nc** is 4 kcal mol^{-1} (BHLYP).

Eight low-lying minima of $As_2F_5^-$ are presented in Figure 2.10, and their relative energies are listed in Table 2.10. Again, as for $As_2F_4^-$, the global minimum (**5aa**; C_2, ^1A) is predicted to be fluorine-bridged for all five functionals. Since the geometrical minima for the neutral and anion global minima are so disparate, a direct comparison of energies is not very meaningful; instead a comparison of dissociation energies is needed to determine relative stabilities. Unlike neutral As_2F_5, the anion is shown to be very stable with respect to As-As bond breaking, since the energy necessary for dissociation into AsF and AsF_4^- is greater than 30 kcal mol^{-1}. The fluorine-bridged isomer **5ab** (C_s, $^1A'$) lies 4.3 kcal mol^{-1} above structure **5aa**. With the default integration grid (75, 302), structure **5ab** has a small imaginary vibrational frequency with BHLYP (60i cm^{-1}) and B3LYP (9i cm^{-1}) functionals. Reoptimizing the structure with the larger integration grid (99, 590) yields a still negative but lower imaginary frequency (43i cm^{-1}) with BHLYP and a positive vibrational frequency with B3LYP (43 cm^{-1}). Therefore, we consider structure **5ab** to be a genuine geometrical minimum. Two F_2-As-As-F_3 isomers of C_s symmetry and $^1A'$ electronic state, **5ac** and **5ad**, differ from each other only by rotation about the As-As bond and are 7 kcal mol^{-1} and 14 kcal mol^{-1} higher in energy than structure **5aa**, respectively (BHLYP). An F_4-As-As-F isomer of C_s symmetry and $^1A'$ electronic state (**5ae**) is predicted to lie 16 kcal mol^{-1} above structure **5aa**. There is another fluorine-bridged isomer, **5nf** (C_s, $^3A''$), that lies 18 kcal mol^{-1} above the global minimum **5aa** (BHLYP). A high symmetry structure **5ag** (C_{4v}, $^3A_1$) derived from the stable AsF_6 anion

is 27 kcal mol^{-1} above 5aa (BHLYP). A third triplet electronic state ($^3A''$) isomer **5ah** is computed to be of C_s symmetry and predicted to lie 37 kcal mol^{-1} above the ground state (**5aa**).

The As-As distance of the global minimum **5aa** (2.438 Å by BHLYP) is shorter than the corresponding distance of the $As_2F_4^-$ global minimum **4aa** with the BHLYP and B3P86 functionals and longer for B3LYP, BP86 and BLYP. The As-F bond lengths are 1.765 Å and 1.810 Å for non-bridging fluorines and 2.195 Å for the bridging fluorine (BHLYP).

2.4.6 As_2F_6 / $As_2F_6^-$

Figure 2.11 shows the structures for the global (**6na**) and low lying local minima (**6nb**-**6nd**) of As_2F_6, while Table 2.11 lists their relative energies. The global minimum (**6na**) is shown to be an F_3-As-As-F_3 structure with C_i symmetry and ^1A_g electronic state. The global minimum has an AsF_3 ···· AsF_3 form, where the two AsF_3 molecules may be described as loosely held by dipole-dipole interactions, and **6na** lies only 2.3-4.7 kcal mol^{-1} (BP86 and BHLYP, respectively) below the energy of two separated AsF_3 molecules. Because of the weak interaction between AsF_3 molecules, the As-As distance is predicted to be very long (3.98 Å for BHLYP). Structure **6nb** is also of AsF_3 - AsF_3 form but with higher symmetry (C_{3v}), and it lies only about 2 kcal mol^{-1} above **6na**. We predict the eclipsed D_{3h} structure to be a sixth order stationary point with the highest imaginary frequency (350i cm^{-1}) leading to structure **6nb**. The staggered isomer of D_{3d} symmetry is not a stationary point, since it dissociates into two AsF_3 molecules when an attempt to optimize the geometry is made. The F_4-As-As-F_2 isomer **6nc** (C_1, ^1A) and the

F_3-As-As-F_3 isomer **6nd** (C_2, ^3B) are predicted to lie 45 kcal mol^{-1} and 111 kcal mol^{-1} (BHLYP) above **6na**, respectively. We predict structure **6nd** to be the lowest triplet electronic state of As_2F_6.

The three geometric minima found for $As_2F_6^-$ are presented in Figure 2.12 and the corresponding relative energies are listed in Table 2.12. We expect the fluorine-linked isomer **6aa** (C_s, $^2A''$) to be the global minimum for this system. We sometimes refer to the **6aa** structure as "fluorine-linked" instead of "fluorine-bridged" for the following reason: there is not a direct bond between the two arsenic atoms; the linking fluorine is necessary to hold the system together. If the structure were F-bridged, there would be an obvious separate As-As bond, similar to the ones in structures **4aa** and **5aa**.

The structure of the global minimum **6aa** can be obtained by putting two AsF_3 molecules together and adding an extra electron to the system. Each of the AsF_3 molecules has a dipole moment due to electron density being gathered around the more electronegative fluorine atoms. The two AsF_3 are oriented so that their dipole moments are parallel and in opposite directions to each other. The extra electron increases the dipole-dipole interaction within $As_2F_6^-$ anion.

The As-F bond distances for the bridging fluorine are 2.204 Å and 2.079Å, while for **4aa** and **5aa** the corresponding bridging distances are reported to be 2.297 Å and 2.194 Å, respectively (B3P86). We can see that the As-F bond distance for the bridging/linking fluorine does not change much as the size of the system increases from $As_2F_4^-$ to $As_2F_6^-$. Unlike the As_2F_6 neutral molecule, **6aa** is a minimum with respect to As-As bond breaking, lower in energy by 19 kcal mol^{-1} (BHLYP) with respect to dissociation to AsF_2 plus AsF_4^-.

The energetically closest $As_2F_6^-$ structure is the F_3-As-As-F_3 isomer **6ab** (C_{2h}, ^2A_g) which is predicted to be 14 kcal mol^{-1} (BHLYP) higher in energy than the global minimum **6aa**. The lowest lying quartet electronic state structure ($^4A'$) is computed to be a planar AsF_4^- ···· AsF_2 structure of C_s symmetry (**6ac**).

2.4.7 As_2F_7 / $As_2F_7^-$

We found four minima on the potential energy surface of As_2F_7 (Figure 2.13); their relative energies are presented in Table 2.13. There is a low imaginary vibrational frequency (lower than 50i cm^{-1}) present for all reported structures. Despite the imaginary frequencies, we expect each reported structure to be a minimum or very close to a minimum on the potential energy surface. In order to get more reliable geometries and energies for these species, we used the larger integration grid (99, 590) instead of the default (75, 302) integration grid for all As_2F_7 structures. All reported structures are very weakly bound by dipole – dipole interactions. The energetically lowest structure **7na** (C_s, $^2A'$) lies only 2-4 kcal mol^{-1} lower than the energy of the separated AsF_3+AsF_4 system. Structures **7nb** (C_s, $^2A'$) and **7nc** (C_s, $^2A'$) are very close in energy to the global minimum **7na**, with relative energies smaller than 2.2 kcal mol^{-1} for **7nb** and 2.7 kcal mol^{-1} for **7nc**. The lowest lying quartet electronic state (**7nd**; C_s, $^4A'$) is predicted to be 88 kcal mol^{-1} higher in energy than the global minimum **7na**.

For the $As_2F_7^-$ anion, the larger integration grid was used as well, due to low imaginary vibrational frequencies present for all reported structures. The optimized geometrical minima of the $As_2F_7^-$ anion are presented in Figure 2.14, and the corresponding relative energies are listed in Table 2.14. Unlike the neutral As_2F_7, the

anion is predicted to be very stable with respect to As-As bond breaking. The *trans* global minimum **7aa** (C_{2h}, ^1A_g) is a fluorine-linked C_s structure and it lies lower by 22 kcal mol^{-1} (B3P86) than dissociation to AsF_3 plus AsF_4^-. The As-F bond length for the bridging fluorine in **7aa**, 2.118 Å, is slightly shorter than the corresponding distance in **4aa** (2.297 Å), **5aa** (2.194 Å) and **6aa** (2.204 Å).

The *cis* fluorine-linked structure **7ab** (C_{2v}, $^1A_1$) is computed to be less than 2 kcal mol^{-1} above the *trans* **7aa** global minimum, and it differs from **7aa** by rotation about the As-As bond by 180º. Structure **7ac** (C_s, $^1A'$) consists of two molecules (AsF_3 and AsF_4^-) loosely held by dipole-dipole interactions, and it is predicted to lie 12 kcal mol^{-1} above structure **7aa** (BHLYP). The two lowest lying structures with a triplet electronic state, **7ad** (C_{4v}, $^3A_1$) and **7ae** (C_s, $^3A'$), lie 44.4 and 95 kcal mol^{-1} higher than the global minimum **7aa** (BHLYP), respectively.

2.4.8 As_2F_8 / $As_2F_8^-$

For the neutral As_2F_8 molecule, five minima or near-minima were located on the potential energy surface (Figure 2.15), with relative energies listed in Table 2.15. Except for **8ab**, all of these structures have low imaginary vibrational frequencies (less than 50i cm^{-1}). Hence the larger integration grid (99, 590) was used to obtain the most reliable geometries and energies. As with As_2F_7, we expect each reported structure to be a minimum or very close to a minimum on the potential energy surface, despite the low imaginary frequencies.

The energy difference between the two energetically lowest structures, **8na** (C_s, $^1A'$) and **8nb** (C_s, $^1A'$), is zero or very small (0.0 kcal mol^{-1} for BP86 and BLYP and

0.1 kcal mol^{-1} for BHLYP, B3P86 and B3LYP). Therefore it is not possible to determine, at this level of theory, which of these two conformers represents the global minimum. Also, both are bound very weakly, by dipole – dipole interactions, since only 0.5 kcal mol^{-1} to 2.1 kcal mol^{-1} is needed for dissociation into the stable closed-shell molecules AsF_3 + AsF_5 (BP86 and BHLYP, respectively).

We predict the F_4-As-As-F_4 structures with D_{2d} (**8nc**; $^1A_1$) and D_{2h} (**8nd**; ^1A_g) symmetries to be 36 kcal mol^{-1} (BHLYP) and 44 kcal mol^{-1} (BHLYP) higher in energy than structure **8na**, respectively. Although energetically above the global minimum, these structures are of particular interest, since both arsenic atoms are pentavalent, analogous to the stable AsF_5 molecule. The two F_5As-AsF_5 structures are quite stable with respect to As-F bond breakage (Table 2.15). The problem ties with the weaker As-As bond. The lowest lying triplet electronic state of the As_2F_8 molecule, **8ae** (C_{2h}, ^3B_u), is predicted to lie 64 kcal mol^{-1} above the global minimum **8na**.

Figure 2.16 (structures **8aa**-**8ad**) displays the geometrical minima found for the $As_2F_8^-$ anion, and Table 2.16 lists their relative energies. Due to low imaginary frequencies present for all structures of $As_2F_8^-$, the larger integration grid (99, 590) was used to obtain the most reliable geometries and energies. From the four minima located on the potential energy surface for $As_2F_8^-$, the lowest in energy is expected to be the fluorine-linked isomer of C_s symmetry **8aa** (C_s, $^2A'$). The energy for dissociating **8aa** into AsF_2 and AsF_6^- varies for different functionals, being between 4 kcal mol^{-1} (BHLYP) and 22 kcal mol^{-1} (BLYP). However, dissociation to AsF_2 + AsF_6^- requires significant rearrangement of As-F bonds and is probably accompanied by a barrier. Since this dissociation energy is positive for all functionals, we conclude that structure **8aa** is stable

with respect to As-As bond breaking. The endothermicities for dissociation into AsF_3 + AsF_5^- and into AsF_4 + AsF_4^- are predicted to be 15 kcal mol^{-1} and 41 kcal mol^{-1}, respectively (BHLYP). Due to the high energy needed for As-As bond breaking of $As_2F_8^-$, we conclude that the $As_2F_8^-$ anion is more energetically more favorable than the As_2F_8 neutral molecule. The As-F bond distances for the linking fluorine are predicted to be 1.897 Å and 2.421Å (B3P86), showing lengthening of one As-F bond (by about 0.2 Å) and shortening of the other As-F bond (by about 0.3 Å) compared to structures **4aa**, **5aa**, **6aa** and **7aa**.

Energetically closest to the global minimum (**8aa**) is an isomer of D_{2d} symmetry (**8ab**, $^2B_2$), which lies 20 kcal mol^{-1} (BHLYP) above **8aa**. The structure of D_{2h} symmetry, (**8nc**, $^2B_{3u}$), has a low imaginary vibrational frequency which increases in magnitude with an increase in the integration grid. The imaginary frequency leads to structure **8ab** when followed. However, the frequency is still lower than 60i cm^{-1}, so it was decided to report **8ac** as a plausible minimum. It is possible, though, that the D_{2d} isomer (**8ac**) is a transition state on the potential energy surface. Imaginary frequencies of the other structures are lower than 50i and decrease in magnitude with increase in the size of the integration grid. Thus structures **8aa**, **8ab** and **8ad** are expected to be true minima on the potential energy surface, or they are very close to the real minima. Structure **8ad** (C_{2h}, ^4B_u), predicted to be the lowest lying quartet electronic state, lies more than 100 kcal mol^{-1} above the global minimum (**8aa**).

2.5 ELECTRON AFFINITIES

Table 2.17 includes all three types of electron affinities for the global minima of the As_2F_n (n = 1-8) molecules for all five density functionals. Zero-point vibrational energies (ZPVE) listed in Table 2.18 were used to compute the ZPVE corrected adiabatic electron affinities. There are neither theoretical nor experimental values on the electron affinities of the As_2F_n species with which to compare the values predicted by DFT.

Note that all values for the adiabatic electron affinity, vertical electron affinity and vertical detachment energy are positive except of the adiabatic electron affinity for As_2F_6 where the BHLYP value is slightly negative (-0.18 eV). This suggests that the process of adding an electron to the neutral molecules is thermodynamically favorable for all the species studied in this work. With few exceptions, the general trend in the electron affinities is that the EA_{ad} and EA_{vert} values predicted by the BHLYP functional are the smallest, and the B3P86 values are the largest.

As noticed before, the two lowest lying minima for the As_2F_2 are very close to each other and the energy ordering depends on the functional used. We suggest the pyramidalized vinylidene-like F_2-As-As isomer (**2aa**) to be the minimum for $As_2F_2^-$. Considering the possibility that the F-As-As-F isomer (**2ab**) is the global minimum, the vertical detachment energies (in parentheses are the adiabatic EAs) have the following values: 2.67 eV (1.80 eV), 3.24 eV (2.40 eV), 2.70 eV (1.87 eV), 2.74 eV (1.91 eV), 2.54 eV (1.71 eV) (BHLYP, B3P86, B3LYP, BP86, BLYP).

The EA_{ad}, EA_{vert} and VDE values for As_2F and As_2F_3 are rather similar due to the small difference in geometry between the anion and the neutral. For As_2F_4, As_2F_5, As_2F_6, As_2F_7 and As_2F_8 the adiabatic electron affinities, the vertical EA and the vertical

detachment energies differ notably, due to the large geometry difference between anion and neutral.

The vertical detachment values for As_2F_n,(n=4-8) are rather large with values of 4.51 eV (As_2F_4), 4.90 eV (As_2F_5), 4.94 eV (As_2F_6), 6.45 eV (As_2F_7) and 5.60 eV (As_2F_8) for the BHLYP functional. This fact supports the thesis that the larger anions are more favorable than the neutrals, a conclusion reached earlier when looking at the relative energies of the individual species with respect to As-As bond breaking.

2.6 CONCLUSIONS

Our systematic DFT study of the arsenic hydrides As_2F_n / $As_2F_n^-$ (n=1-8) shows that all of these species are likely to be at least marginally stable with respect to As-As bond dissociation. The stabilization energies for As_2F_n / $As_2F_n^-$ (n=1-4) global minima are between 20 kcal mol^{-1} and 80 kcal mol^{-1}; the As-As bond distance increases for these species with an addition of each fluorine. The $As_2F_n^-$ (n=5, 6, 7) molecules resist dissociation by at least 19 kcal mol^{-1} and all of them are F-bridged or F-linked. The dissociation energy of the F-linked global minimum of As_2F_8 is very dependant upon the functional used and ranges from 4 kcal mol^{-1} (BHLYP) to 22 kcal mol^{-1} (BLYP), still suggesting a favorable structure. Because of the bridging or linking fluorine atoms, the As-As bond distances for $As_2F_n^-$ (n=5-8) are large, having values between 2.5 Å and 4.5 Å. The global minima of the neutral As_2F_5, As_2F_6, As_2F_7 and As_2F_8 species are expected to be bound only weakly (1-4 kcal mol^{-1}) and are likely to have AsF_{n-3} – AsF_3 form. Electron density is preferentially located around the more electronegative atoms (fluorines), causing the arsenics to be partially positively charged. Each of the two

arsenics present in As_2F_n (n=5-8) is surrounded by several fluorines and gives rise to a significant dipole moment (Table 2.19). The two dipole moments interact with each other providing the final structure of the global minima of As_2F_n (n=5-8) presented in Figures 2.9, 2.11, 2.13 and 2.15. As-As distances are very long in this case, having values about 4 Å – 4.5 Å.

The fact that anions are more likely to be stable with respect to As-As bond dissociation is supported by electron affinity values, which are expected to be positive for all studied species. The EA_{ad} values of As_2F_n increase in a zigzag pattern as *n* increases from 1 to 8. The larger EAs correspond to closed shell anionic species As_2F^-, $As_2F_3^-$, $As_2F_5^-$ and $As_2F_7^-$. Figure 2.18 shows this zigzag pattern of EAs and demonstrates a remarkable parallelism in the predictions made by the five methods DFT methods (the B3P86 EAs are too large and not discussed elsewhere in this paper). The vertical detachment energies are rather large, especially for molecules with larger number of fluorines (4-8), having values about 4 – 6.7 eV.

It is clear that neutral As_2F_n molecules will dissociate preferentially into AsF_3 + AsF_{n-3} for all As_2F_n, n > 2, and into As + AsF_n for As_2F and As_2F_2. For the anions, dissociation into AsF_4^- + AsF_{n-4} is favored for species with n > 3, and dissociation into As + AsF_n^- is preferred for molecules with n ≤ 3.

The neutral As_2F_n species with smaller numbers of fluorines and all anions $As_2F_n^-$ seem ikely to be made and observed. We hope that the present theoretical study will provide strong motivation for future experimental studies.

2.7 ACKNOWLEDGEMENTS

This research was supported by the U. S. National Science Foundation, Grant CHE-0136186. We would like to thank Nancy A. Richardson, Joseph D. Larkin and Brian N. Papas for helpful suggestions concerning this research.

2.8 REFERENCES

[1] M. Sobczyk, A. Sawicka, and P. Skurski, Eur. J. Inorg. Chem. (20), 3790 (2003).

[2] K. O. Christe and W. Maya, Inorg. Chem. **8** (6), 1253 (1969).

[3] S. Brownstein, Canad. J. Chem. **47** (4), 605 (1969).

[4] M. Al-Mukhtar, J. H. Holloway, E. G. Hope, and G. J. Schrobilgen, J. Chem. Soc.,Dalton Trans. (11), 2831 (1991).

[5] C. G. Barraclough, J. Besida, P. G. Davies, and T. A. O'Donnell, J. Fluorine Chem. **38** (3), 405 (1988).

[6] J. Y. Calves and R. J. Gillespie, J. Am. Chem. Soc. **99** (6), 1788 (1977).

[7] K. O. Christe, X. Z. Zhang, R. Bau, J. Hegge, G. A. Olah, G. K. Surya Prakash, and J. A. Sheehy, J. Am. Chem. Soc. **122** (3), 481 (2000).

[8] P. A. Dean, R. J. Gillespie, and R. J. Hulme, J. Chem. Soc. Chem. Commun., 900 (1969).

[9] B. Frlec, D. Gantar, and J. H. Holloway, Vestn. Slov. Chem. Drus. **26**, 415 (1979).

[10] R. J. Gillespie, P. A. W. Dean, R. Hulme, and D. A. Humphreys, J. Chem. Soc. A (2), 341 (1971).

[11] G. L. Gutsev and A. I. Boldyrev, J. Struct. Chem. **25** (5), 678 (1984).

[12] O. Knop, S. C. Choi, and D. C. Hamilton, Can. J. Chem. **70** (10), 2574 (1992).

[13] A. T. Kozulin, A. V. Gogolev, and S. G. Shishkin, Izvestiya Vysshikh Uchebnykh Zavedenii, Fizika **20** (4), 42 (1977).

[14] T. J. Bastow and H. J. Whitfield, J. Magnetic Resonance **37** (2), 269 (1980).

[15] M. Baudler and H. J. Stassen, Z. Anorg. Allg. Chem. **345** (3-4), 182 (1966).

[16] M. Baudler and H. J. Stassen, Z. Anorg. Allg. Chem. **343** (5-6), 244 (1966).

[17] J. T. Hewitt and T. F. Winmill, Pr. Chem. Soc. **23**, 150 (1907).

[18] A. S. Alikhanyan, A. V. Steblevskii, V. B. Lazarev, V. T. Kalinnikov, Y. K. Grinberg, E. G. Zhukov, L. M. Agamirova, and V. I. Gorgoraki, Izvestiya Akademii Nauk SSSR, Neorganicheskie Materialy **16**, 73 (1980).

[19] T. K. Davies and K. C. Moss, J. Chem. Soc (A) **7**, 1054 (1970).

[20] C. E. Doiron and T. B. McMahon, Inorganic Chemistry **19** (10), 3037 (1980).

[21] J. A. Zimmerman, S. B. H. Bach, C. H. Watson, and J. R. Eyler, J. Phys. Chem. **95** (1), 98 (1991).

[22] E. J. Caine and E. J. Charles, J. Electron. Mater. **13** (2), 341 (1984).

[23] K. O. Christe, W. W. Wilson, J. A. Sheehy, and J. A. Boatz, Angew. Chem., Int. Ed. **38** (13-14), 2004 (1999).

[24] F. Illas, J. Rubio, and J. M. Ricart, Phys. Rev. B **31** (12), 8068 (1985).

[25] R. A. King, V. S. Mastryukov, and H. F. Schaefer, J. Chem. Phys. **105** (16), 6880 (1996).

[26] G. L. Li, Q. S. Li, W. G. Xu, Y. Xie, and H. F. Schaefer, Mol. Phys. **99** (12), 1053 (2001).

[27] Q. S. Li, G. L. Li, W. G. Xu, Y. Xie, and H. F. Schaefer, J. Chem. Phys. **111** (17), 7945 (1999).

[28] Q. S. Li, G. L. Li, W. G. Xu, Y. Xie, and H. F. Schaefer, ChemPhysChem **3** (2), 179 (2002).

[29] C. B. Lindhal, Kirk-Othmer Encycl. Chem. Technol. **10**, 682 (1980).

[30] F. R. McFeely, J. F. Morar, N. D. Shinn, G. Landgren, and F. J. Himpsel, Phys. Rev. B **30** (2), 764 (1984).

[31] Y. Ni, X. Wang, M. Suto, and L. C. Lee, J. Phys. B **21**, 1281 (1988).

[32] T. A. Schoolcraft and B. J. Garrison, J. Am. Chem. Soc. **113** (22), 8221 (1991).

[33] P. J. v. d. Hoek, W. Ravenek, and E. J. Baerends, Phys. Rev. B **38** (17), 12508 (1988).

[34] W. G. Xu, G. L. Li, G. Yu, Y. Zhao, Q. S. Li, Y. Xie, and H. F. Schaefer, J. Phys. Chem. A **107** (2), 258 (2003).

[35] C. Ye, M. Suto, L. C. Lee, and T. J. Chuang, J. Phys. B **22** (16), 2527 (1989).

[36] J. Yota and V. A. Burrows, J. Appl. Phys. **69** (10), 7369 (1991).

[37] C. Pak, Y. Xie, T. J. Van Huis, and H. F. Schaefer, J. Am. Chem. Soc. **120** (43), 11115 (1998).

[38] R. A. King, J. M. Galbraith, and H. F. Schaefer, J. Phys. Chem. **100** (15), 6061 (1996).

[39] G. S. Tschumper, J. T. Fermann, and H. F. Schaefer, J. Chem. Phys. **104** (10), 3676 (1996).

[40] T. J. Van Huis, J. M. Galbraith, and H. F. Schaefer, Mol. Phys. **89** (2), 607 (1996).

[41] Q. S. Li, W. G. Xu, Y. Xie, and H. F. Schaefer, J. Phys. Chem. A **103** (37), 7496 (1999).

[42] C. Pak, J. C. Rienstra-Kiracofe, and H. F. Schaefer, J. Phys. Chem. A **104** (47), 11232 (2000).

[43] R. A. King, N. D. Pettigrew, and H. F. Schaefer, J. Chem. Phys. **107** (20), 8536 (1997).

[44] A. D. Becke, Phys. Rev. A **38** (6), 3098 (1988).

[45] C. Lee, W. Yang, and R. G. Parr, Phys. Rev. B **37** (2), 785 (1988).

[46] A. D. Becke, J. Chem. Phys. **98** (7), 5648 (1993).

[47] A. D. Becke, J. Chem. Phys. **98** (2), 1372 (1993). The BHLYP method adopted in the GAUSSIAN programs (and elsewhere subsequently) differs from the precise prescription of Becke.

[48] J. P. Perdew, Phys. Rev. B **33** (12), 8822 (1986).

[49] J. P. Perdew, J. Phys. Rev. B **34**, 7046 (1986).

[50] M. J. Frisch, G. W. Trucks, H. B. Schlegel, P. M. W. Gill, B. G. Johnson, M. A. Robb, J. R. Cheeseman, T. A. Keith, G. A. Petersson, J. A. Montgomery, K. Raghavachari, M. A. Al – Laham, V. G. Zakrzewski, J. V. Ortiz, J. B. Foresman, J. Cioslowski, B. B. Stefanov, A. Nanayakkara, M. Challacombe, C. Y. Peng, P. Y. Ayala, W. Chen, M. W. Wong, J. L. Andres, E. S. Replogle, R. Gomperts, R. L. Martin, D. J. Fox, J. S. Binkley, D. J. Defrees, J. Baker, J. P. Stewart, M. Head – Gordon, C. Gonzales, and J. A. Pople, GAUSSIAN 94, Revision C.3, Gaussian, Inc.: Pittsburgh, PA, 1995.

[51] T. H. Dunning, J. Chem. Phys. **53**, 2823 (1970).

[52] S. J. Huzinaga, J. Chem. Phys. **42** (4), 1293 (1965).

[53] A. Schäfer, H. Horn, and R. Ahlrichs, J. Chem. Phys. **97** (4), 2571 (1992).

[54] T. J. Lee and H. F. Schaefer, J. Chem. Phys. **83** (4), 1784 (1985).

[55] T. J. Lee, D. J. Fox, H. F. Schaefer, and R. M. Pitzer, J. Chem. Phys. **81** (1), 356 (1984).

[56] L. Sari, M. C. McCarthy, H. F. Schaefer, and P. Thaddeus, J. Am. Chem. Soc. **125** (37), 11409 (2003).

Table 2.1: Relative energies for As_2F in kcal mol^{-1}.[a]

Molecule	Point Group	Structure	BHLYP	B3LYP	BP86	BLYP
As+AsF			48.9	58.2	65.2	63.6
As_2+F			58.1	64.8	70.5	68.8
As_2F	C_s	1na	0.0	0.0	0.0	0.0
	C_s	1nb	22.1	27.1	29.9	30.1
	C_{2v}	1nc	38.4	36.8	22.1	21.1

[a]ZPVE corrections not included.

Table 2.2: Relative energies for As_2F^- in kcal mol^{-1}.[a]

Molecule	Point Group	Structure	BHLYP	B3LYP	BP86	BLYP
As_2+F^-			42.8	40.9	43.9	39.5
As+AsF^-			79.6	89.7	98.3	95.0
As^-+AsF			84.4	93.8	101.4	98.3
As_2F^-	C_s	1aa	0.0	0.0	0.0	0.0
	C_s	1ab	19.3	23.8	26.6	26.6
	C_{2v}	1ac	66.9	69.1	71.8	70.3

[a]ZPVE corrections not included.

Table 2.3: Relative energies for As_2F_2 in kcal mol^{-1}.[a]

Molecule	Point Group	Structure	BHLYP	B3LYP	BP86	BLYP
As+AsF_2			39.9	50.0	56.7	55.5
AsF+AsF			46.6	55.3	61.9	59.4
As_2F+F			83.5	94.4	100.9	99.6
As_2F_2	C_{2h}	2na	0.0	0.0	0.0	0.0
	C_{2v}	2nb	3.0	2.7	2.3	2.4
	C_s	2nc	7.3	13.8	16.5	17.6
	C_2	2nd	14.8	19.3	21.1	21.3
	C_1	2ne	35.0	36.0	2.3	2.4

[a]ZPVE corrections not included.

Table 2.4: Relative energies for $As_2F_2^-$ in kcal mol^{-1}.[a]

Molecule	Point Group	Structure	BHLYP	B3LYP	BP86	BLYP
As_2F+F^-			60.5	56.3	57.4	52.8
$As+AsF_2^-$			57.7	62.6	69.2	65.2
As^-+AsF_2			67.7	71.4	76.0	72.7
AsF^-+AsF			69.6	72.7	78.1	73.3
$As_2F_2^-$	C_s	2aa	0.0	0.0	0.0	0.0
	C_2	2ab	3.4	0.5	-0.8	-1.5
	C_2	2ac	4.1	1.2	0.2	-0.8
	C_{2v}	2ad	32.0	32.2	32.9	31.5
	C_{2h}	2ae	43.4	40.9	39.5	37.9
	C_s	2af	44.7	43.0	41.9	40.6
	C_s	2ag	42.3	43.5	43.7	41.2

[a]ZPVE corrections not included.

Table 2.5: Relative energies for As_2F_3 in kcal mol^{-1}.[a]

Molecule	Point Group	Structure	BHLYP	B3LYP	BP86	BLYP
$As+AsF_3$			16.4	22.6	26.9	26.5
$AsF+AsF_2$			32.1	35.2	38.8	36.1
As_2F_2+F			78.1	82.4	86.3	84.5
As_2F_3	C_s	3na	0.0	0.0	0.0	0.0
	C_s	3nb	3.4	3.2	2.9	3.0
	C_1	3nc	3.9	3.5	3.1	3.2
	C_s	3nd	26.0	28.6	27.3	30.7

[a]ZPVE corrections not included.

Table 2.6: Relative energies for $As_2F_3^-$ in kcal mol^{-1}.[a]

Molecule	Point Group	Structure	BHLYP	B3LYP	BP86	BLYP
$As+AsF_3^-$			52.7	57.6	62.6	59.5
As^-+AsF_3			54.3	59.7	63.6	62.3
$AsF+AsF_2^-$			60.0	63.5	68.7	64.5
$As_2F_2+F^-$			65.1	60.1	60.1	56.3
AsF^-+AsF_2			65.2	68.2	72.4	68.7
$As_2F_3^-$	C_s	3aa	0.0	0.0	0.0	0.0
	C_s	3ab	1.5	1.4	1.0	1.4
	C_{3v}	3ac	13.1	14.4	12.1	15.8
	C_s	3ad	16.0	18.5	19.4	19.5
	C_s	3ae	24.4	27.4	28.3	28.7
	C_1	3af	30.6	28.3	25.7	25.7

[a]ZPVE corrections not included.

Table 2.7: Relative energies for As_2F_4 in kcal mol^{-1}.[a]

Molecule	Point Group	Structure	BHLYP	B3LYP	BP86	BLYP
$AsF+AsF_3$			23.2	27.2	30.8	28.8
AsF_2+AsF_2			32.2	34.4	37.5	34.5
$As+AsF_4$			83.9	90.6	92.4	93.5
As_2F_3+F			92.6	101.8	108.0	106.1
As_2F_4	C_{2h}	4na	0.0	0.0	0.0	0.0
	C_2	4nb	2.8	2.4	2.1	2.1
	C_s	4nc	39.7	40.4	38.2	40.6
	C_{2v}	4nd	43.3	50.5	51.1	55.2
	C_{2v}	4ne	80.9	79.5	-	-

[a]ZPVE corrections not included.

Table 2.8: Relative energies for $As_2F_4^-$ in kcal mol^{-1}.[a]

Molecule	Point Group	Structure	BHLYP	B3LYP	BP86	BLYP
$As+AsF_4^-$			20.4	27.7	34.6	32.9
AsF^-+AsF_3			40.0	43.6	48.5	46.2
$AsF+AsF_3^-$			43.2	45.6	50.5	46.6
$AsF_2^-+AsF_2$			43.8	46.2	51.5	47.7
$As_2F_3+F^-$			63.3	62.9	66.0	62.8
As^-+AsF_4			105.4	111.2	113.2	114.1
$As_2F_4^-$	C_1	4aa	0.0	0.0	0.0	0.0
	C_s	4ab	9.0	10.4	12.4	12.0
	C_2	4ac	12.5	10.8	9.7	10.4
	C_s	4ad	12.2	13.4	15.0	14.8
	C_{2v}	4ae	8.9	15.9	18.1	22.1
	C_s	4af	19.3	26.0	30.5	30.4
	C_2	4ag	43.9	42.6	42.5	41.6

[a]ZPVE corrections not included.

Table 2.9: Relative energies for As_2F_5 in kcal mol^{-1}.[a]

Molecule	Point Group	Structure	BHLYP	B3LYP	BP86	BLYP
AsF_2+AsF_3			4.2	3.2	2.1	2.5
$AsF+AsF_4$			71.6	72.1	69.0	71.0
$As+AsF_5$			67.9	77.9	78.4	85.6
As_2F_4+F			73.6	78.7	80.7	81.4
As_2F_5	C_1	5na	0.0	0.0	0.0	0.0
	C_s	5nb	31.9	32.6	27.6	33.6
	C_s	5nc	36.2	36.8	32.2	37.6

[a]ZPVE corrections not included.

Table 2.10: Relative energies for $As_2F_5^-$ in kcal mol^{-1}.[a]

Molecule	Point Group	Structure	BHLYP	B3LYP	BP86	BLYP
$AsF+AsF_4^-$			31.6	36.3	41.8	38.7
$AsF_2^-+AsF_3$			39.3	42.2	46.8	44.0
$AsF_2+AsF_3^-$			47.7	48.9	52.5	48.5
$As_2F_4+F^-$			67.7	66.9	69.4	66.3
$As+AsF_5^-$			65.5	75.5	80.6	80.9
AsF^-+AsF_4			111.8	115.7	117.3	116.7
As^-+AsF_5			112.9	125.7	129.8	134.5
$As_2F_5^-$	C_2	5aa	0.0	0.0	0.0	0.0
	C_s	5ab	4.3	4.1	3.8	3.8
	C_s	5ac	7.3	8.4	10.0	9.5
	C_s	5ad	14.4	15.2	16.4	15.7
	C_s	5ae	16.3	20.6	25.1	22.4
	C_s	5af	17.5	22.7	23.6	27.0
	C_{4v}	5ag	26.7	38.7	42.2	47.4
	C_1	5ah	37.1	37.1	37.2	36.6

[a]ZPVE corrections not included.

Table 2.11: Relative energies for As_2F_6 in kcal mol^{-1}.[a]

Molecule	Point Group	Structure	BHLYP	B3LYP	BP86	BLYP
AsF_3+AsF_3			4.7	3.5	2.3	2.7
AsF_2+AsF_4			81.0	79.6	75.9	76.9
$AsF+AsF_5$			84.0	90.8	90.5	95.4
As_2F_5+F			102.0	110.1	116.3	113.6
As_2F_6	C_i	6na	0.0	0.0	0.0	0.0
	C_{3v}	6nb	3.1	2.3	1.7	1.7
	C_1	6nc	45.1	44.2	38.5	43.4
	C_2	6nd	110.8	104.3	93.3	97.1

[a]ZPVE corrections not included.

Table 2.12: Relative energies for $As_2F_6^-$ in kcal mol^{-1}.[a]

Molecule	Point Group	Structure	BHLYP	B3LYP	BP86	BLYP
$AsF_2+AsF_4^-$			19.0	19.1	19.4	19.1
$AsF_3+AsF_3^-$			26.1	24.4	23.4	23.2
$As+AsF_6^-$			33.8	50.6	56.3	63.7
$AsF+AsF_5^-$			59.6	63.6	63.4	65.2
$As_2F_5+F^-$			74.1	73.6	75.6	73.0
$AsF_2^-+AsF_4$			94.0	93.8	91.2	92.9
AsF^-+AsF_5			102.1	109.7	109.5	115.5
$As_2F_6^-$	C_s	6aa	0.0	0.0	0.0	0.0
	C_{2h}	6ab	13.9	11.7	8.2	10.6
	C_s	6ac	71.0	69.7	66.7	67.4

[a]ZPVE corrections not included.

Table 2.13: Relative energies for As_2F_7 in kcal mol^{-1}.[a,b]

Molecule	Point Group	Structure	BHLYP	B3LYP	BP86	BLYP
AsF_3+AsF_4			4.0	2.8	1.8	1.9
AsF_2+AsF_5			15.9	21.1	22.9	26.0
As_2F_6+F			24.5	33.0	41.9	38.3
As_2F_7	C_s	7na	0.0	0.0	0.0	0.0
	C_s	7nb	2.2	1.6	1.1	0.9
	C_s	7nc	2.7	2.0	1.5	1.4
	C_s	7nd	87.7	85.9	82.6	82.8

[a]ZPVE corrections not included.
[b]All energies were obtained using the larger integration grid (99,590).

Table 2.14: Relative energies for $As_2F_7^-$ in kcal mol^{-1}.[a,b]

Molecule	Point Group	Structure	BHLYP	B3LYP	BP86	BLYP
$AsF_3+AsF_4^-$			22.4	21.7	21.2	21.0
$AsF+AsF_6^-$			53.2	66.1	70.3	75.7
$AsF_2+AsF_5^-$			72.1	73.4	71.8	72.7
$As_2F_6+F^-$			77.1	75.8	77.1	74.7
$AsF_3^-+AsF_4$			106.0	103.1	98.8	99.4
$AsF_2^-+AsF_5$			109.4	114.7	114.1	118.8
$As_2F_7^-$	C_{2h}	7aa	0.0	0.0	0.0	0.0
	C_{2v}	7ab	2.0	1.8	1.6	1.7
	C_s	7ac	11.8	8.1	11.0	7.8
	C_{4v}	7ad	44.4	57.5	62.1	67.4
	C_s	7ae	95.0	91.4	84.4	87.5

[a]ZPVE corrections not included.
[b]All energies were obtained using the larger integration grid (99,590).

Table 2.15: Relative energies for As_2F_8 in kcal mol^{-1}.[a,b]

Molecule	Point Group	Structure	BHLYP	B3LYP	BP86	BLYP
AsF_3+AsF_5			2.1	1.3	0.5	0.8
AsF_4+AsF_4			66.4	58.6	52.5	50.6
As_2F_7+F			87.6	89.7	93.4	88.0
As_2F_8	C_s	8na	0.0	0.0	0.0	0.0
	C_s	8nb	0.1	0.1	0.0	0.0
	D_{2d}	8nc	36.5	34.6	28.2	33.0
	C_{2h}	8nd	44.1	42.0	35.3	39.7
	C_{2h}	8ne	63.6	57.0	52.0	49.8

[a]ZPVE corrections not included.
[b]All energies were obtained using the larger integration grid (99,590).

Table 2.16: Relative energies for $As_2F_8^-$ in kcal mol^{-1}.[a,b]

Molecule	Point Group	Structure	BHLYP	B3LYP	BP86	BLYP
$AsF_2+AsF_6^-$			4.3	13.5	18.4	21.7
$AsF_3+AsF_5^-$			14.6	14.1	13.8	13.7
$AsF_4^-+AsF_4$			41.0	38.1	36.3	35.8
$AsF_3^-+AsF_5$			60.3	62.1	61.9	64.4
$As_2F_7+F^-$			96.5	93.1	93.0	90.5
$As_2F_8^-$	C_s	8aa	0.0	0.0	0.0	0.0
	D_{2d}	8ab	19.7	14.5	9.8	11.2
	D_{2h}	8ac	23.1	17.9	13.2	14.2
	C_{2h}	8ad	115.1	108.8	100.4	102.9

[a]ZPVE corrections not included.
[b]All energies were obtained using the larger integration grid (99,590).

Table 2.17: Adiabatic electron affinities (EA_{ad}), zero-point corrected EA_{ad} (EA_{ad}^{ZPVE}), vertical electron affinities (EA_{vert}) and vertical detachment energies (VDE) for As_2F_n (n = 1-8) in eV.

		EA_{ad}	EA_{ad}^{ZPVE}	EA_{vert}	VDE
As_2F	BHLYP	2.28	2.28	2.09	2.49
	B3LYP	2.51	2.52	2.33	2.73
	BP86	2.61	2.62	2.43	2.83
	BLYP	2.40	2.42	2.22	2.64
As_2F_2	BHLYP	1.94	1.95	1.49	2.91
	B3LYP	1.89	1.91	1.50	4.34
	BP86	1.88	1.89	1.45	3.70
	BLYP	1.65	1.66	1.28	3.48
As_2F_3	BHLYP	2.38	2.39	2.03	2.77
	B3LYP	2.57	2.59	2.22	2.96
	BP86	2.63	2.65	2.28	3.01
	BLYP	2.45	2.47	2.11	2.83
As_2F_4	BHLYP	1.67	1.71	0.58	4.51
	B3LYP	1.85	1.89	0.83	4.35
	BP86	1.94	1.98	0.92	4.12
	BLYP	1.79	1.83	0.79	3.94
As_2F_5	BHLYP	2.69	2.72	1.24	4.90
	B3LYP	3.04	3.07	1.47	4.83
	BP86	3.27	3.30	1.53	4.60
	BLYP	3.02	3.05	1.42	4.48
As_2F_6	BHLYP	1.73	1.79	-0.18	4.94
	B3LYP	1.96	2.02	0.24	4.73
	BP86	2.00	2.05	0.51	4.45
	BLYP	1.91	1.97	0.43	4.32
As_2F_7	BHLYP	5.22	5.26	3.32	6.45
	B3LYP	5.40	5.43	3.68	6.21
	BP86	5.29	5.32	3.68	5.84
	BLYP	5.25	5.27	3.70	5.76
As_2F_8	BHLYP	3.33	3.40	0.66	5.60
	B3LYP	3.69	3.77	1.61	5.61
	BP86	3.75	3.82	2.00	5.37
	BLYP	3.78	3.86	2.11	5.35

Table 2.18: Zero – point vibrational energies within the harmonic approximation for the global minima of As_2F_n / $As_2F_n^-$ (n=1-8) in eV.

	B3LYP	BLYP	BP86	BHLYP
As_2F	0.07	0.07	0.07	0.07
As_2F^-	0.06	0.05	0.06	0.06
As_2F_2	0.13	0.12	0.12	0.14
$As_2F_2^-$	0.11	0.10	0.11	0.13
As_2F_3	0.18	0.17	0.17	0.19
$As_2F_3^-$	0.17	0.15	0.16	0.18
As_2F_4	0.24	0.22	0.23	0.26
$As_2F_4^-$	0.20	0.19	0.20	0.22
As_2F_5	0.30	0.28	0.29	0.32
$As_2F_5^-$	0.27	0.25	0.26	0.29
As_2F_6	0.37	0.35	0.36	0.40
$As_2F_6^-$	0.32	0.30	0.31	0.34
As_2F_7	0.42	0.38	0.40	0.46
$As_2F_7^-$	0.39	0.36	0.37	0.42
As_2F_8	0.53	0.49	0.50	0.58
$As_2F_8^-$	0.46	0.42	0.43	0.51

Table 2.19: Dipole moments of AsF_n (n=1, 2, 3) in Debyes.

	BHLYP	B3LYP	BP86	BLYP
AsF	2.05	1.99	1.81	1.94
AsF_2	2.62	2.56	2.34	2.51
AsF_3	2.89	2.88	2.69	2.87

Table 2.20: Harmonic vibrational frequencies (in cm^{-1}) for As_2F_n (n=1-8). Given in parentheses are the IR intensities in km/mole.

	sym	BHLYP	B3LYP	BP86	BLYP		sym	BHLYP	B3LYP	BP86	BLYP
As_2F	A´	652(137)	609(123)	590(109)	569(109)		A_u	751(179)	702(154)	675(133)	659(132)
	A´	312(2)	342(3)	335(3)	324(3)		A_u	715(284)	668(263)	644(243)	627(245)
	A´	177(6)	169(5)	161(4)	158(4)		A_u	679(367)	635(340)	610(320)	595(317)
As_2F_2	A_g	667(0)	636(0)	621(0)	597(0)		A_u	352(56)	324(44)	305(36)	297(35)
	A_g	392(0)	362(0)	345(0)	331(0)		A_u	274(26)	254(18)	240(14)	235(14)
	A_g	217(0)	201(0)	190(0)	184(0)		A_u	271(10)	250(10)	235(9)	229(9)
	A_u	140(9)	125(8)	116(6)	111(7)		A_u	70(6)	77(6)	76(6)	71(6)
	B_u	669(251)	638(219)	625(193)	600(195)		A_u	58(18)	56(11)	55(7)	53(7)
	B_u	118(8)	102(8)	84(7)	81(7)		A_u	44(0)	39(6)	22(10)	19(10)
As_2F_3	A´	692(114)	653(95)	630(70)	611(55)	As_2F_7 [a]	A´	772(77)	710(72)	672(61)	653(61)
	A´	675(128)	639(118)	624(118)	605(136)		A´	743(95)	693(80)	664(75)	649(71)
	A´	318(6)	299(5)	289(4)	280(4)		A´	704(181)	656(176)	631(173)	615(172)
	A´	264(10)	240(9)	227(8)	221(8)		A´	618(153)	563(117)	546(114)	518(97)
	A´	176(0)	161(0)	153(0)	147(0)		A´	566(60)	516(67)	493(62)	473(71)
	A´	128(15)	120(14)	114(12)	113(12)		A´	347(25)	316(18)	297(14)	290(14)
	A˝	671(119)	635(109)	612(100)	591(102)		A´	339(16)	301(10)	279(7)	266(6)
	A˝	134(1)	120(1)	110(0)	109(0)		A´	326(41)	291(29)	268(21)	258(18)
	A˝	37(6)	52(6)	59(5)	59(6)		A´	276(26)	253(21)	238(20)	232(17)
As_2F_4	A_g	700(0)	662(0)	642(0)	624(0)		A´	195(6)	173(7)	159(8)	150(8)
	A_g	345(0)	319(0)	305(0)	295(0)		A´	91(1)	79(1)	76(2)	70(2)
	A_g	263(0)	239(0)	225(0)	220(0)		A´	53(5)	44(4)	41(4)	37(4)
	A_g	157(0)	140(0)	131(0)	126(0)		A´	31(5)	24(5)	24(4)	17(4)
	A_u	688(241)	653(222)	634(205)	614(207)		A˝	778(138)	713(131)	677(125)	655(126)
	A_u	73(0)	61(0)	49(0)	51(0)		A˝	689(113)	642(102)	616(88)	602(91)
	A_u	49i(5)	51i(5)	50i(4)	49i(4)		A˝	285(0)	253(1)	236(1)	228(3)
		[40(5)] [a]	[38(5)] [a]	[35(4)] [a]	[34(5)] [a]		A˝	269(5)	246(4)	231(2)	223(1)
	B_g	668(0)	635(0)	617(0)	597(0)		A˝	189(15)	165(12)	152(10)	144(10)
	B_g	186(0)	169(0)	158(0)	155(0)		A˝	81(0)	69(0)	66(0)	59(0)
	B_u	691(237)	654(208)	635(182)	616(187)		A˝	27(3)	21(3)	19(2)	16(2)
	B_u	263(20)	241()17	227(14)	222(14)		A˝	19i(0)	21i(0)	24i(0)	24i(0)
	B_u	106(20)	88(18)	73(15)	75(17)	As_2F_8 [a]	A´	844(136)	776(126)	734(121)	715(119)
As_2F_5	A	744(104)	695(89)	668(77)	651(75)		A´	795(216)	737(191)	703(168)	683(163)
	A	721(115)	679(94)	658(79)	639(81)		A´	754(7)	695(71)	668(74)	651(74)
	A	703(127)	657(122)	634(114)	616(116)		A´	746(70)	689(2)	650(1)	630(1)
	A	698(167)	653(152)	629(141)	611(142)		A´	706(187)	658(169)	635(150)	617(152)
	A	662(166)	624(152)	605(139)	587(136)		A´	653(12)	611(12)	585(9)	570(10)
	A	347(29)	320(23)	302(18)	295(18)		A´	404(79)	380(68)	363(58)	356(58)
	A	280(10)	260(8)	247(6)	242(6)		A´	386(4)	362(1)	345(0)	339(0)
	A	274(8)	252(6)	238(5)	233(5)		A´	370(62)	345(48)	329(38)	323(38)
	A	272(8)	249(6)	236(6)	231(6)		A´	345(23)	315(21)	295(20)	288(19)
	A	133(10)	125(10)	124(9)	122(10)		A´	267(14)	245(9)	231(6)	226(6)
	A	79(3)	79(7)	77(6)	73(6)		A´	133(0)	120(0)	110(0)	108(0)
	A	71(5)	70(4)	70(4)	68(5)		A´	58(3)	41(4)	30(3)	32(3)
	A	63(7)	60(3)	57(1)	56(2)		A´	48(3)	35(1)	23(1)	27(0)
	A	44(3)	43(1)	41(1)	41(1)		A´	21(1)	14(1)	11(1)	11(1)
	A	37(1)	35(0)	32(0)	34(0)		A˝	836(139)	771(129)	731(122)	711(121)
As_2F_6	A_g	744(0)	696(0)	671(0)	654(0)		A˝	707(133)	659(124)	636(117)	618(117)
	A_g	712(0)	665(0)	641(0)	624(0)		A˝	387(0)	362(0)	345(0)	339(0)
	A_g	674(0)	630(0)	604(0)	591(0)		A˝	368(50)	345(42)	329(36)	323(35)
	A_g	351(0)	324(0)	305(0)	297(0)		A˝	268(7)	245(5)	230(4)	226(5)
	A_g	290(0)	265(0)	249(0)	242(0)		A˝	132(0)	119(0)	110(0)	108(0)
	A_g	269(0)	250(0)	236(0)	231(0)		A˝	56(1)	40(1)	28(1)	29(1)
	A_g	121(0)	107(0)	94(0)	89(0)		A˝	27(2)	21(1)	13(0)	14(1)
	A_g	73(0)	69(0)	67(0)	62(0)		A˝	12i(0)	8(1)	2(1)	3i(1)
	A_g	44(0)	38(0)	33(0)	31(0)						

[a] Frequencies were obtained using the larger integration grid (99,590).

Table 2.21: Harmonic vibrational frequencies (in cm^{-1}) for $As_2F_n^-$ (n=1-8). Given in parentheses are the IR intensities in km/mole.

	sym	BHLYP	B3LYP	BP86	BLYP		sym	BHLYP	B3LYP	BP86	BLYP
As_2F^-	A′	460(185)	411(155)	394(150)	369(82)		A′	150(21)	142(11)	138(5)	131(5)
	A′	394(34)	372(50)	366(40)	353(105)		A′	98(8)	95(2)	94(0)	88(0)
	A′	177(8)	158(8)	148(7)	144(7)		A′	43(2)	51(1)	52(1)	46(2)
$As_2F_2^-$	A′	589(241)	521(232)	488(223)	467(223)		A″	664(147)	615(139)	589(130)	569(132)
	A′	303(31)	286(28)	281(21)	268(23)		A″	297(1)	266(2)	248(2)	239(2)
	A′	278(14)	251(9)	234(6)	226(6)		A″	193(11)	167(11)	150(9)	144(11)
	A′	180(12)	161(11)	158(8)	156(8)		A″	106(5)	105(5)	103(4)	103(4)
	A″	544(119)	473(113)	440(109)	417(110)		A″	46(4)	51(3)	55(2)	55(2)
	A″	145(0)	130(1)	132(1)	129(1)		A″	36(0)	33(0)	26(0)	23(0)
$As_2F_3^-$	A′	604(190)	544(128)	519(15)	499(13)	$As_2F_7^-$ [a]	A_g	702(0)	651(0)	623(0)	606(0)
	A′	560(143)	526(184)	508(276)	488(279)		A_g	571(0)	534(0)	515(0)	498(0)
	A′	332(15)	315(13)	309(12)	299(12)		A_g	350(0)	318(0)	297(0)	288(0)
	A′	287(30)	267(24)	257(20)	249(20)		A_g	294(0)	268(0)	252(0)	245(0)
	A′	200(2)	185(2)	177(1)	172(1)		A_g	153(0)	142(0)	136(0)	131(0)
	A′	140(9)	129(7)	122(6)	120(6)		A_g	97(0)	89(0)	85(0)	81(0)
	A″	559(103)	495(94)	461(87)	441(87)		B_g	665(0)	614(0)	587(0)	568(0)
	A″	158(0)	144(0)	136(0)	135(0)		B_g	285(0)	257(0)	240(0)	232(0)
	A″	56(6)	58(6)	60(6)	53(7)		B_g	123(0)	109(0)	101(0)	96(0)
$As_2F_4^-$	A	639(128)	585(124)	553(117)	534(120)		A_u	673(291)	621(274)	594(257)	575(261)
	A	600(240)	531(274)	505(267)	489(266)		A_u	297(4)	266(3)	248(3)	239(3)
	A	503(128)	482(84)	465(74)	453(73)		A_u	204(14)	178(12)	162(10)	155(11)
	A	379(150)	351(115)	350(92)	333(96)		A_u	14(4)	14(3)	12(2)	12(1)
	A	324(21)	302(14)	292(9)	282(10)		A_u	23(0)	20(1)	16(1)	16(3)
	A	303(5)	256(5)	235(5)	228(5)		B_u	708(220)	655(193)	625(169)	608(170)
	A	223(21)	204(39)	198(39)	192(35)		B_u	556(362)	517(357)	498(360)	481(355)
	A	202(25)	171(9)	156(5)	150(4)		B_u	355(37)	319(34)	299(78)	287(33)
	A	139(2)	130(6)	124(6)	120(6)		B_u	314(23)	280(54)	271(652)	262(612)
	A	134(3)	115(2)	109(8)	101(3)		B_u	257(767)	260(724)	257(48)	247(132)
	A	91(10)	82(8)	98(3)	91(12)		B_u	172(57)	155(30)	142(16)	137(19)
	A	82(2)	77(7)	70(1)	66(1)		B_u	18(2)	14(2)	9i(2)	10i(2)
$As_2F_5^-$	A	651(7)	602(12)	574(19)	555(26)	$As_2F_8^-$ [a]	A′	726(134)	671(112)	640(99)	623(98)
	A	582(325)	537(296)	519(268)	502(259)		A′	710(69)	652(82)	619(83)	599(91)
	A	381(79)	359(94)	354(90)	340(90)		A′	633(125)	585(133)	556(120)	542(132)
	A	350(54)	330(21)	318(5)	306(8)		A′	592(290)	540(245)	518(246)	496(216)
	A	288(1)	260(0)	245(1)	238(0)		A′	547(27)	499(24)	476(17)	456(21)
	A	193(0)	174(0)	164(0)	157(0)		A′	454(231)	403(243)	372(231)	358(233)
	A	118(1)	112(1)	106(1)	101(1)		A′	355(7)	316(10)	294(52)	286(54)
	A	68(1)	72(0)	75(0)	77(0)		A′	346(74)	313(55)	289(7)	276(2)
	B	650(262)	601(241)	572(221)	552(225)		A′	334(74)	285(55)	257(54)	242(50)
	B	544(57)	501(66)	486(71)	470(73)		A′	272(17)	249(11)	233(6)	226(3)
	B	293(6)	265(4)	251(3)	244(3)		A′	231(3)	211(5)	201(7)	195(6)
	B	222(53)	209(53)	200(49)	192(50)		A′	181(14)	160(17)	153(20)	143(19)
	B	195(20)	171(12)	162(9)	154(9)		A′	116(11)	105(8)	99(5)	93(5)
	B	113(3)	102(2)	95(3)	93(2)		A′	69(6)	64(7)	66(6)	60(6)
	B	54i(25)	30(22)	73(17)	59(18)		A′	36(2)	31(1)	28(1)	26(1)
$As_2F_6^-$	A′	698(144)	649(119)	620(100)	603(98)		A″	687(170)	634(154)	607(142)	590(141)
	A′	673(88)	624(84)	599(79)	580(81)		A″	593(272)	531(247)	506(224)	478(222)
	A′	565(66)	527(23)	510(2)	493(2)		A″	355(12)	315(6)	291(4)	278(2)
	A′	539(282)	508(315)	493(337)	476(329)		A″	306(0)	278(0)	262(0)	254(0)
	A′	353(17)	320(14)	301(49)	288(9)		A″	274(6)	249(5)	234(4)	228(4)
	A′	315(24)	285(390)	284(621)	272(666)		A″	230(2)	209(1)	196(1)	191(1)
	A′	306(155)	280(10)	261(17)	251(1)		A″	81(2)	75(2)	75(2)	70(2)
	A′	270(595)	261(377)	253(75)	244(86)		A″	21(1)	22(1)	23(1)	23(1)
	A′	184(23)	170(17)	161(11)	153(12)		A″	14i(1)	11i(1)	10i(1)	6i(1)

[a] Frequencies were obtained using the larger integration grid (99,590).

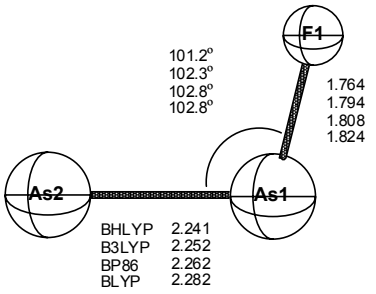

1na (C_s, $^2A'$)

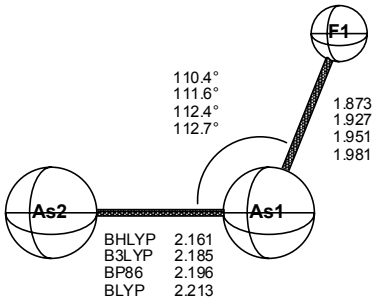

1aa (C_s, $^1A'$)

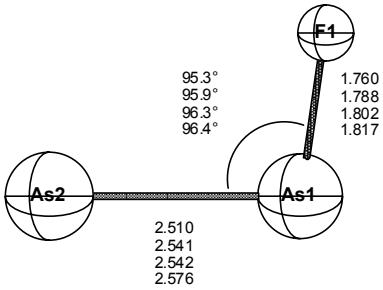

1nb (C_s, $^4A'$)

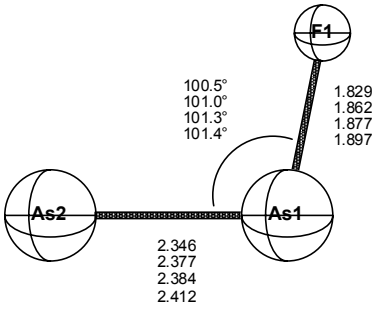

1ab (C_s, $^3A''$)

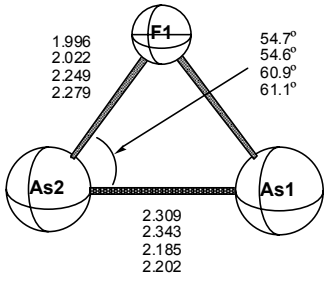

1nc (C_{2v}, $^2A_2$)

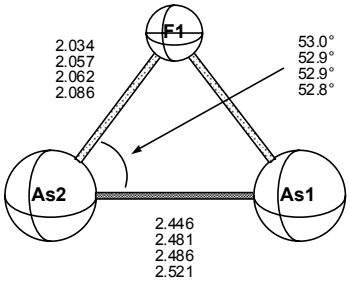

1ac (C_{2v}, $^1A_1$)

Figure 2.1: Geometries of the low-lying minima of As_2F (bond lengths in Å).

Figure 2.2: Geometries of the low-lying minima of As_2F^- (bond lengths in Å).

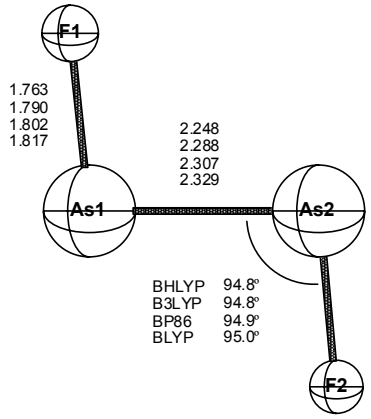

2na (C_{2h}, ^1A_g)

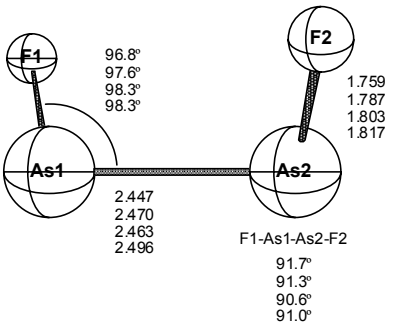

2nd (C_2, ^3B)

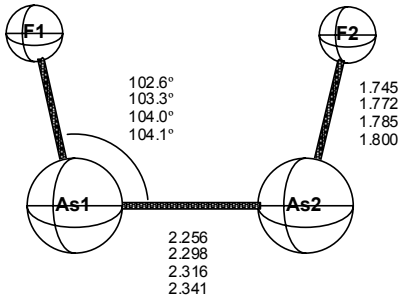

2nb (C_{2v}, $^1A_1$)

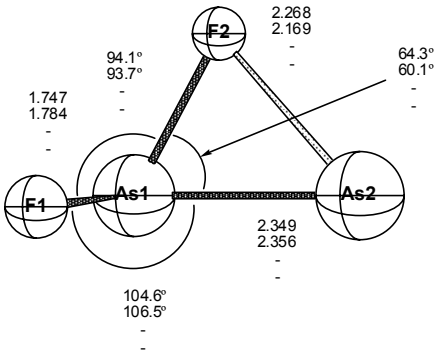

2ne (C_1, ^1A)

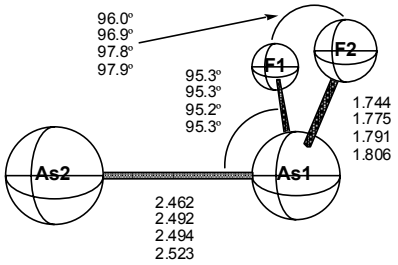

2nc (C_s, $^3A''$)

Figure 2.3: Geometries of the low-lying minima of As_2F_2 (bond lengths in Å).

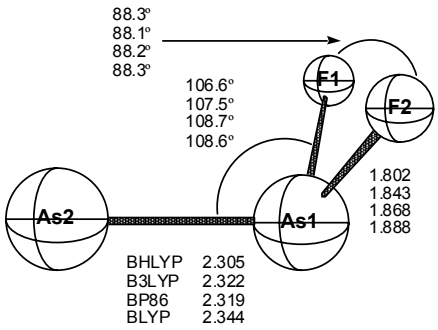

2aa (C_s, $^2A'$)

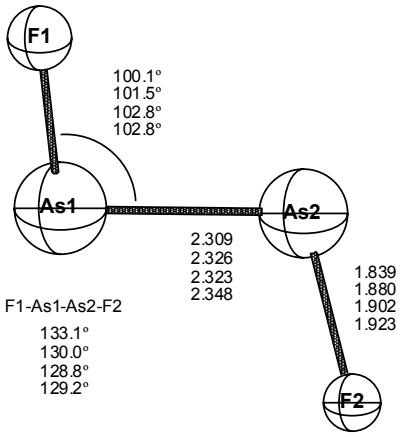

2ac (C_2, ^2B)

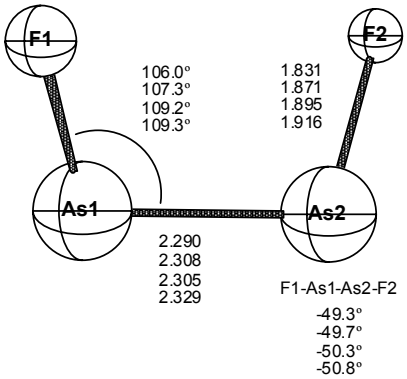

2ab (C_2, ^2A)

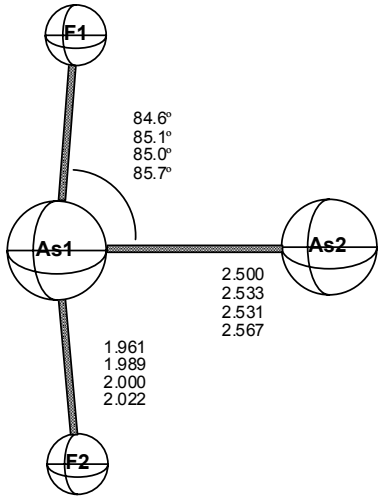

2ad (C_{2v}, $^4B_2$)

Figure 2.4: Geometries of the low-lying minima of $As_2F_2^-$ (bond lengths in Å).

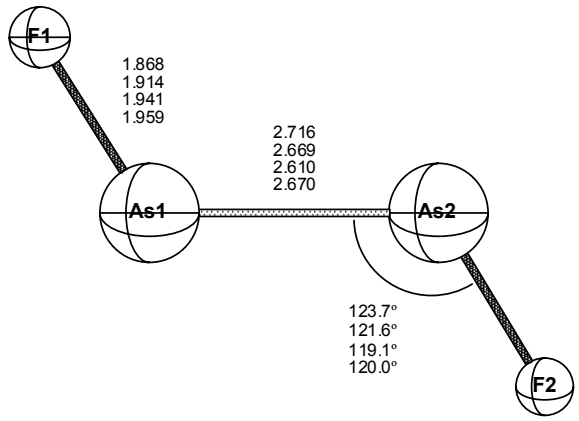

2ae (C_{2h}, ^4A_g)

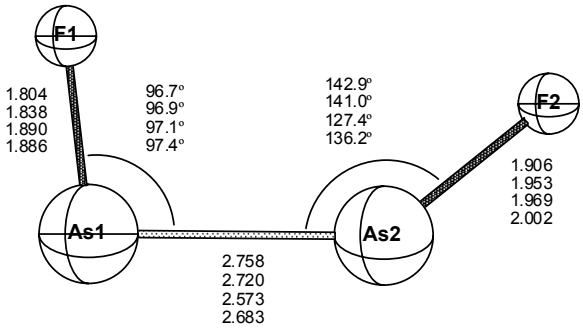

2af (C_s, $^4A'$)

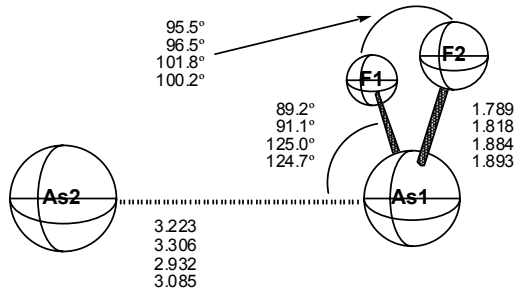

2ag (C_s, $^4A''$)

Figure 2.4 (Continued)

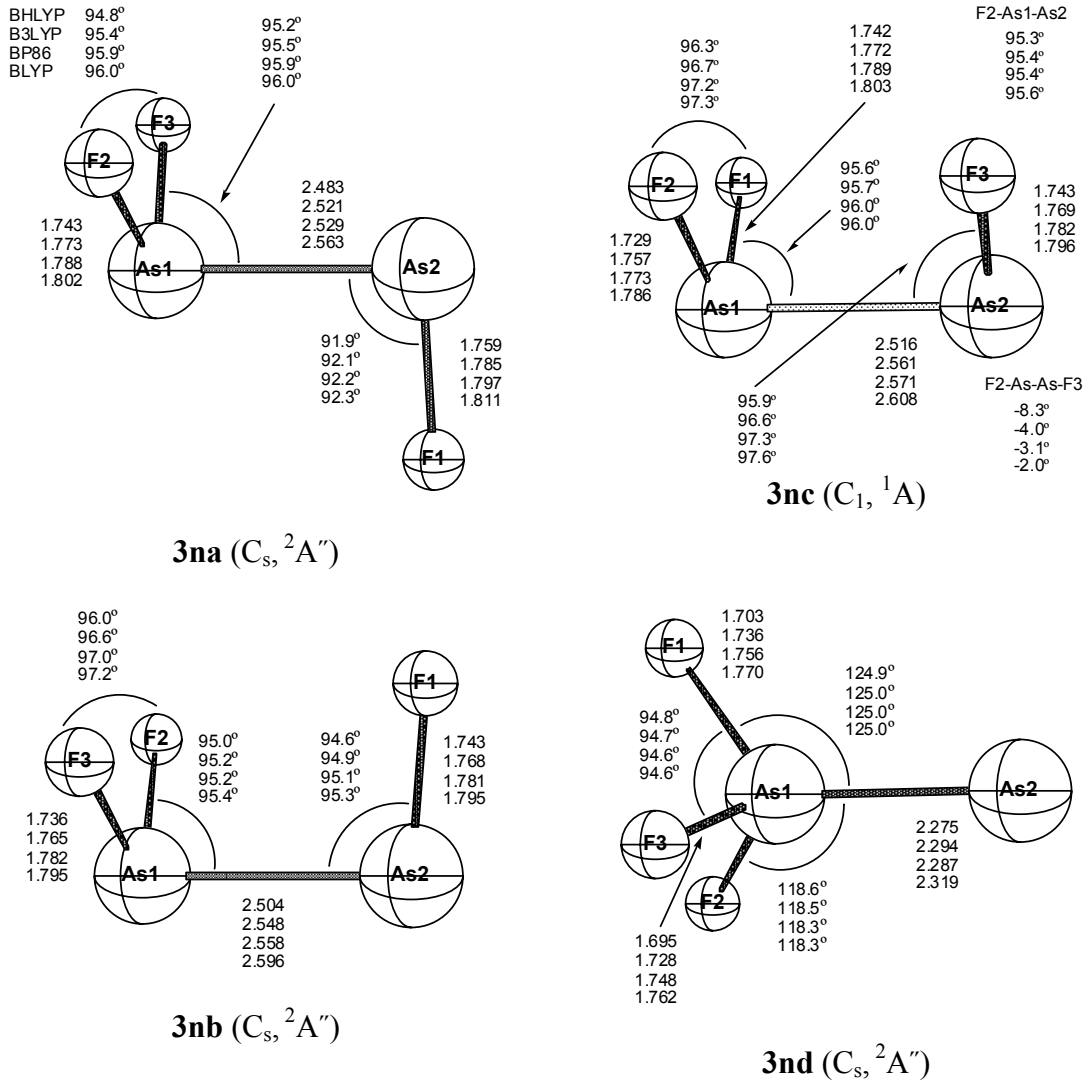

Figure 2.5: Geometries of the low-lying minima of As_2F_3 (bond lengths in Å).

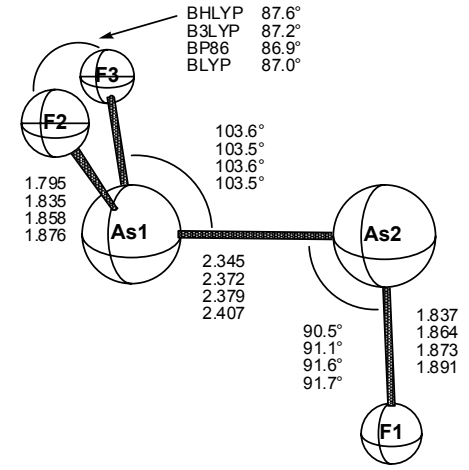

3aa (C_s, $^1A'$)

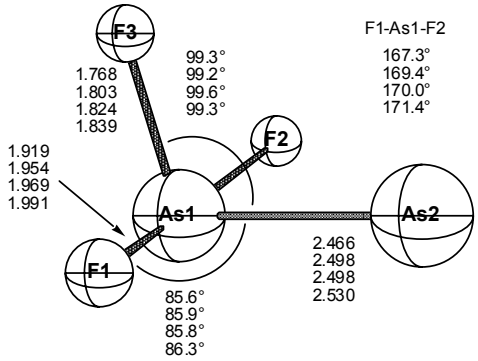

3ad (C_s, $^3A''$)

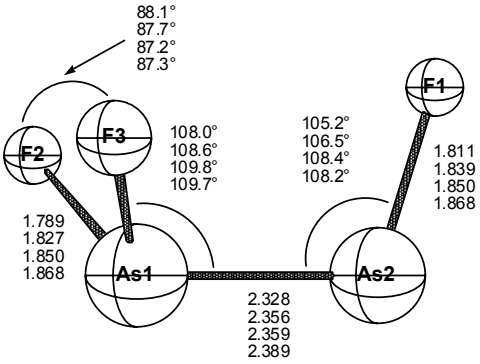

3ab (C_s, $^1A'$)

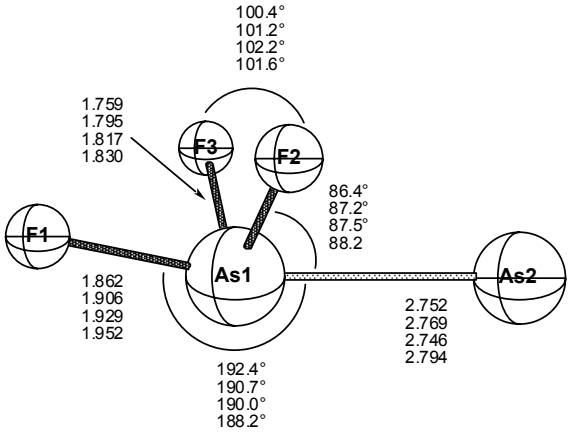

3ae (C_s, $^3A''$)

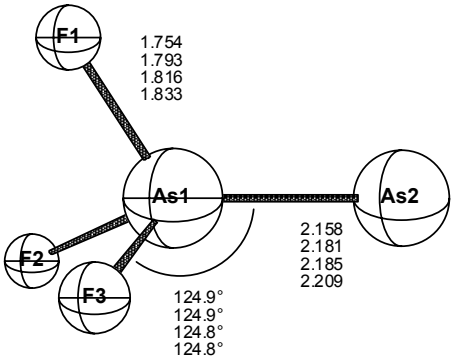

3ac (C_{3v}, $^1A_1$)

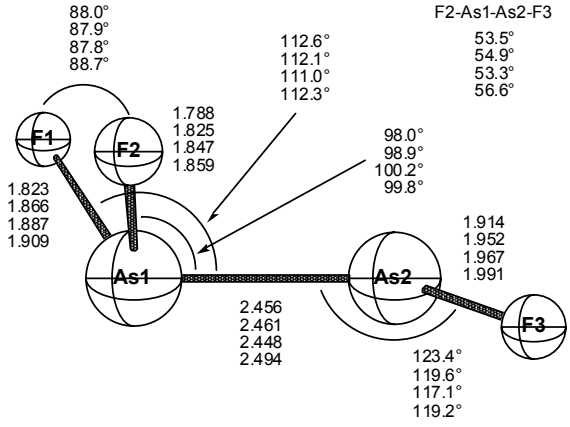

3af (C_1, ^3A)

Figure 2.6: Geometries of the low-lying minima of $As_2F_3^-$ (bond lengths in Å).

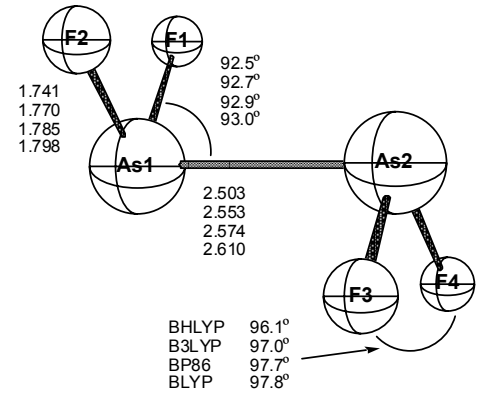

4na (C_{2h}, ^1A_g)

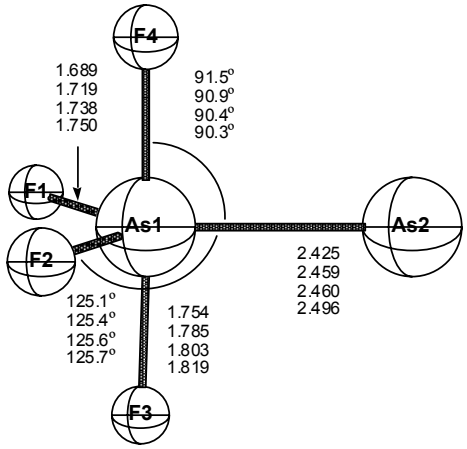

4nd (C_{2v}, $^3A_2$)

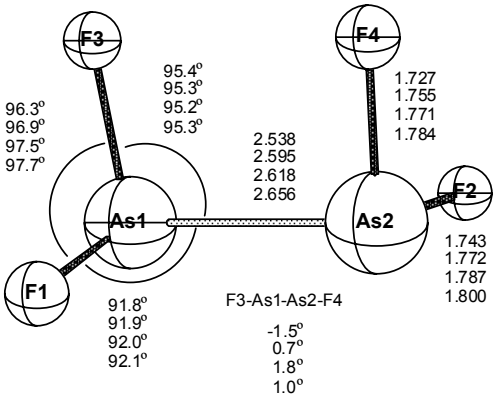

4nb (C_2, ^1A)

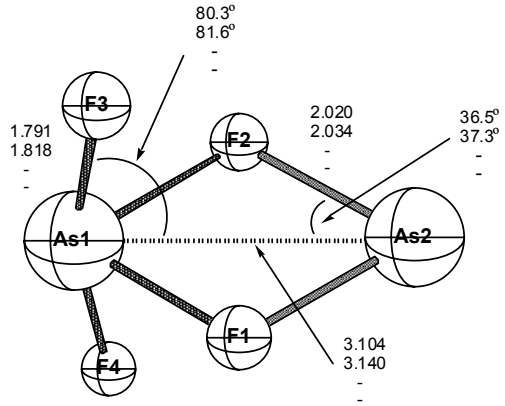

4ne (C_{2v}, $^1A_1$)

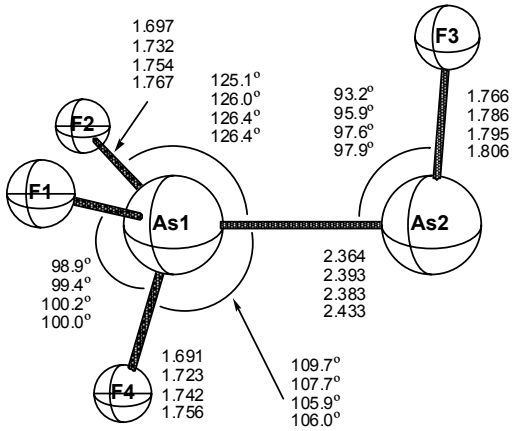

4nc (C_s, $^1A'$)

Figure 2.7: Geometries of the low-lying minima of As_2F_4 (bond lengths in Å).

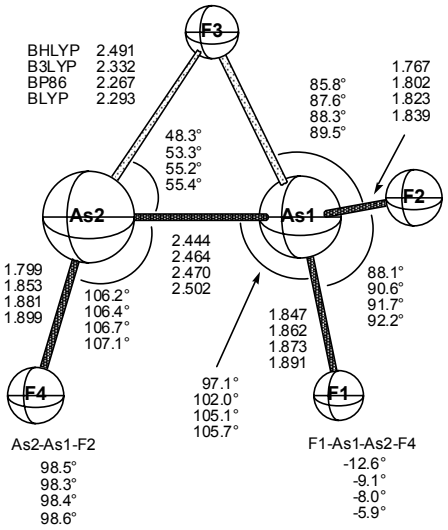

4aa (C_1, ^2A)

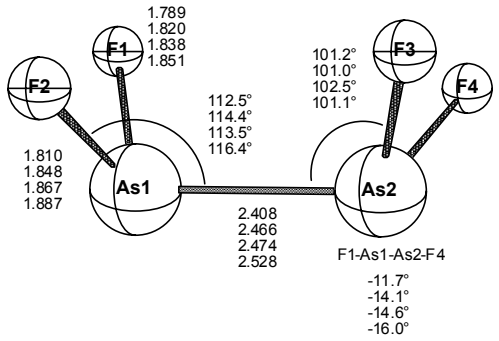

4ac (C_2, ^2B)

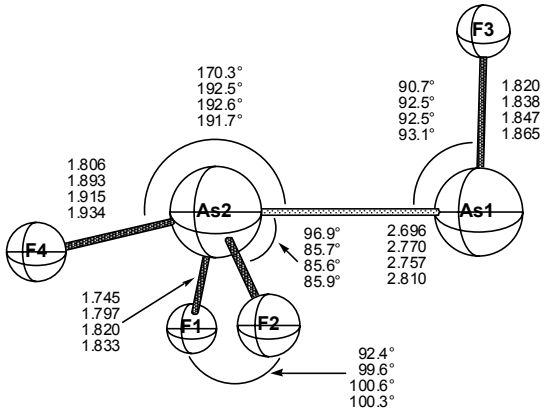

4ab (C_s, $^2A''$)

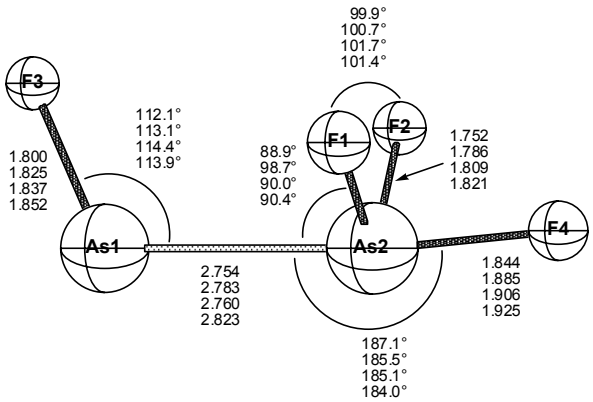

4ad (C_s, $^2A''$)

Figure 2.8: Geometries of the low-lying minima of $As_2F_4^-$ (bond lengths in Å).

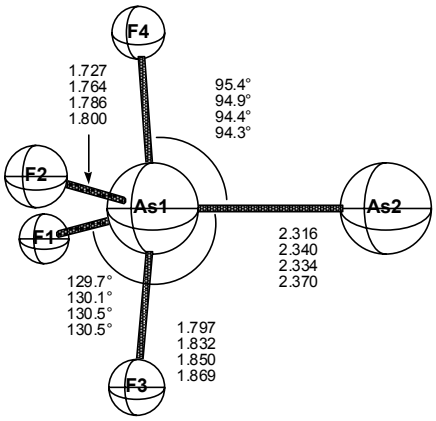

4ae (C_{2v}, $^2B_1$)

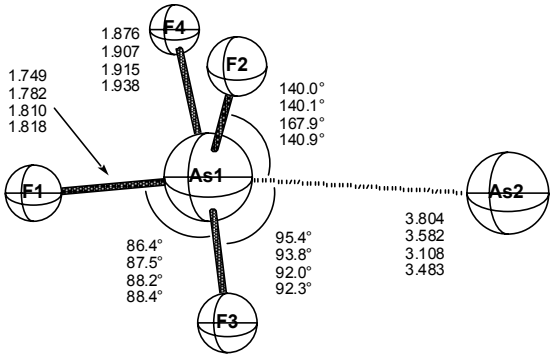

4af (C_s, $^4A''$)

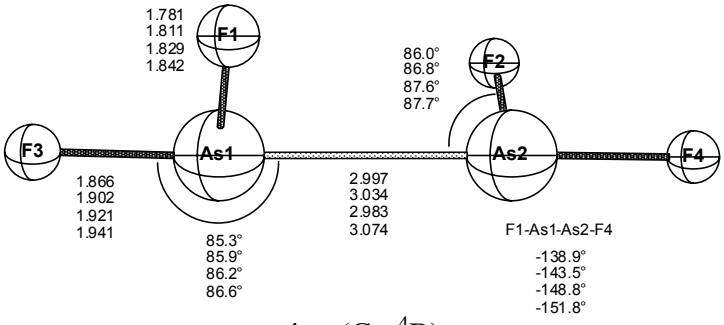

4ag (C_2, ^4B)

Figure 2.8 (Continued)

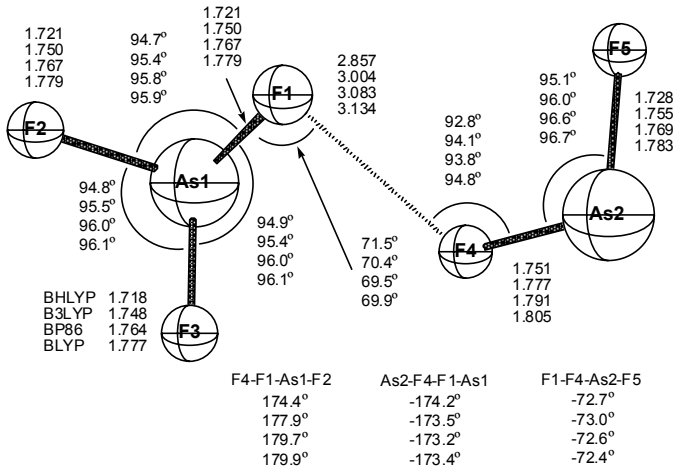

5na (C_1, ^2A)

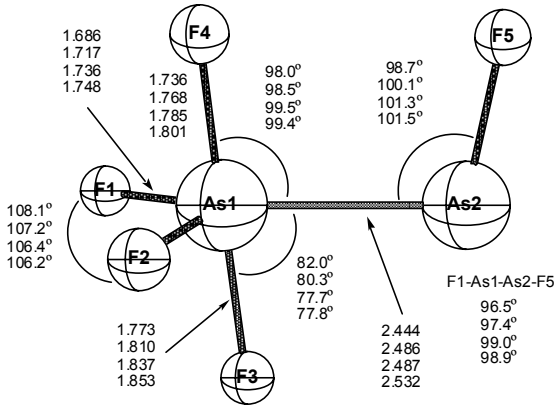

5nb (C_s, $^2A''$)

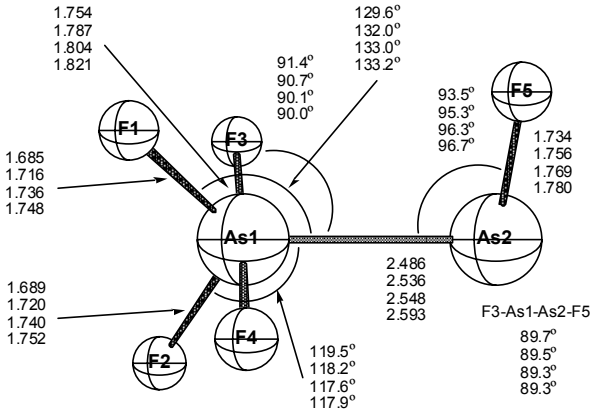

5nc (C_s, $^2A''$)

Figure 2.9: Geometries of the low-lying minima of As_2F_5 (bond lengths in Å).

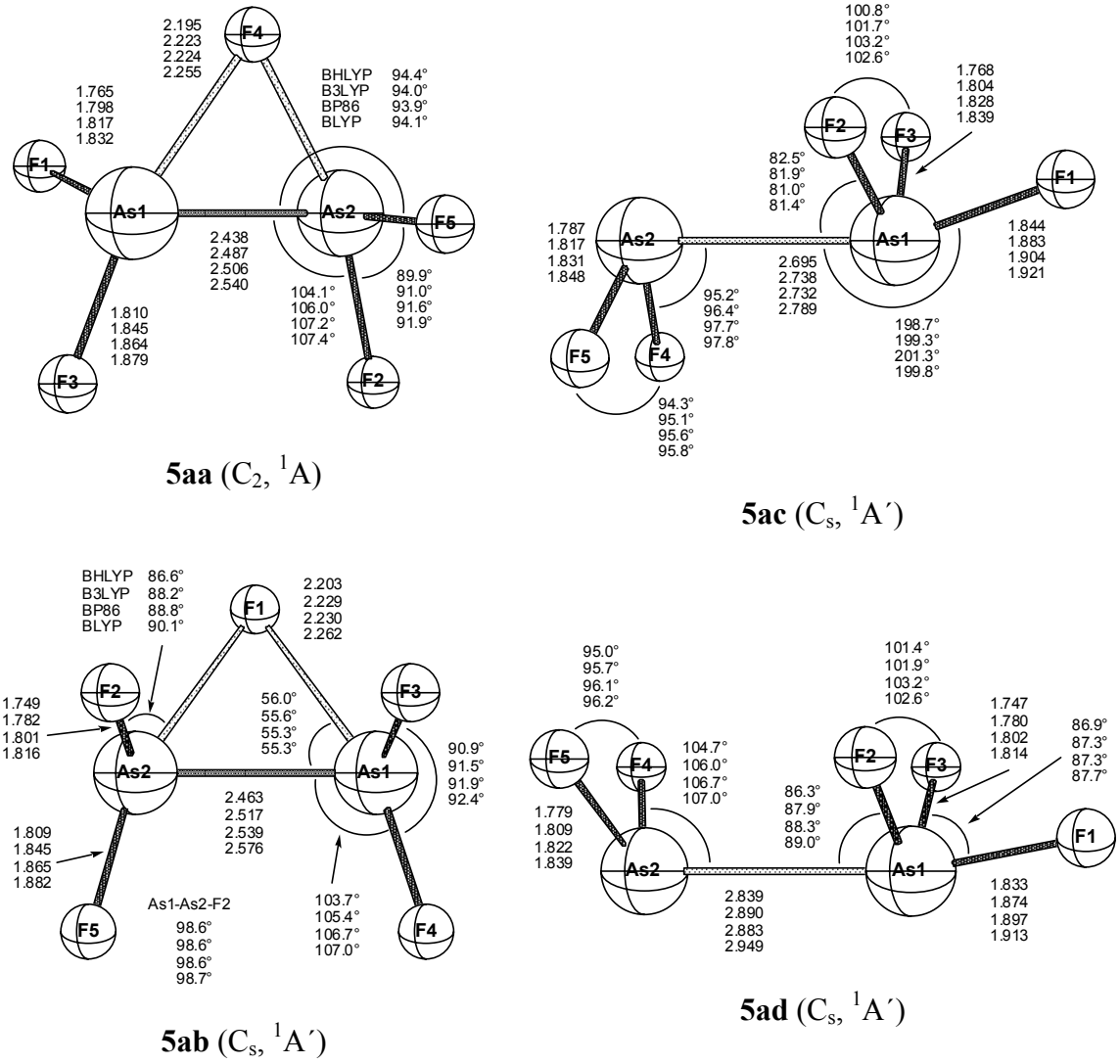

Figure 2.10: Geometries of the low-lying minima of $As_2F_5^-$ (bond lengths in Å).

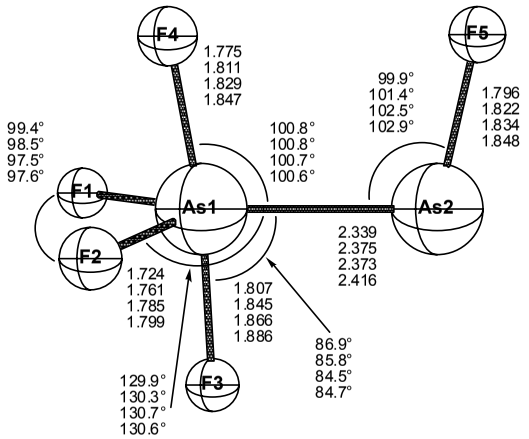

5ae (C_s, $^1A'$)

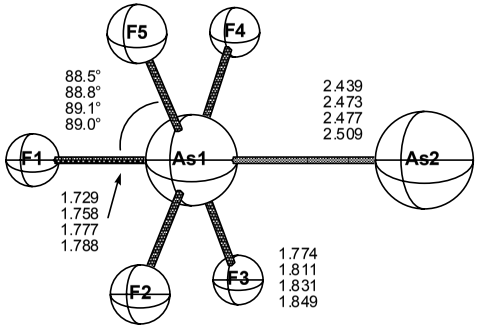

5ag (C_{4v}, $^3A_1$)

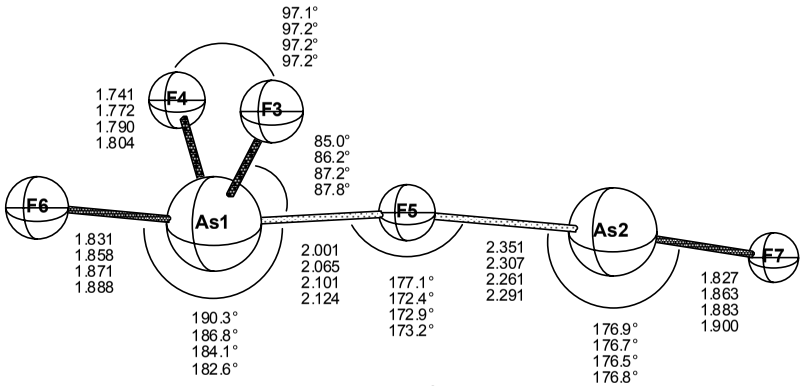

5af (C_s, $^3A''$)

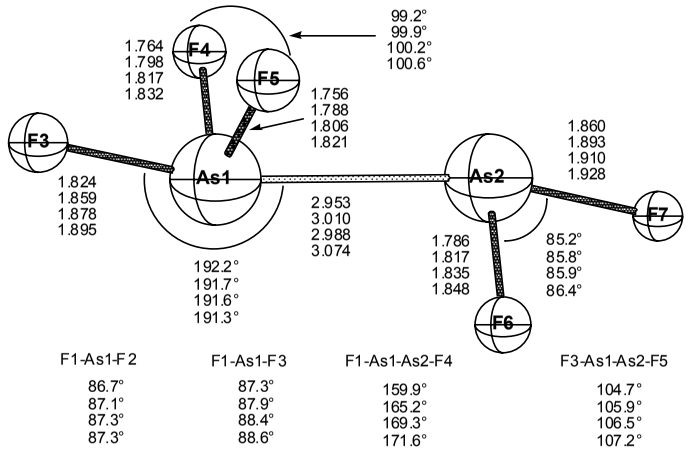

5ah (C_1, ^3A)

Figure 2.10 (Continued)

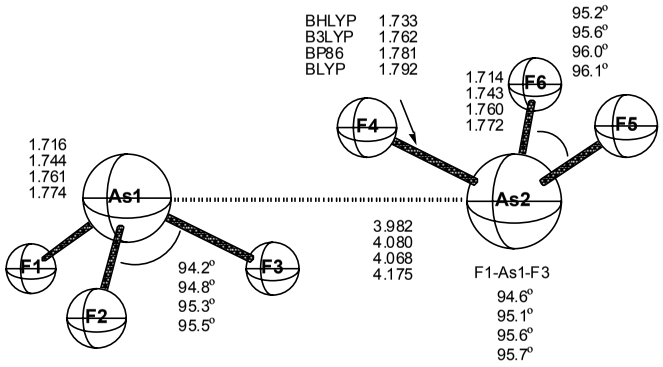

6na (C_i, ^1A_g)

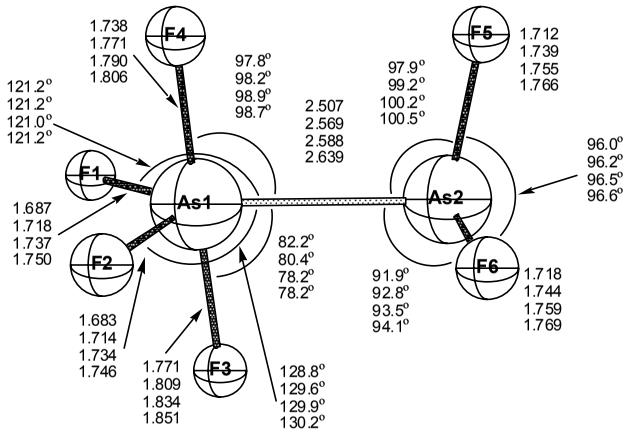

6nc (C_1, ^1A)

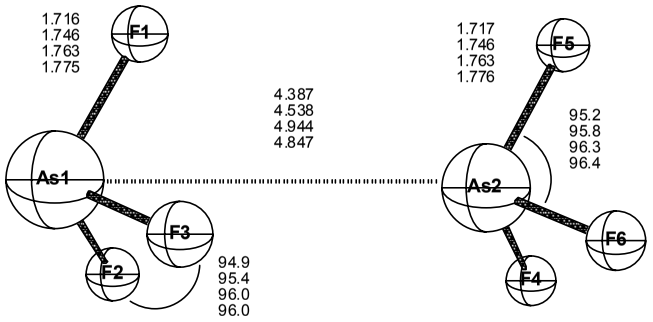

6nb (C_{3v}, $^1A_1$)

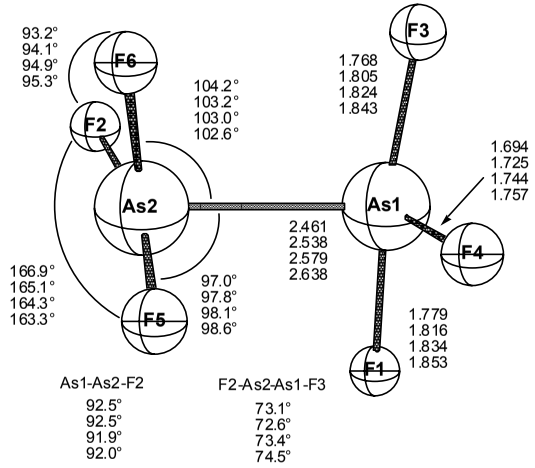

6nd (C_2, ^3B)

Figure 2.11: Geometries of the low-lying minima of As_2F_6 (bond lengths in Å).

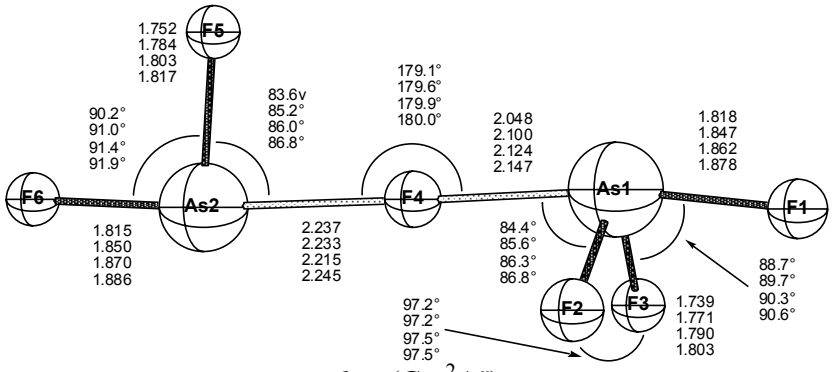

6aa (C_s, $^2A''$)

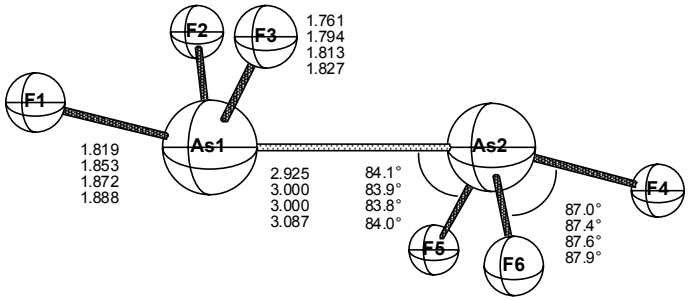

6ab (C_{2h}, ^2A_g)

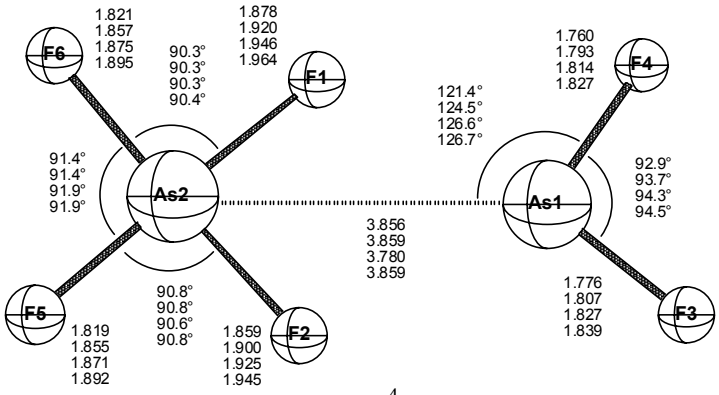

6ac (C_s, $^4A'$)

Figure 2.12: Geometries of the low-lying minima of $As_2F_6^-$ (bond lengths in Å).

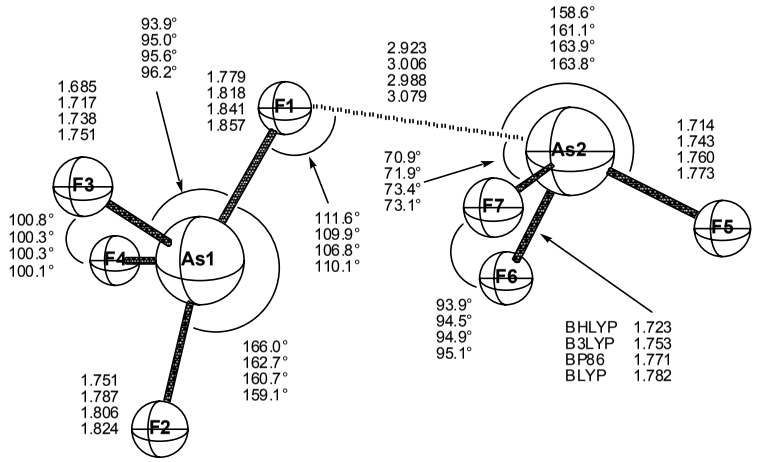

7na (C_s, $^2A'$)

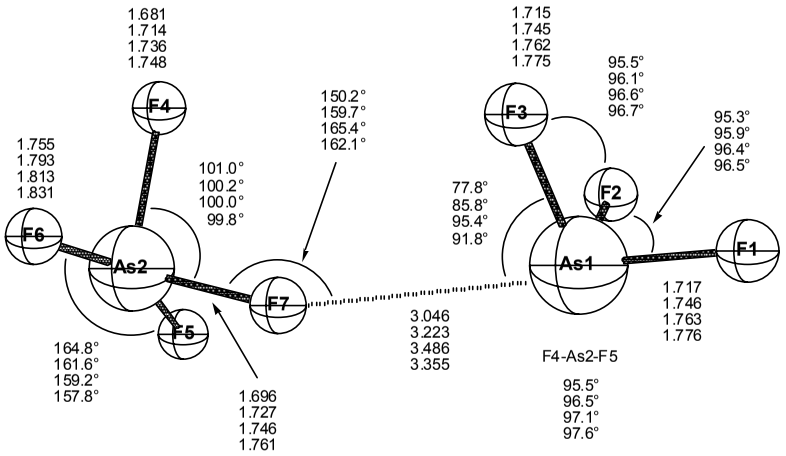

7nc (C_s, $^2A'$)

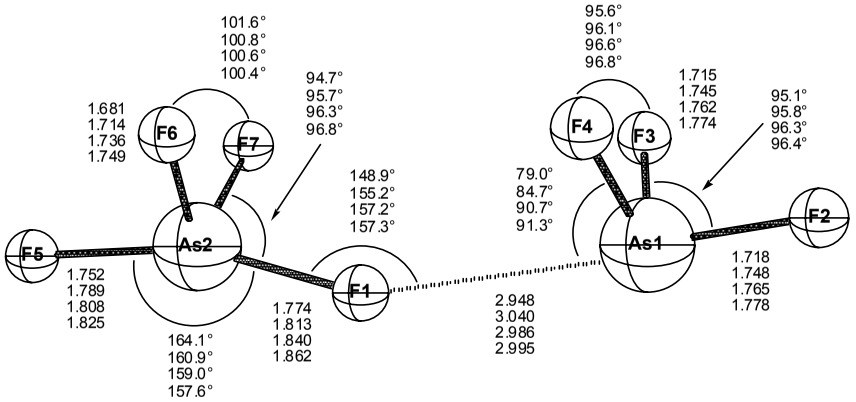

7nb (C_s, $^2A'$)

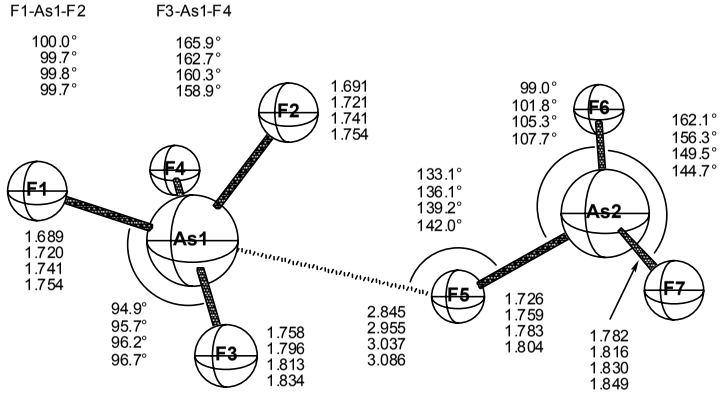

7nd (C_s, $^4A'$)

Figure 2.13: Geometries of the low-lying minima of As_2F_7 (bond lengths in Å).

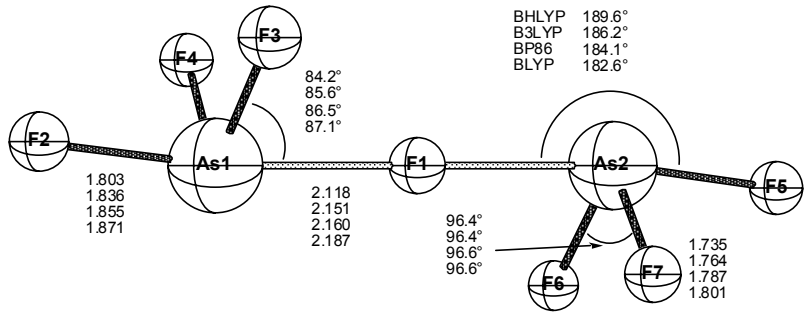

7aa (C_{2h}, ^1A_g)

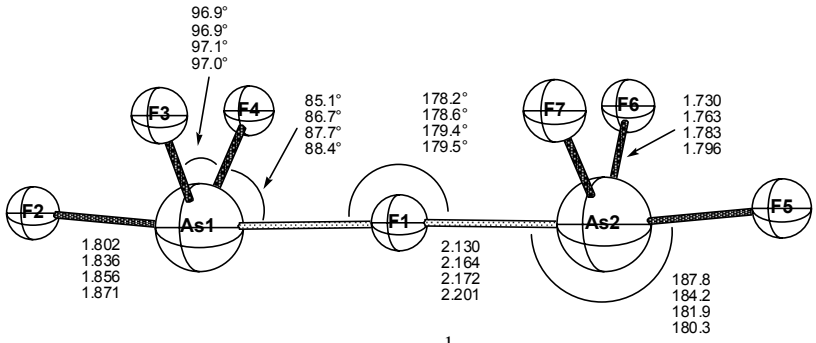

7ab (C_{2v}, $^1A_1$)

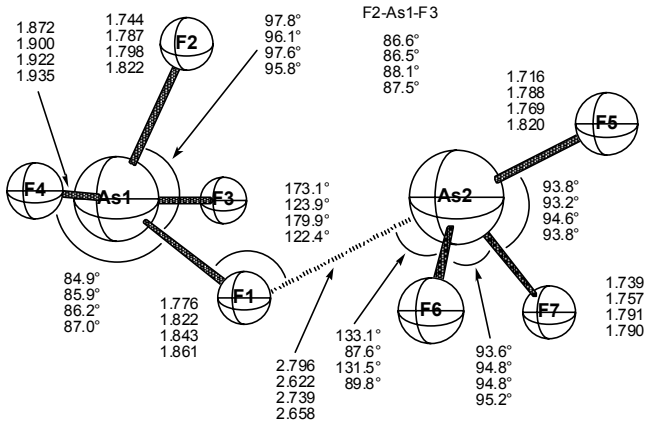

7ac (C_s, $^1A'$)

Figure 2.14: Geometries of the low-lying minima of $As_2F_7^-$ (bond lengths in Å).

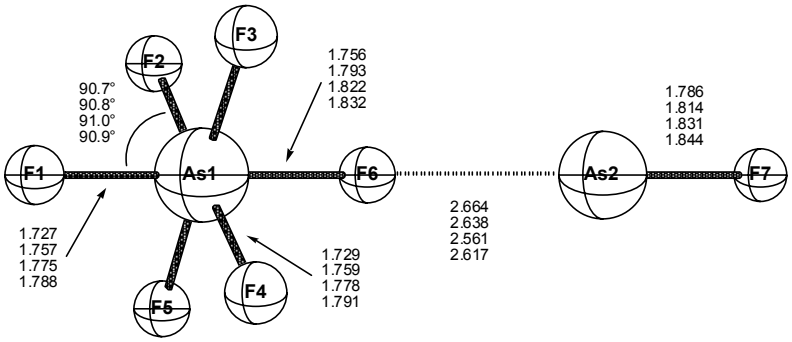

7ad (C_{4v}, $^3A_1$)

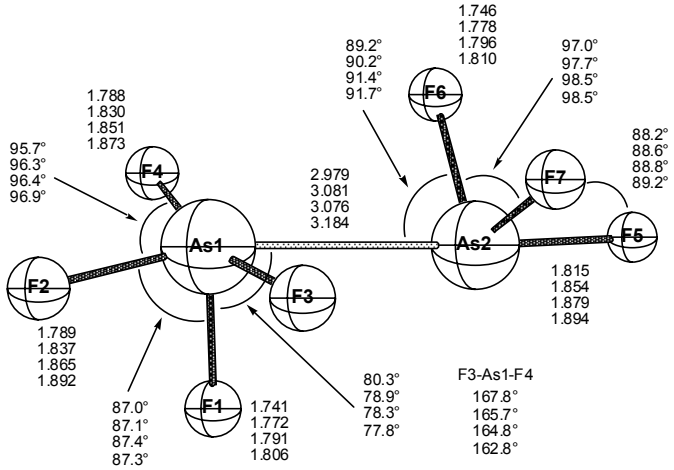

7ae (C_s, $^3A'$)

Figure 2.14 (Continued)

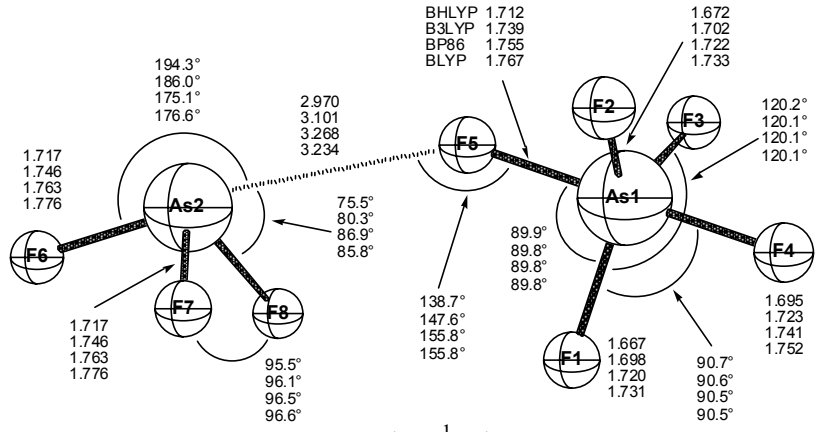

8na (C_s, $^1A'$)

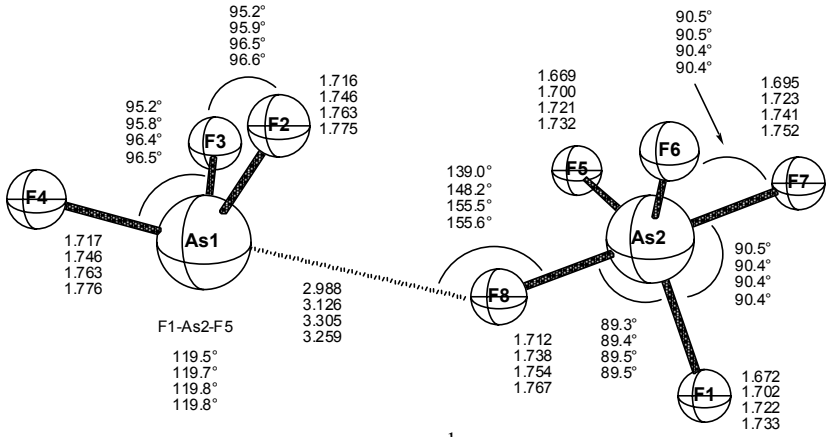

8nb (C_s, $^1A'$)

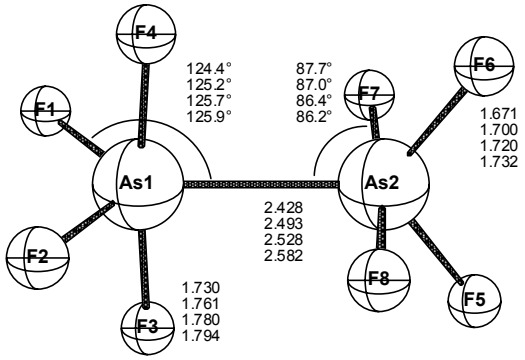

8nc (D_{2d}, $^1A_1$)

Figure 2.15: Geometries of the low-lying minima of As_2F_8 (bond lengths in Å).

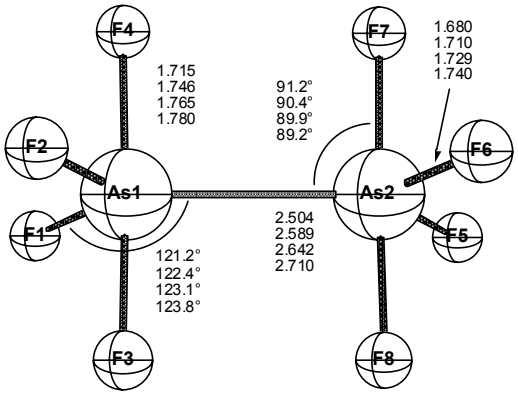

8nd (D_{2h}, ^1A_g)

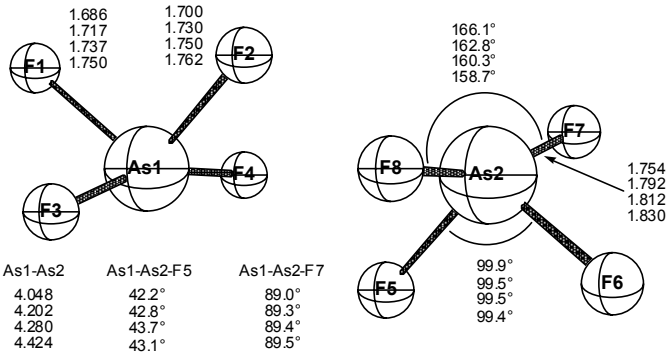

8ne (C_{2h}, ^3B_u)

Figure 2.15 (Continued)

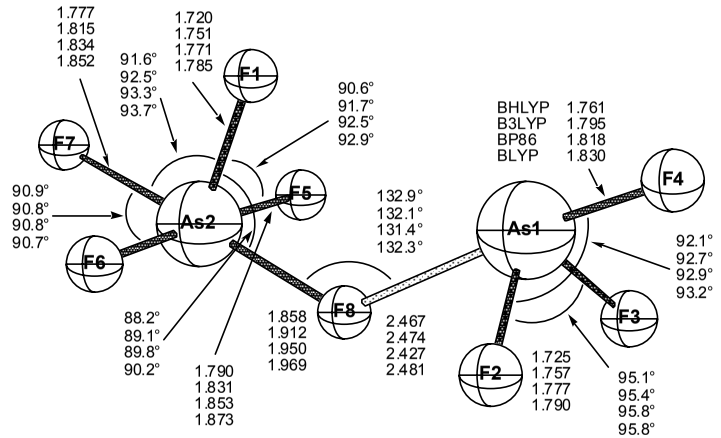

8aa (C_s, $^2A'$)

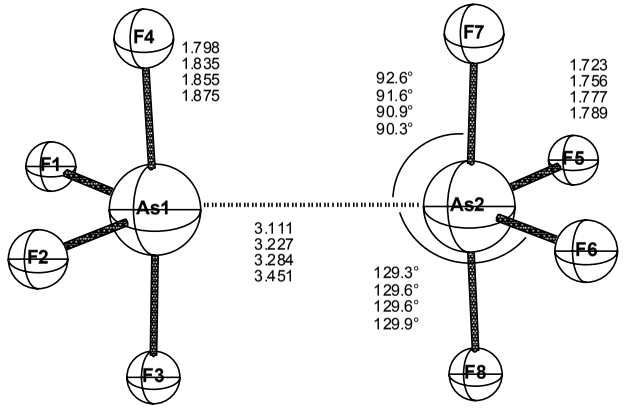

8ac (D_{2h}, $^2B_{3u}$)

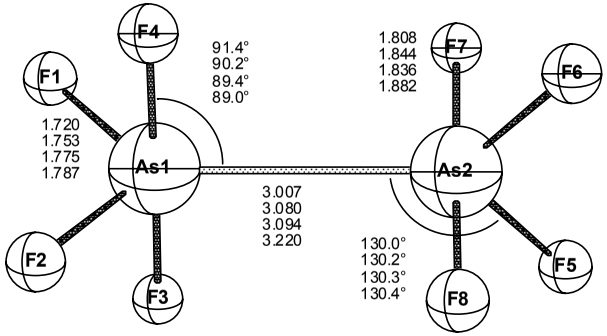

8ab (D_{2d}, $^2B_2$)

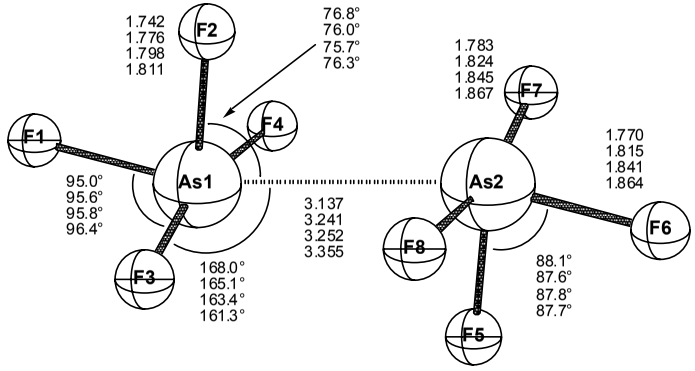

8ad (C_{2h}, ^4B_u)

Figure 2.16: Geometries of the low-lying minima of $As_2F_8^-$ (bond lengths in Å).

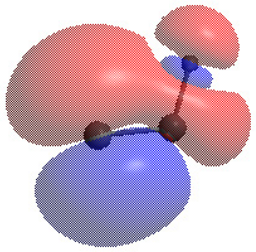

(a)

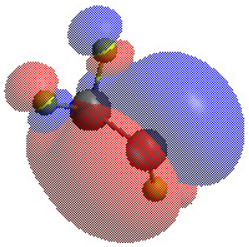

(b)

Figure 2.17: The highest occupied molecular orbitals (HOMO) of (a) As_2F^- and (b) $As_2F_3^-$

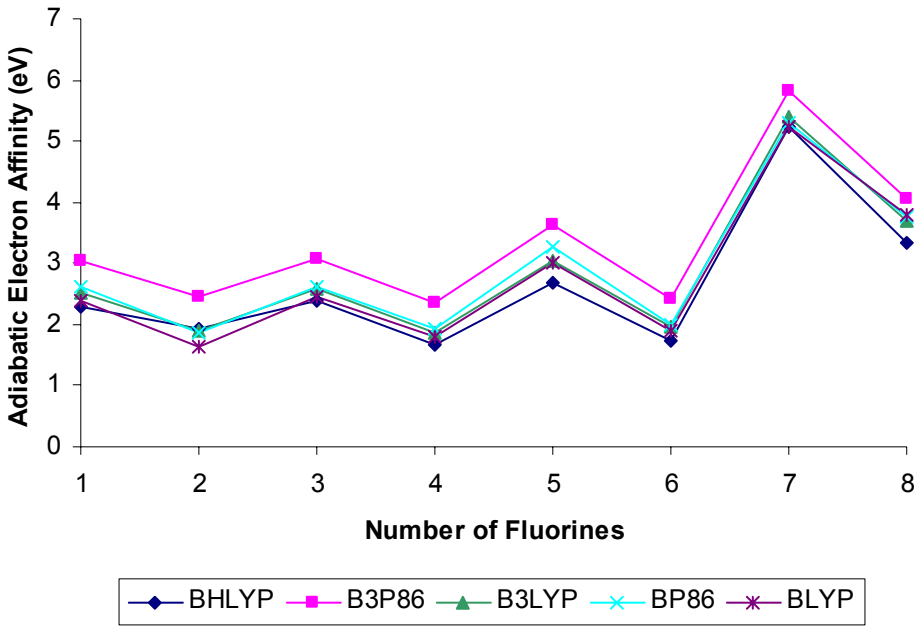

Figure 2.18: Adiabatic electron affinities as a function of the number of fluorines in As_2F_n for all five functionals.

CHAPTER 3

MODEL SYSTEMS FOR PROBING METAL CATION HYDRATION: THE $V^+(H_2O)$ AND $ArV^+(H_2O)$ COMPLEXES[*]

[*] V. Kasalová, W. D. Allen, E. D. Pillai, M. A. Duncan, H. F. Schaefer III. Submitted to *The Journal of Chemical Physics*, 12/21/2005

3.1 ABSTRACT

In support of mass-selected infrared photodissociation (IRPD) spectroscopy experiments, coupled cluster methods including all single and double excitations (CCSD) and a perturbative contribution from connected triple excitations [CCSD(T)] have been used to study the $V^+(H_2O)$ and $ArV^+(H_2O)$ complexes. Equilibrium geometries, harmonic vibrational frequencies, and dissociation energies were computed for the four lowest-lying quintet states ($^5A_1$, $^5A_2$, $^5B_1$ and $^5B_2$), all of which appear within a 6 kcal mol^{-1} energy range. Moreover, anharmonic vibrational analyses with complete quartic force fields were executed for the $^5A_1$ states of $V^+(H_2O)$ and $ArV^+(H_2O)$. Two different basis sets were used: a Wachters+f V[8*s*6*p*4*d*1*f*] basis with triple-zeta plus polarization (TZP) for O, H and Ar; and an Ahlrichs QZVPP V[11*s*6*p*5*d*3*f*2*g*] and Ar[9*s*6*p*4*d*2*f*1*g*] basis with aug-cc-pVQZ for O and H. The ground state is predicted to be $^5A_1$ for $V^+(H_2O)$, but argon tagging changes the lowest-lying state to $^5B_1$ for $ArV^+(H_2O)$. Our computations show an opening of 2°-3º in the equilibrium bond angle of H_2O due to its interaction with the metal ion. Zero-point vibrational averaging increases the *effective* bond angle further by 2.0°-2.5º, mostly due to off-axis motion of the heavy vanadium atom rather than changes in the water bending potential. The total theoretical shift in the bond angle of about +4° is significantly less than the widening near 9º deduced from IRPD experiments. The binding energies (D_0) for successive addition of H_2O and Ar to the vanadium cation are 36.2 and 9.4 kcal mol^{-1}, respectively.

3.2 INTRODUCTION

Fundamental to understanding the bulk solvation of metal ions is the interaction of the individual ions and solvent molecules. Metal-cation/water complexes are of the most fundamental interest. However, the details of metal-solvation processes are difficult to determine experimentally, and gas-phase spectroscopic structures of water molecules in contact with a metal cation are rare in the literature.

Photodissociation spectroscopy has been used previously for many metal-ligand complexes to obtain vibrationally resolved spectra for electronic states, as well as rotationally resolved spectra that have provided some of the first direct structural determinations for these molecules. In the early and mid-1990s Duncan and co-workers[1-3] were the first to perform *electronic* laser photodissociation spectroscopy with detection by time-of-flight mass spectrometry. Lisy *et al*.[4-7] subsequently applied *infrared* photodissociation spectroscopy (IRPD) to metal-ion/ligand systems, including alkali-cation/water complexes. Beginning in 2002, more extensive mass-selected IRPD studies were executed within the Duncan group,[8-16] on a variety of main group transition-metal/ligand complexes produced by laser vaporization sources. In 2004 Nishi and co-workers[17,18] reported IR photodissociation studies on $Mg^+(H_2O)$ and $Al^+(H_2O)$. Finally, the most recent 2005 work in the Duncan laboratory has applied mass-selected IRPD to investigate progressively argon-solvated $Mg^+(H_2O)Ar_n$ clusters[19] and solvation dynamics of $Ni^+(H_2O)_n$ complexes.[20]

A stronger metal-ligand bond in complexes with a transition metal, as compared to alkali metals,[21-28] makes these systems challenging candidates for spectroscopy. The bond energy of transition-metal-cation/water complexes is too high for single-photon

infrared photodissociation; therefore, multiphoton dissociation or "argon tagging" is necessary. The principle behind "argon tagging" is that clusters with rare gas atoms loosely attached have dissociation channels that are accessible at lower photon energies, thus allowing mass spectrometric detection of infrared absorption across wider frequency ranges. It is generally assumed that the argon in such mixed complexes acts as a spectator and does not induce significant structural changes in the clusters or shift the vibrations by substantial amounts.

Recently, the Duncan group applied mass-selected IRPD spectroscopy to the vanadium-cation/water complex.[12] This study provided the first gas-phase IR data on a transition-metal-cation/water system. Vanadium was chosen because it has a single isotope, thus simplifying the mass analysis. $V^+(H_2O)$, $V^+(H_2O)Ar_n$, $V^+(D_2O)$ and $V^+(D_2O)Ar_n$ were produced by laser vaporization of a metal target rod and entrainment in an Ar steam gas. The argon atom is attached to the vanadium cation on the opposite side of the water molecule. After mass selecting the target species, the O-H and O-D stretches in the water moiety were vibrationally excited, and fragment-ion versus energy photodissociation spectra were recorded.

The IRPD spectrum of $ArV^+(H_2O)$ contains peaks at 3605 and 3690 cm^{-1}.[12] These bands are ~50 cm^{-1} and ~70 cm^{-1} to the red of the symmetric (3657 cm^{-1}) and antisymmetric (3756 cm^{-1}) stretches in free water. Vibrational frequencies of $ArV^+(H_2O)$ evaluated at the B3LYP/6-31G* level of theory (3630 and 3689 cm^{-1}) agree qualitatively with the measured red shifts. For the theoretically predicted $^5B_1$ ground state, the DFT computed H-O-H angle is 107.5˚.

The rotational constants of $ArV^+(H_2O)$, corresponding to the Ar-V-O principal axis, surmised from the profile of the IRPD spectrum of the H_2O antisymmetric stretch were $A' = 7.96$ cm^{-1} and $A'' = 12.52$ cm^{-1}.[12] The A'' value would indicate an H-O-H angle (113.8°) much more greatly expanded upon complexation than predicted by B3LYP/6-31G* density functional theory. The large difference between A' and A'' would point to a prodigious vibrationally-averaged geometry distortion in the complex for the O-H antisymmetric stretching fundamental level.

Prior to the IRPD experiment performed by Duncan's group,[12] the $V^+(H_2O)$ complex was probed by various experimental methods, including collision induced dissociation (CID),[22,23,25] resonant one-photon dissociation spectroscopy,[29] and charge stripping mass spectrometry.[30] The vanadium-cation/water complex showed characteristics of an electrostatically bound species, with a dissociation energy $D_0 = 35\pm4$ kcal mol^{-1} (see Table 3.1) and a V-O stretching frequency $\omega_e'' = 420\pm75$ cm^{-1}.

Various computational methods have been applied to $V^+(H_2O)$, including the modified coupled pair functional (MCPF) approach,[31,32] Møller-Plesset perturbation theory,[33,34] configuration interaction,[33] density functional theory[35-37,30] and limited coupled cluster methods.[34-36,30] These theoretical studies focused on structures and dissociation energies for the ground state ($^5A_1$) and the lowest-lying ($^5A_2$, $^5B_1$, and $^5B_2$) states. Also it was confirmed that the HV^+OH intermediate, hypothesized by experimentalists,[22] is a well-defined minimum on the potential energy surface, lying 53.8 kcal mol^{-1} above $V^+(H_2O)$.[35] To our best knowledge, no theoretical data is available for the $ArV^+(H_2O)$ complex.

Motivated by the IRPD experiments, the $V^+(H_2O)$ and $ArV^+(H_2O)$ complexes are studied here as model systems for metal cation hydration. Accurate structures are obtained for the lowest-lying states of the $V^+(H_2O)$ and $ArV^+(H_2O)$ complexes, and the effects of vibrational averaging on the structures (in particular the H-O-H angle expansion) are analyzed. Definitive dissociation energy and adiabatic excitation energies are determined as well.

3.3 THEORETICAL METHODS

To ensure against spin contamination, reference electronic wave functions were determined by the single-configuration restricted open-shell Hartree-Fock (ROHF) method.[38-41] Electron correlation was then included by the coupled cluster singles and doubles method (CCSD),[42] as well as CCSD with a perturbative contribution from connected triple excitations [CCSD(T)].[42,43] All open-shell coupled-cluster energies were determined from a spin-orbital formulation into which ROHF orbitals were substituted.[42] The 1*s*, 2*s* and 2*p* core orbitals of vanadium and argon, as well as the 1*s* core orbital of oxygen, were frozen in the correlation treatments. When investigating the multireference character of $V^+(H_2O)$, state-averaged (SA) complete active space self-consistent field (CASSCF)[44,45] single point computations were performed with a 12 electron/13 MO active space.

Two basis sets were utilized in this study. The smaller basis set, denoted Wf(TZP), was constructed from the Wachters[46] set with supplemental diffuse *p*, diffuse *d*, and *f*-polarization functions[47-49] for vanadium, the valence triple-zeta basis set of Dunning[50] with added polarization functions (TZP) for oxygen and hydrogen [$\alpha_p(H)$ =

0.75, α_d(O) = 0.85], and the Schäfer, Huber and Ahlrichs TZV[51] basis set with added polarization functions[52] for argon. The final Wf(TZP) contraction schemes are V(14*s*11*p*6*d*3*f*/8*s*6*p*4*d*1*f*), O(11*s*6*p*1*d*/5*s*3*p*1*d*), H(5*s*1*p*/3*s*1*p*), and Ar(14*s*9*p*1*d*/5*s*4*p*1*d*). A larger basis set of quadruple-zeta quality, denoted collectively as QZVPP here, consisted of the QZVPP[53] basis, published by Weigend, Furche, and Ahlrichs in 2003 for the vanadium and argon atoms, and Dunning's augmented correlation-consistent polarized-valence quadruple-zeta (aug-cc-pVQZ) basis set[54,55] for oxygen and hydrogen. The final contraction schemes for the QZVPP basis set are V(24*s*18*p*9*d*3*f*2*g*/11*s*6*p*5*d*3*f*2*g*), Ar(20*s*14*p*4*d*2*f*1*g*/9*s*6*p*4*d*2*f*1*g*), O(13*s*7*p*4*d*3*f*2*g*/6*s*5*p*4*d*3*f* 2*g*) and H(7*s*4*p*3*d*2*f*/5*s*4*p*3*d*2*f*). The QZVPP basis functions for vanadium are designed to have sufficient flexibility in the outer core region to correlate the 3*s* and 3*p* electrons.

Tightly optimized geometrical structures (with all gradient components $< 10^{-6}$ a.u.) were obtained at each level of theory. The harmonic vibrational frequencies for the geometric minima of $V^+(H_2O)$ and $ArV^+(H_2O)$ were computed for both basis sets with the ROHF, CCSD, and CCSD(T) methods. To determine fundamental frequencies and zero-point vibrational (ZPV) effects on rotational constants, quartic force fields for $V^+(H_2O)$, $ArV^+(H_2O)$, and H_2O were computed at the Wf(TZP) CCSD and CCSD(T) levels of theory and employed in concert with second-order vibrational perturbation theory (VPT2)[56-60] to determine anharmonic constants. Adopting the atomic labeling of Figure 3.1, the following symmetry-adapted internal coordinates were utilized for $V^+(H_2O)$ and $ArV^+(H_2O)$:

$$S_1(a_1) = r_{12} \quad \text{(V-O stretch)}$$

$$S_2(a_1) = \frac{1}{\sqrt{2}}\left(r_{23} + r_{24}\right) \quad (H_2O \text{ symmetric stretch})$$

$$S_3(a_1) = \theta_{324}$$ (H_2O scissor)

$$S_4(b_1) = \gamma_{1234}$$ (H_2O wag)

$$S_5(b_2) = \frac{1}{\sqrt{2}}\left(r_{23} - r_{24}\right)$$ (H_2O antisymmetric stretch)

$$S_6(b_2) = \frac{1}{\sqrt{2}}\left(\theta_{123} - \theta_{124}\right)$$ (H_2O rock)

$$S_7(a_1) = r_{51}$$ (Ar-V stretch)

$$S_8(b_1) = \frac{1}{\sqrt{2}}\left(\alpha^{x}_{3215} + \alpha^{x}_{4215}\right)$$ (Ar-V-O linear bend in xz plane)

$$S_9(b_2) = \frac{1}{\sqrt{2}}\left(\alpha^{y}_{3215} + \alpha^{y}_{3215}\right)$$ (Ar-V-O linear bend in yz plane)

where r_{ij} denotes the bond distance between atoms *i* and *j*, θ_{ijk} is the *i-j-k* bond angle, γ_{ijkl} is the out-of-plane angle of the *ij* bond with respect to the *j-k-l* plane, and α^{x}_{ijkl} and α^{y}_{ijkl} are linear bends of the *jkl* chain perpendicular to (α^{x}) or within (α^{y}) the *ijk* plane. The full quartic (quadratic) force fields for $V^{+}(H_2O)$ and $ArV^{+}(H_2O)$ were computed via 183 (17) and 568 (30) energies points, respectively. The step size for displacements was 0.01 Å and 0.02 rad for bond lengths and angles, respectively. Great effort was made to ensure continuity of both Hartree-Fock and coupled cluster solutions by slow incremental variations from equilibrium when the species were distorted from C_{2v} symmetry. The program INTDIF2004[61,62] was employed to determine the required displacements as well as compute the force constants in internal coordinates. The transformation of the force constants from internal to normal coordinates and the computation of spectroscopic constants were performed using the programs INTDER2000[63-65] and ANHARM,[66,67] respectively.

All electronic structure computations were performed using the ACES II[68] and MOLPRO[69] suites of programs. Most of the computations were nonrelativistic; however, final energetic predictions for the $V^+(H_2O)$ ground state were scrutinized by including the one-electron mass-velocity and Darwin scalar relativistic terms[70-74] via the first-order perturbation scheme implemented in ACESII.

3.4 RESULTS AND DISCUSSION: THE $V^+(H_2O)$ COMPLEX

For vanadium cation, the lowest-lying quintet state ^5D arises from the $3d^4$ configuration, and the first excited state is ^5F ($3d^3$ $4s$). The $^5D_0 \rightarrow {}^5F_1$ excitation energy between the lowest-lying spin-orbit sublevels in these manifolds is 2604.82 cm^{-1}.[75] Applying our single-reference electronic structure methods (without spin-orbit coupling) in C_{2v} symmetry to atomic $V^+(^5D)$, we find a four-fold degeneracy for the lowest energy solution, with the fifth component ($3d^1_{xy}\,3d^1_{yz}\,3d^1_{xz}\,3d^1_{x^2-y^2}$) very slightly higher in energy. The degeneracy splitting is 0.17 kcal mol^{-1} for ROHF/Wf(TZP), but an utterly negligible 0.00055 kcal mol^{-1} for CCSD(T)/Wf(TZP). We conclude that artifactual degeneracy splitting within the $V^+(^5D)$ manifold is not a concern here and that the CCSD(T) method is sufficient to effectively restore the five-fold degeneracy that must be present in the full CI limit.

Complexation with water genuinely splits the five degenerate components of the V^+ ground state and in C_{2v} symmetry (Figure 3.1) gives rise to two $^5A_1$ states, as well as $^5A_2$, $^5B_1$, and $^5B_2$ states. The V^+ atomic configurations to which these states asymptotically correlate are $^5A_1(\,3d^1_{xy}\,3d^1_{yz}\,3d^1_{xz}\,3d^1_{z^2}\,)$, $^5A_1(\,3d^1_{xy}\,3d^1_{yz}\,3d^1_{xz}\,3d^1_{x^2-y^2}\,)$, $^5A_2(\,3d^1_{x^2-y^2}\,3d^1_{yz}\,3d^1_{xz}\,3d^1_{z^2}\,)$, $^5B_1(\,3d^1_{yz}\,3d^1_{x^2-y^2}\,3d^1_{xy}\,3d^1_{z^2}\,)$, and $^5B_2(\,3d^1_{xz}\,3d^1_{x^2-y^2}\,3d^1_{xy}\,3d^1_{z^2}\,)$,

assuming the axis convention in Fig. 3.1. Because the open-shell vanadium *d* orbitals retain their atomic character in the electrostatic $V^+(H_2O)$ and $ArV^+(H_2O)$ complexes, there is little mixing of the two low-lying $^5A_1$ states. In particular, (12 e^-/13 MO) state-specific CASSCF computations on $V^+(H_2O)$ with the Wf(TZP) basis set gave leading CI coefficients in the natural orbital basis of (0.9780, –0.0769) and (0.0769, 0.9780) for the two $^5A_1$ states, with no other coefficients larger than 0.06. In this work, only the lowest $^5A_1$ state will be fully examined, because we are mostly interested in the ground state for this system.

Relative energies, optimum geometries, dissociation energies, and vibrational frequencies for the four lowest-lying states of $V^+(H_2O)$ are presented in Tables 3.1-3.4. All four states are within 6 kcal mol^{-1} of one another. The ground state is the $^5A_1$ state for all applied levels of theory. The electronic configuration for the singly occupied orbitals of the ground state in C_{2v} symmetry is $1a_2 4b_2 4b_1 9a_1$, which agrees with previous results.[31,32,34] All of these molecular orbitals correspond to atomic orbitals on vanadium: $1a_2$ to $3d_{xy}$, $4b_2$ to $3d_{yz}$, $4b_1$ to $3d_{xz}$, and $9a_1$ to a mixture of the $3d_{z^2}$ and 4*s* orbitals, as mentioned by Rosi and Bauschlicher.[31,32] The fascinating hybrid character of the $9a_1$ orbital is illustrated in Fig 3.2.

The V-O distance, O-H distance and H-O-H angle for the ground state of $V^+(H_2O)$ are 2.049 Å, 0.963 Å and 106.8˚, respectively, at the CCSD(T)/ QZVPP level of theory (Table 3.3). The H-O-H angle computed at the same level of theory for free water is 104.4˚, which is 2.4˚ less than that of the $V^+(H_2O)$ complex. The H-O-H angle expansion resulting from addition of the vanadium cation is much smaller than the aforementioned IRPD spectroscopic result (9.3°) of Duncan et al.[12] The complexation

effect on the H-O-H angle is not particularly sensitive to level of theory; indeed among the six sets of optimum geometries we computed in this study (Table 3.3), the angle widening lies in the range 1.0°-2.9°. The predicted H-O-H angle for $V^+(H_2O)$ is even less sensitive to the computational method than for the corresponding angle in free water. For $V^+(H_2O)$, the change in the H-O-H angle due to basis set and electron correlation improvements [ROHF/Wf(TZP) to CCSD(T)/QZVPP] only approaches 0.8° for the $^5A_1$ and $^5A_2$ states of $V^+(H_2O)$, and is only 0.2° for the $^5B_1$ state of $V^+(H_2O)$. For comparison, the angle for free water computed with CCSD(T)/QZVPP (104.4°) is 2.0° smaller than that computed with ROHF/Wf(TZP) (106.4°).

Moving an electron in $V^+(H_2O)$ from the $1a_2$ ($3d_{xy}$) to the $10a_1$ ($3d_{x^2-y^2}$) orbital results in a $^5A_2$ state that is almost degenerate with the ground state, as the energy difference is only 0.15 kcal mol^{-1} for the CCSD(T)/ QZVPP level of theory (Table 3.2). The $T_e(^5A_2)$ excitation energy is not very sensitive to electron correlation or basis set, varying by only 0.1-0.2 kcal mol^{-1} in Table 3.2. Our $^5A_2 - {}^5A_1$ separation of 0.15 kcal mol^{-1} generally validates the relative energies of 0.09 kcal mol^{-1} obtained by Rosi and Bauschlicher,[31,32] and 0.07 kcal mol^{-1} obtained by Trachtman et al.[34] The geometry difference between the $^5A_2$ state and the $^5A_1$ ground state is also very small. The V-O bond distance for the $^5A_2$ state is only 0.002 Å longer than the corresponding distance for the $^5A_1$ state [CCSD(T)/QZVPP]. The H-O-H angle for the $^5A_2$ state differs from the $^5A_1$ ground state value by less than 0.1˚ [CCSD(T)/QZVPP].

The $^5B_1$ and $^5B_2$ states of $V^+(H_2O)$ are 0.4 and 5.1 kcal mol^{-1} [CCSD(T)/QZVPP], respectively, above the ground state. Electron correlation lowers both states substantially, by almost 4 kcal mol^{-1} for the $^5B_1$ state, making ($^5A_1$, $^5A_2$, $^5B_1$) isoenergetic within

0.5 kcal mol^{-1}. The trend with increasing basis set is further lowering of the $^5B_1$ and $^5B_2$ excited states. The B3LYP results of Klippenstein and Yang[36] also give a ($^5A_1$, $^5A_2$, $^5B_1$) cluster of states within 0.5 kcal mol^{-1}, but the ($^5A_2$, $^5B_1$) ordering is switched with respect to our high-level CCSD(T)/QZVPP predictions. The ordering of $^5B_1$ and $^5B_2$ states reported by Rosi and Bauschlicher[31,32] (T_e = 6.0 kcal mol^{-1} for $^5B_1$ and 1.5 kcal mol^{-1} for $^5B_2$) is reversed compared to our best results. This disparity might merely be a labeling issue for the C_{2v} irreducible representations, although their axis conventions appear to be the same as ours. The CCSD(T)/QZVPP method yields optimum H-O-H angles for the $^5B_1$ and $^5B_2$ states that are respectively 0.29° above and 0.45° below the corresponding ground state value of 106.76°. Finally, the $^5B_1$ state exhibits the shortest equilibrium V-O bond distance [2.0193 Å, CCSD(T)/QZVPP] among the four lowest-lying electronic states.

Correlation of the 3*s*3*p* shell on vanadium is important for the evaluation of the excitation energies. The QZVPP basis was explicitly constructed to allow polarization of the 3*s*3*p* shell, and it has been recommended that this shell be included in correlation treatments with this basis set of the 3*d* series of transition metals.[53] We performed CCSD(T)/QZVPP single-point energy computations with V(3*s*) and V(3*p*) included in the core to see what changes in excitation energies would be engendered. The corresponding small-core optimum geometries were employed. The resulting excitation energies were 0.15 kcal mol^{-1}, 0.88 kcal mol^{-1}, and 4.95 kcal mol^{-1} for the $^5A_2$, $^5B_1$, and $^5B_2$ states, respectively. The ordering of the states of $V^+(H_2O)$ is preserved for these large core computations, but the excitation energies change for the $^5B_1$ and $^5B_2$ states by +0.51 kcal mol^{-1} and −0.14 kcal mol^{-1}, respectively (cf. Table 3.2).

In our optimum geometric structures, the V-O distance decreases substantially with improvements in both the basis set and electron correlation treatment. However, this occurrence is typical of electrostatically bound complexes between polarizable species. Note that for the $^5B_1$ and $^5B_2$ states of $V^+(H_2O)$, the contraction of the V-O distance from ROHF/Wf(TZP) to CCSD(T)/QZVPP approaches 0.2 Å. Our best [CCSD(T)/QZVPP] predictions for r(V-O) are as much as 0.05 Å shorter than previous theoretical values but are probably still upper bounds on the exact equilibrium distances.

The lowest-lying triplet electronic state of $V^+(H_2O)$ reported by Rosi and Bauchslicher,[31,32] $^3B_2$, lies 22 kcal mol^{-1} higher in energy than the quintet ground state (MCPF/Wachters+f TZP). Irigoras et al.[35] found the lowest triplet state to be $^3A_1$, lying 18.1 kcal mol^{-1} above the $^5A_1$ state [B3LYP/TZVP+G(3df,2p)]. We performed CCSD(T)/Wf(TZP) single-point energy computations for various triplet electronic states at the $V^+(H_2O)$ $^5A_1$ CCSD(T)/Wf(TZP) geometry. We found the lowest triplet state of $V^+(H_2O)$ to be $^3B_2$ with a vertical excitation energy of 19.6 kcal mol^{-1}. In summary, the triplet states of $V^+(H_2O)$ are sufficiently higher in energy than the low-lying quintet manifold to be excluded from further consideration in this work.

The ZPVE corrected dissociation energy (D_0) of the $V^+(H_2O)$ ground state, corresponding to dissociation into $V^+(^5D) + H_2O$, is computed to be 36.2 kcal mol^{-1} at our best level of theory [CCSD(T)/QZVPP]. The basis set and electron correlation trends in Table 3.1 suggest that our D_0 value is converged to within 1 kcal mol^{-1}. Indeed, our (nonrelativistic) dissociation energy of 36.2 ± 1.0 kcal mol^{-1} is within the error bars of all experimental studies (Table 3.1) and provides the most accurate dissociation energy of the $V^+(H_2O)$ complex to date. Among the theoretical studies on $D_0(V^+\text{-}H_2O)$, the

6-311++G** CCSD(T) dissociation energy reported in Ref. 34 is unusually large (ΔH^0_{298} = –41.8 kcal mol^{-1}). We performed single-point CCSD(T)/6-311++G** energy computations at the CCSD(T)/QZVPP optimized geometry and found that the dissociation energy D_e for production of $V^+(^5D)$ is 34.0 kcal mol^{-1}, while dissociation into $V^+(^5F)$ requires 41.3 kcal mol^{-1} of energy. For this reason, we conclude that the CCSD(T) dissociation energy reported in Ref. 34 likely corresponds to an incorrect dissociation asymptote.

The effects of core correlation and special relativity on the binding energy of $V^+(H_2O)$ warrant consideration. If the 3*s* and 3*p* outer-core orbitals on vanadium are not correlated, against the recommendation of Weigend, Furche, and Ahlrichs,[53] the V^+-H_2O dissociation energy decreases by almost 5 kcal mol^{-1} at our best level of theory [CCSD(T)/QZVPP]. When ZPVE is added, the dissociation energy becomes D_0~31.4 kcal mol^{-1}, an anomalously small value compared to experimental measurements. Clearly, large-core correlation treatments are not advisable for this system, at least with the QZVPP basis. With regard to relativistic corrections, the one-electron mass-velocity and Darwin terms shift the dissociation energy of the $V^+(H_2O)$ $^5A_1$ ground state by +0.48 kcal mol^{-1} at the CCSD(T)/QZVPP level, i.e., well within our stated error bars. To further pinpoint the various auxiliary effects on $D_0(V^+$-$H_2O)$ would require multicomponent relativistic treatments and an accounting of shifts in the atomic V^+ spin-orbit splittings engendered by H_2O complexation.

The harmonic vibrational frequencies of the four lowest-lying states of $V^+(H_2O)$ are listed with associated results for free water in Table 3.4. At the highest level of theory [CCSD(T)/QZVPP], analogous frequencies of the four electronic states of $V^+(H_2O)$ never

differ by more than 20 cm^{-1}, and for the $^5A_1$ and $^5A_2$ states the ω_1 values are almost identical. It is thus sufficient to focus our discussion on the ground-state $^5A_1$ frequencies.

First note in Table 3.4 that CCSD(T) theory with the aug-cc-pVQZ basis reproduces the empirical harmonic frequencies of H_2O to exceptional accuracy (within 2 cm^{-1} in every case). Because the QZVPP set for $V^+(H_2O)$ contains the aug-cc-pVQZ basis on the H_2O moiety, we expect the frequencies of the H_2O modes to be very accurately predicted with the CCSD(T)/QZVPP method. The O-H symmetric and antisymmetric harmonic stretching frequencies of $^5A_1$ $V^+(H_2O)$ are ω_1 = 3794 cm^{-1} and ω_5 = 3876 cm^{-1} [CCSD(T)/QZVPP], representing red shifts of 37 cm^{-1} and 64 cm^{-1}, respectively, from free water. Among the correlated electronic structure methods in Table 3.4, there is striking agreement (within 1 cm^{-1}) on the magnitude of these red shifts, enhancing the credence of the predictions. As shown below (Table 3.8), vibrational anharmonicity increases the red shifts of the symmetric and antisymmetric O-H stretches to 43 cm^{-1} and 72 cm^{-1}, respectively. These theoretical results nicely substantiate the red shifts of ~50 cm^{-1} and ~70 cm^{-1} observed by Duncan's group.[12] This general agreement is maintained when the effects of argon tagging are considered in the next section (3.5), despite some subtle changes brought on by the Ar "spectator".

The H_2O harmonic scissoring frequency of $^5A_1$ $V^+(H_2O)$ is ω_2 = 1675 cm^{-1} [CCSD(T)/QZVPP], constituting a blue shift of 26 cm^{-1} relative to free water. Vibrational anharmonicity has no discernable effect on this complexation shift (Table 3.8). It is remarkable that a blue shift occurs in the scissoring frequency simultaneously with H-O-H angle widening (2°-3º) and O-H bond elongation (~0.004 Å).

The harmonic frequencies for the interfragment modes of $V^+(H_2O)$ occur in the 300-550 cm^{-1} range. Perhaps the most noteworthy trend for these modes is the increase in the V-O stretching frequency with improvements in both the basis set and electron correlation treatment, in accord with the bond length contractions observed in Table 3.3. Our best prediction [CCSD(T)/QZVPP] for the V-O stretching frequency of $^5A_1$ $V^+(H_2O)$ is ω_3 = 449 cm^{-1}, or ν_3 = 438 cm^{-1} if vibrational anharmonicity is included (Table 3.8). Consistent with this theoretical result, Lessen and co-workers[29] report a V-O stretch of ω_e'' = 420±75 cm^{-1} from a resonant one-photon fragmentation spectrum of $V^+(H_2O)$.

3.5 RESULTS AND DISCUSSION: THE $ArV^+(H_2O)$ COMPLEX

Similarly to $V^+(H_2O)$, the four lowest-lying quintet electronic states were investigated for the $ArV^+(H_2O)$ complex. Relative energies, geometries, dissociation energies, and harmonic vibrational frequencies for the $^5A_1$, $^5A_2$, $^5B_1$ and $^5B_2$ states are listed in Tables 3.2 and 3.5-3.7. Fundamental vibrational frequencies and anharmonicities of $ArV^+(H_2O)$, $V^+(H_2O)$, and free H_2O are compared in Table 3.8.

As in the $V^+(H_2O)$ case, the triplet electronic states are sufficiently high in energy to be excluded from detailed consideration here. Specifically, CCSD(T)/Wf(TZP) single-point energy computations on the triplet electronic states of $ArV^+(H_2O)$ at the $^5A_1$ CCSD(T)/Wf(TZP) optimized geometry gave two $^3B_2$ and two $^3B_1$ states in a range of 29.0 to 33.3 kcal mol^{-1}. Therefore, triplet electronic states of $ArV^+(H_2O)$ were not considered further.

The dissociation energy profile with respect to Ar-V distance of $ArV^+(H_2O)$ for various levels of theory is presented in Figure 3.3. The striking feature of Figure 3.3 is

that electron correlation is required to gain any significant binding of Ar to $V^+(H_2O)$, even though the basic nature of the attraction is "electrostatic". While Figure 3.3 explicitly shows only the $^5A_1$ potential curves, the curves for the other states are nearly identical. At the ROHF/Wf(TZP) level, the equilibrium Ar-V bond is extremely large (> 4 Å) for all four states. With ROHF/QZVPP there is a double minimum for all four studied states of $ArV^+(H_2O)$. Geometrical structures are reported for both minima in Table 3.5, and the one with shorter Ar-V distance is consistently designated min 1. In Tables 3.2 and 3.6 relative energies and dissociation energies are reported for the lower-energy minimum only (min 1 for $^5B_1$; min 2 for $^5A_1$, $^5A_2$, and $^5B_2$). Minima designated as min 2 are no longer present when correlation is introduced at the CCSD level.

When argon is added to the $V^+(H_2O)$ complex, the ordering of the lowest-lying states changes, even though Ar would generally be considered a spectator atom. At the ROHF level of theory, no reordering of states is seen due to the large Ar-V distance; the $^5A_1$ state is the lowest energetically (Table 3.2). However, the $^5B_1$ state is predicted to be the ground electronic state of $ArV^+(H_2O)$ for correlated methods, except in the CCSD/Wf(TZP) case, where $^5A_1$ is a mere 0.01 kcal mol^{-1} below $^5B_1$. Our best level of theory [CCSD(T)/QZVPP] gives a $^5A_1 - {}^5B_1$ separation of T_e = 0.49 kcal mol^{-1}, and the $^5A_2$ state is predicted to be only slightly higher (T_e = 0.62 kcal mol^{-1}).

The CCSD(T)/QZVPP argon-vanadium distance for the $^5B_1$ ground state (2.538 Å) differs by less than 0.008 Å from the corresponding distances for the other three states (Table 3.5). In general, the Ar-V distance for all four states gets smaller as correlation is added to the system. The CCSD(T)/QZVPP vanadium-oxygen distance varies from 2.039 Å ($^5B_1$) to 2.096 Å ($^5B_2$), the O-H distance is predicted to be 0.963 Å

for the ground state and 0.962 Å for the $^5A_1$, $^5A_2$ and $^5B_2$ states, and the H-O-H angle ranges from 105.99º ($^5B_2$) to 106.62º ($^5B_1$). The r(V-O) contraction in $ArV^+(H_2O)$ with improvements in both the basis set and treatment of electron correlation is not as large as in the untagged ion. The contraction of the V-O distance from ROHF/Wf(TZP) to CCSD(T)/QZVPP is between ~0.08 Å ($^5A_1$, $^5A_2$) and ~0.14 Å ($^5B_1$, $^5B_2$). Our best CCSD(T)/QZVPP prediction for r(V-O) of the $^5B_1$ ground state is 2.039 Å.

Comparison of data in Tables 3.3 and 3.5 reveals the effect of argon tagging in the geometric structure of $V^+(H_2O)$. Forming the Ar adduct while maintaining the electronic state as $^5A_1$ shifts r(V-O), r(O-H), and θ(H-O-H) by +0.0206 Å, –0.0007 Å, and –0.39º, respectively, at the CCSD(T)/QZVPP level. However, argon addition changes the ground electronic state to $^5B_1$, and if this state switching is considered, the tagging effect [CCSD(T)/QZVPP] on r(V-O), r(O-H), and θ(H-O-H) is –0.0105 Å, +0.0003 Å, and –0.14º, respectively, or roughly half as much. In brief, intricacies are encountered upon argon tagging, but the overall structural shifts can certainly be categorized as small perturbations.

Argon binding energies for various levels of theory for both the $^5B_1$ and $^5A_1$ states of $ArV^+(H_2O)$ are contained in Table 3.6. The dissociation energy (D_e) of the $ArV^+(H_2O)$ $^5B_1$ ground state, corresponding to fragmentation into Ar (^1S) and the $^5A_1$ ground state of $V^+(H_2O)$, is computed to be 9.9 kcal mol^{-1} at the CCSD(T)/ QZVPP level of theory. While with correlated methods the $^5A_1$ – $^5B_1$ separation for $ArV^+(H_2O)$ is smaller than 0.5 kcal mol^{-1}, at the ROHF level of theory it is larger than 4 kcal mol^{-1} in favor of the $^5A_1$ state due to the very weak Ar-V bond (Ar-V equilibrium bond length > 4 Å). This explains the negative ROHF energies for the process $^5B_1$ $ArV^+(H_2O) \rightarrow Ar(^1S) + {}^5A_1$

$V^+(H_2O)$. The argon binding energy of each of the states of $ArV^+(H_2O)$ gets larger as the basis set is enlarged and the electron correlation treatment improved, which is consonant with the shrinking Ar-V distance. It is striking that without correlation the binding energy is less than 1 kcal mol^{-1}, whereas the final D_e (9.9 kcal mol^{-1}) is quite large for an ion-quadrupole complex.

The $ArV^+(H_2O)$ complex is further characterized by the harmonic vibrational frequencies in Table 3.7. The new modes formed by addition of the Ar atom all have frequencies (ω_4, ω_6, ω_9) substantially less than 200 cm^{-1}. The CCSD/Wf(TZP) frequencies allow quantification of argon tagging shifts when the $^5A_1$ electronic state is retained. The O-H bond stretches in the H_2O moiety are both shifted +10 cm^{-1} in going from $^5A_1$ $V^+(H_2O)$ to $^5A_1$ $ArV^+(H_2O)$, with an attendant reduction in the H_2O scissoring frequency by less than 2 cm^{-1}. The interfragment V-O stretch, H_2O wag, and H_2O rock are all reduced in frequency by about 10 cm^{-1}. Vibrational anharmonicity (Table 3.8) does not appreciably affect any of the argon tagging shifts, provided the $^5A_1$ state is maintained.

The change in the ground state to $^5B_1$ upon argon complexation has some significant consequences, as shown in the CCSD(T)/QZVPP frequencies of $V^+(H_2O)$ and $ArV^+(H_2O)$. First, the H_2O modes are now all shifted by about –5 cm^{-1} (opposite direction) due to the presence of argon. The interfragment V-O stretch and H_2O rock now exhibit larger tagging effects of –16 cm^{-1} and +79 cm^{-1}, respectively. Finally, the H_2O wag appears to be strongly influenced by vibronic interactions with the nearby quintic electronic states, as promoted by Ar addition. In fact, we were only able to determine b_1 vibrational frequencies for $^5B_1$ $ArV^+(H_2O)$ at the CCSD(T)/Wf(TZP) level, because

insuperable convergence difficulties were encountered in searching for $^5B_1$ electronic solutions along these modes with the QZVPP basis. This issue is addressed in more detail in the following section (III.C).

3.6 VIBRATIONAL ANHARMONICITY EFFECTS

The computation of the non-totally-symmetric vibrational frequencies of $V^+(H_2O)$ and $ArV^+(H_2O)$ requires extreme care due to the intricate vibronic interactions within the lowest-lying manifold of quintet states precipitated when the equilibrium C_{2v} symmetry is lowered. Nonetheless, complete vibrational analyses of the $^5A_1$ ground state of $V^+(H_2O)$ and its $^5A_1$ counterpart in $ArV^+(H_2O)$ were executed here without severe difficulties. The principal problem we encountered involved the b_1 vibrational modes of the $^5B_1$ state of $ArV^+(H_2O)$. The $^5B_1$ state is the ground state of $ArV^+(H_2O)$ at the CCSD(T)/Wf(TZP), CCSD/QZVPP, and CCSD(T)/QZVPP levels of theory; however, the $^5A_1$ state is lower in energy for the ROHF reference wave function. Because the $^5B_1$ and $^5A_1$ states retain their V^+ atomic character in $ArV^+(H_2O)$, we were able (with much care) to continuously follow the $^5B_1$ ROHF solutions into C_s and C_1 regions where the ($^5B_1$, $^5A_1$) pair is of the same spatial symmetry. Accordingly, a complete and mathematically correct numerical differentiation of the potential energy surface of the $^5B_1$ state of $ArV^+(H_2O)$ was achieved through quartic terms, despite loss of the variational principle for the b_1 modes. The resulting CCSD(T)/Wf(TZP) anharmonic force field for $^5B_1$ $ArV^+(H_2O)$ is given as Supplementary Material (Table 3.S1). A number of intriguing cubic and quartic constants are exhibited that are anomalously large in magnitude, all involving the b_1 modes (S_4 and S_8). Many of these anomalous force constants also involve the a_1 V-O stretching

coordinate, which appears to exacerbate the problem. The probable origin of this phenomenon is seen in Figures 3.4 and 3.5, where the potential curves vs. r(V-O) for the lowest-lying quintet states of $ArV^+(H_2O)$ exhibit crossings very near the equilibrium distance. In the full geometric configuration space, conical intersections of the quintet potential energy surfaces are thus present in the vicinity of the equilibrium structures, giving rise to near singularities in the $^5B_1$ force field expansion for $ArV^+(H_2O)$.

In Tables 3.9 and 3.10, the Wf(TZP) CCSD and CCSD(T) quartic force fields are given for the $^5A_1$ ground state of $V^+(H_2O)$, along with the CCSD/Wf(TZP) force field for the analogous $^5A_1$ state of $ArV^+(H_2O)$. For comparison, the Wf(TZP) CCSD and CCSD(T) quartic force fields of free H_2O are given in Table 3.11. As shown in Tables 3.9 and 3.10, no anomalous force constants occur for $ArV^+(H_2O)$ in the $^5A_1$ state, in contrast to its close-lying $^5B_1$ counterpart. Therefore, our analysis of vibrational anharmonicity in the $V^+(H_2O)$ and $ArV^+(H_2O)$ species centers on the $^5A_1$ electronic state throughout. The issues of concern here can be addressed via a VPT2 treatment based on quartic force fields, although it must be recognized that a rigorous analysis would entail a detailed variational treatment of nonadiabatic vibrational phenomena. In essence, we focus here on inherent (adiabatic) anharmonic vibrational effects unspoiled by vibronic coupling within the manifold of low-lying quintet electronic states.

As previously introduced, the VPT2 anharmonicities and rovibration interaction constants of $ArV^+(H_2O)$, $V^+(H_2O)$, and free H_2O are compared in Table 3.8, at a common level of theory [CCSD/Wf(TZP)]. Corresponding results for five sets of isotopic derivatives of these species are given in Supplementary Tables 3.S2-3.S5. Finally, CCSD(T)/Wf(TZP) anharmonicities for $V^+(H_2O)$ and H_2O are provided in

Supplementary Table 3.S6. We investigated the influence of a number of potential anharmonic resonances on the fundamental frequencies of the isotopologs. The exclusion of resonance interactions based on a 20 cm^{-1} cutoff for zeroth-order state separations changed the computed VPT2 anharmonicities by more than 1 cm^{-1} in only one case: the $2\omega_5(H_2O$ wag) – ω_3(V-O stretch) Fermi resonance in $^{40}Ar^{51}V^+(D_2O)$. Thus, in our tabulated results no anharmonic resonances were removed, except for the $2\omega_5-\omega_3$ interaction in $^{40}Ar^{51}V^+(D_2O)$ (Table 3.S2). The ω_6[Ar-V-O lin. bend (b_1)] – ω_9[Ar-V-O lin. bend (b_2)] Coriolis resonance has a strong influence on the α_6^A and α_9^A constants for all $ArV^+(H_2O)$ isotopologs. Exclusion of this interaction from the VPT2 treatment was necessary to obtain valid rovibration interaction constants in all cases, but the overall ZPV shift on the rotational constants is completely invariant to the removal of such Coriolis resonances.

In Table 3.8 the theoretical fundamental frequencies of H_2O lie within a few cm^{-1} of the observed band origins, ν_1 = 3657.1, ν_2 = 1594.7, and ν_3 = 3755.9 cm^{-1}.[76,77] Thus, the CCSD/Wf(TZP) method is providing a particularly advantageous cancellation of errors in the electronic structure treatment. The CCSD/Wf(TZP) O-H stretching anharmonicities are equally well matched with experiment (Δ_1 = –173 cm^{-1}, Δ_3 = –185 cm^{-1}),[78-80] whereas the computed anharmonicity for the H_2O scissor is about 12 cm^{-1} smaller in magnitude than the empirically derived value (Δ_2 = –55 cm^{-1}).[78-80]

Formation of the $V^+(H_2O)$ complex increases the magnitude of the O-H stretching anharmonicities by 5-8 cm^{-1}, while leaving the scissoring anharmonicity unaffected. The interfragment V-O stretching and H_2O rocking modes of $V^+(H_2O)$ have small anharmonicities of –11 cm^{-1} and –3 cm^{-1}, respectively. In contrast, the H_2O wag has an

enormous anharmonicity in the positive direction (Δ_4 = +120 cm^{-1}), displaying strong characteristics of a quartic oscillator.

Argon tagging (without electronic state switching) has remarkably little effect (1.3 cm^{-1} on average) on the vibrational anharmonicities of $V^+(H_2O)$, including the large positive value for the H_2O wag. The anharmonicity of the newly formed Ar-V stretching mode is only –7.5 cm^{-1}. On the other hand, the Ar-V-O linear bends $\nu_6(b_1)$ and $\nu_9(b_2)$ have proportionately large anharmonicities of +21.7 and +10.0 cm^{-1}, respectively. These sizable, positive values can be directly traced to the large rotational A_e constant of the $ArV^+(H_2O)$ adduct and the associated Coriolis contributions [$A_e\left(\zeta_{rs}^a\right)^2\left(\omega_r/\omega_s+\omega_s/\omega_r\right)$] to the off-diagonal χ_{rs} anharmonicity constants.

The rovibration interaction constants (α_i) are of particular interest here, because they allow a determination of zero-point vibrational effects on the geometric structures of $V^+(H_2O)$ and $ArV^+(H_2O)$. As shown in Table 3.8, the binding of vanadium cation to water has dramatic effects on the α_i constants of the H_2O vibrational modes. In contrast, further argon tagging of $V^+(H_2O)$ has no significant effect, particularly for the all-important α_i^A constants. For the α_i^B and α_i^C parameters, argon complexation merely reduces the magnitude of these already-small rovibration interaction constants.

A key question is whether some of the disparity between the water bond angle widening in $V^+(H_2O)$ theoretically predicted here (2°-3°) and that surmised from the IRPD experiments in the Duncan laboratory[12] (9.3°) can be attributed to zero-point vibrational effects on the effective geometric structure. In the equilibrium structures of $V^+(H_2O)$ and $ArV^+(H_2O)$, only the light hydrogen atoms contribute to the A rotational constants; however, vibrational motion along the b_1 and b_2 modes displaces the massive

vanadium and/or argon atoms off the *a* principal axis, potentially increasing the effective I_A moment of inertia by a substantial amount. To investigate this effect, we used our CCSD/Wf(TZP) α_i constants to synthesize (A_0, B_0, C_0) rotational constants for several isotopologs of $V^+(H_2O)$ and $ArV^+(H_2O)$ and then to extract vibrationally averaged r_0 structures by least-squares fits. The molecular structure refinements were performed using a robust computer program MolStruct recently developed by one of us.[81] The following $V^+(H_2O)$ isotopologs were employed in the least-squares refinment: (^{51}V, ^{16}O, H, H), (^{51}V, ^{18}O, H, H), (^{51}V, ^{16}O, D, D), and (^{50}V, ^{16}O, H, H). For $ArV^+(H_2O)$, the same isotopologs were used with ^{40}Ar included, and one more isotopolog was added: (^{36}Ar, ^{51}V, O, H, H). All the necessary rovibration interaction constants appear in Table 3.8 and Supplementary Tables 3.S2-3.S5. Our best CCSD(T)/QZVPP equilibrium geometries were employed as reference structures for the determination of $r_e - r_0$ shifts. We found that the standard errors of the r_0 fits were significantly reduced by excluding the A_0 rotational constants from the refinements, so unless otherwise stated, only the much smaller (B_0, C_0) values were included in the MolStruct data set.

Our vibrationally-averaged structural parameters for the $^5A_1$ state of $V^+(H_2O)$ differ from the equilibrium structural parameters by the following amounts: θ_0(H-O-H) − θ_e(H-O-H) = +2.35°, r_0(O-H) − r_e(O-H) = +0.0025 Å, and r_0(V-O) − r_e(V-O) = +0.0066 Å. If the A_0 rotational constants are included in the refinement, then θ_0(H-O-H) − θ_e(H-O-H) = +1.82°, r_0(O-H) − r_e(O-H) = −0.0018 Å, and r_0(V-O) − r_e(V-O) = +0.0066 Å, still showing a substantial angle expansion. If the interfragment modes of $V^+(H_2O)$ are excluded from the vibrational averaging by omitting all α_3, α_4, and α_6 constants, then θ_0(H-O-H) − θ_e(H-O-H) = +0.40°, and r_0(O-H) − r_e(O-H) = +0.0146 Å.

Császár and co-workers[82] have very recently published effective rotational constants (A_0, B_0, C_0) of water isotopologs arising from variational vibrational computations on the near spectroscopic quality, empirically adjusted CVRQD potential energy surface.[83] Applying our MolStruct procedure to these (A_0, B_0, C_0) rotational constants yields the following shifts for free H_2O from the highly accurate CVRQD water surface: r_0(O-H) − r_e(O-H) = +0.0025 Å and θ_0(H-O-H) − θ_e(H-O-H) = +0.69°. An analogous refinement using our Wf(TZP) CCSD α_i constants for free water instead of the CVRQD vibrational corrections of Ref. 82 gives r_0(O-H) − r_e(O-H) = +0.0029 Å and θ_0(H-O-H) − θ_e(H-O-H) = +0.64°. Finally, for the $^5A_1$ state of $ArV^+(H_2O)$ we find θ_0(H-O-H) − θ_e(H-O-H) = 2.08°, r_0(O-H) − r_e(O-H) = −0.007 Å, r_0(V-O) − r_e(V-O) = +0.005 Å, and r_0(Ar-V) − r_e(Ar-V) = +0.011 Å .

The primary conclusions to be derived from our r_0 structural data are: (1) the results for free H_2O indicate the validity of performing MolStruct r_0 fits based on Wf(TZP) CCSD rovibration interaction constants; (2) zero-point vibrational averaging in $V^+(H_2O)$ widens the H-O-H bond angle by 2.4°, and argon tagging reduces this shift by about +0.3°; (3) most of the ZPV effect on the H-O-H angle is due to off-axis motions of the massive V atom, rather than flattening of the potential energy curve for H_2O bending due to complexation with the vanadium cation; (4) adding the computed effects of vibrational averaging to our best equilibrium structures [CCSD(T)/QZVPP] for the ground states of $V^+(H_2O)$ and $ArV^+(H_2O)$ gives θ_0(H-O-H) angles of 109.1° and 108.7°, respectively. The H_2O bond angle value derived from the IRPD experiments (113.8°)[12] is still about 5° higher than predicted by our high-level theoretical analysis; however, consideration of zero-point vibrational effects has lowered this disparity by 2°-3°. The

remaining discrepancy is evident by directly comparing our best purely theoretical A_0 rotational constants for the $^5A_1$ states of $V^+(H_2O)$ and $ArV^+(H_2O)$ (13.70 cm^{-1} and 13.65 cm^{-1}, respectively) with the significantly smaller IRPD value (12.52 cm^{-1}).[12]

3.7 CONCLUSIONS

The model systems $V^+(H_2O)$ and $ArV^+(H_2O)$, exemplary of mass-selected infrared photodissociation (IRPD) spectroscopy on hydrated metal cations, have been thoroughly investigated by high-level electronic structure theory. Our best predictions are based on restricted open-shell CCSD(T) theory implemented with a massive V[11*s*6*p*5*d*3*f*2*g*], Ar[9*s*6*p*4*d*2*f*1*g*], O[6*s*5*p*4*d*3*f*2*g*], and H[5*s*4*p*3*d*2*f*] (QZVPP) basis set, and with the outer-core V(3*s*,3*p*) electrons correlated. The microsolvation of V^+ with one water molecule gives an equilibrium V-O distance of 2.049 Å and a binding energy (D_0) of 36.2 kcal mol^{-1}. Formation of the $V^+(H_2O)$ complex shifts the H_2O fundamentals (ν_1, ν_2, ν_3) by (–43, +26, –72) cm^{-1}. Our computed red shifts for the O-H stretching modes (ν_1, ν_3) are in excellent agreement with the IRPD results (~50, ~70) cm^{-1} from the Duncan laboratory.[12] When H_2O binds to V^+, the H-O-H equilibrium bond angle widens by +2.4°, with a concomitant increase in the O-H distance of +0.004 Å. The H_2O molecule splits the degenerate ground-state manifold of $V^+(^5D)$, yielding electronic states in C_{2v} symmetry with the following relative energies: $T_e(^5A_1,^5A_2,^5B_1,^5B_2)$ = (0, 0.15, 0.37, 5.09) kcal mol^{-1}. A second $^5A_1$ state of $V^+(H_2O)$ appears somewhat higher in energy, and the lowest-lying triplet state is more than 15 kcal mol^{-1} above the ground $^5A_1$ state.

Argon tagging of $V^+(H_2O)$ places the Ar atom 2.538 Å from the V^+ center and 180° removed from the H_2O ligand, in accord with simple expectation for an electrostatic

complex. The argon binding energy is D_0 [Ar - $V^+(H_2O)$] = 9.4 kcal mol^{-1}. Surprisingly, virtually all of this binding energy is attributable to electron correlation effects, in that Hartree-Fock theory yields only a 0.25 kcal mol^{-1} stabilization even with the large QZVPP basis set. Argon tagging engenders only small perturbations in the $V^+(H_2O)$ structure: δr_e(V-O) = –0.0105 Å, δr_e(O-H) = +0.0003 Å, and $\delta\theta_e$(H-O-H) = –0.14°. However, the Ar "spectator" is responsible for a number of subtle effects, such as switching the electronic ground state. For $ArV^+(H_2O)$ our best theory predicts a $^5B_1$ ground state and excitation energies $T_e(^5A_1,^5A_2,^5B_2)$ = (0.49, 0.62, 4.17) kcal mol^{-1}. Argon tagging shifts the vibrational frequencies of $V^+(H_2O)$ by no more than 10 cm^{-1}, but the direction of the shift is in most cases dependent on whether the final electronic state in question is $^5A_1$ or $^5B_1$.

An analysis of vibrational anharmonicity effects in $V^+(H_2O)$ and $ArV^+(H_2O)$ has been executed by computing complete quartic force fields and then applying second-order vibrational perturbation theory (VPT2) to determine anharmonic constants and rovibration interaction constants. This approach probes inherent anharmonic vibrational properties of single electronic states in these species. Rigorous variational computations of the vibronic coupling in these systems is not currently practical. For free H_2O our quartic force fields reproduce the observed O-H stretching fundamentals to within 5 cm^{-1}, bolstering confidence in our analogous results for $V^+(H_2O)$ and $ArV^+(H_2O)$. Our rovibration interaction constants allow quantification of the influence of zero-point vibrational (ZPV) averaging on the molecular structures of $V^+(H_2O)$ and $ArV^+(H_2O)$. A peculiar phenomenon is observed for the *effective* bond angle θ_0(H-O-H), specifically, a ZPV increase of 2°-3° as a consequence of off-axis motion of the heavy vanadium atom,

as opposed to flattening and/or skewing of the water bending potential. Nonetheless, the total complexation effect on the water bond angle computed here (about +4°) is substantially less than the 9° widening surmised from the IRPD experiments.[12] Thermal averaging over excited vibrational states in the $V^+(H_2O)$ and $ArV^+(H_2O)$ complexes might increase the effective H-O-H angle more and further reduce the disparity between theory and experiment. However, it is clear that the interpretation of geometric parameters extracted from IRPD profiles is complicated by numerous effects, and thus care must be taken in equating effective bond angle widening with changes in electronic structure upon complexation.

A number of issues of theoretical interest were encountered in our study of $V^+(H_2O)$ and $ArV^+(H_2O)$: (1) The $V^+(H_2O)$ binding energy appears to be very sensitive to vanadium (3*s*,3*p*) core electron correlation. (2) There is large quartic anharmonicity in the H_2O wagging mode in $V^+(H_2O)$ and $ArV^+(H_2O)$. (3) Curve crossings within the lowest-lying quintet manifold of $ArV^+(H_2O)$ occur near the equilibrium geometry, giving rise to anomalous force constants in the local representations of the potential energy surfaces of some of the electronic states. These crossings arise along the Ar-V stretching mode, and thus are precipitated by the presence of the argon "spectator" atom. (4) Finally, the intricate vibronic coupling within the $({}^5A_1,{}^5A_2,{}^5B_1,{}^5B_2)$ manifold of $V^+(H_2O)$ and $ArV^+(H_2O)$ remains unexplored. All of these issues would be worthy targets of future investigations.

3.8 ACKNONWLEDGEMENTS

This research project was supported by the U.S. National Science Foundation, grant number CHE-0451445 and the U.S. Department of Energy, grant number DE-FG02-96ER14658.

3.9 REFERENCES

[1] K. F. Willey, C. S. Yeh, D. L. Robbins, J. S. Pilgrim, and M. A. Duncan, J. Chem. Phys. **97**, 8886 (1992).

[2] C. T. Scurlock, S. H. Pullins, J. E. Reddic, and M. A. Duncan, J. Chem. Phys. **104**, 4591 (1996).

[3] M. A. Duncan, Annu. Rev. Phys. Chem. **48**, 69 (1997).

[4] J. M. Lisy, Int. Rev. Phys. Chem. **16**, 267 (1997).

[5] O. M. Cabarcos, C. J. Weinheimer, and J. M. Lisy, J. Chem. Phys. **108**, 5151 (1998).

[6] O. M. Cabarcos, C. J. Weinheimer, and J. M. Lisy, J. Chem. Phys. **110**, 8429 (1999).

[7] T. D. Vaden, B. Forinash, and J. M. Lisy, J. Chem. Phys. **117**, 4628 (2002).

[8] G. Gregoire and M. A. Duncan, J. Chem. Phys. **117**, 2120 (2002).

[9] D. van Heijnsbergen, G. von Helden, G. Meijer, P. Maitre, and M. A. Duncan, J. Am. Chem. Soc. **124**, 1562 (2002).

[10] R. S. Walters, T. Jaeger, and M. A. Duncan, J. Phys. Chem. A **106**, 10482 (2002).

[11] M. A. Duncan, Int. Rev. Phys. Chem. **22**, 407 (2003).

[12] N. R. Walker, R. S. Walters, E. D. Pillai, and M. A. Duncan, J. Chem. Phys. **119**, 10471 (2003). Note: The basis set used for the DFT computations in this reference was 6-31G*; due to a typographical error, the basis set is reported as 3-31G* therein.

[13] R. S. Walters and M. A. Duncan, Aust. J. Chem. **57**, 1145 (2003).

[14] T. Jaeger, E. D. Pillai, and M. A. Duncan, J. Phys. Chem. A **108**, 6605 (2004).

[15] N. R. Walker, R. S. Walters, and M. A. Duncan, J. Chem. Phys. **120**, 10037 (2004).

[16] N. R. Walker, R. S. Walters, G. A. Grieves, and M. A. Duncan, J. Chem. Phys. **121**, 10498 (2004).

[17] Y. Inokuchi, K. Ohshimo, F. Misaizu, and N. Nishi, J. Phys. Chem. **108**, 5034 (2004).

[18] Y. Inokuchi, K. Ohshimo, F. Misaizu, and N. Nishi, Chem. Phys. Lett. **390**, 140 (2004).

[19] N. R. Walker, R. S. Walters, M.-K. Tsai, K. D. Jordan, and M. A. Duncan, J. Phys. Chem. A **109**, 7057 (2005).

[20] R. S. Walters, E. D. Pillai, and M. A. Duncan, J. Am. Chem. Soc. **127**, 16599 (2005).

[21] Organomettalic Ion Chemistry, edited by B. S. Freiser (Kluwer, Dordrecht, 1996) (1006).

[22] T. F. Magnera, D. E. David, and J. Michl, J. Am. Chem. Soc. **111**, 4100 (1989).

[23] P. J. Marinelli and R. R. Squires, J. Am. Chem. Soc. **111**, 4101 (1989).

[24] D. E. Clemmer, Y.-M. Chen, N. Aristov, and P. B. Armentrout, J. Phys. Chem. **98**, 7538 (1994).

[25] N. F. Dalleska, K. Honma, L. S. Sunderlin, and P. B. Armentrout, J. Am. Chem. Soc. **116**, 3519 (1994).

[26] Gas Phase Metal Ion Chemistry, edited by J. A. Leary and P. B. Armentrout, special issue of Int. J. Mass. Spectrom. **204**, 1 (2001).

[27] M. A. Duncan, Adv. Met. Semicond. Clusters **5** (2002).

[28] P. B. Armentrout, Int. J. Mass. Spectrom. **227**, 289 (2003).

[29] D. E. Lessen, R. L. Asher, and P. J. Brucat, J. Chem. Phys. **93**, 6102 (1990).

[30] D. Schröder, M. Engeser, H. Schwarz, and J. N. Harvey, CHEMPHYSCHEM **3**, 584 (2002).

[31] M. Rosi and C. W. Bauschlicher, Jr., J. Chem. Phys. **90**, 7264 (1989).

[32] M. Rosi and C. W. Bauschlicher, Jr., J. Chem. Phys. **92**, 1876 (1990).

[33] E. Magnusson and N. W. Moriarty, J. Comp. Chem. **14**, 961 (1993).

[34] M. Trachtman, G. D. Markham, J. P. Glusker, P. George, and C. W. Bock, Inorg. Chem. **37**, 4421 (1998).

[35] A. Irigoras, J. E. Fowler, and J. M. Ugalde, J. Am. Chem. Soc. **121**, 574 (1999).

[36] S. J. Klippenstein and C.-N. Yang, International Journal of Mass Spectrometry **201**, 253 (2000).

[37] R. C. Dunbar, J. Phys. Chem. A **106**, 7328 (2002).

[38] W. J. Hehre, L. Radom, P. v. R. Schleyer, and J. A. Pople, Ab initio Molecular Orbital Theory (Wiley-Interscience, New York, 1986).

[39] A. Szabo and N. S. Ostlund, Modern Quantum Chemistry: Introduction to Advanced Electronic Structure Theory, 1st ed. revised (McGraw-Hill, New York, 1989).

[40] C. C. J. Roothaan, Rev. Mod. Phys. **23**, 69 (1951).

[41] J. A. Pople and R. K. Nesbet, J. Chem. Phys. **22**, 571 (1954).

[42] P. J. Knowles, C. Hampel, and H.-J. Werner, J. Chem. Phys. **99**, 5219 (1993).

[43] J. D. Watts, J. Gauss, and R. J. Bartlett, J. Chem. Phys. **98**, 8718 (1993).

[44] P. J. Knowles and H.-J. Werner, Chem. Phys. Lett. **115**, 259 (1985).

[45] H.-J. Werner and P. J. Knowles, J. Chem. Phys. **82**, 5053 (1985).

[46] A. J. H. Wachters, J. Chem. Phys. **52**, 1033 (1970).

[47] Basis sets were obtained from the Extensible Computational Chemistry Environment Basis Set Database, Version 02/25/04, as developed and distributed by the Molecular Science Computing Facility, Environmental and Molecular Sciences Laboratory which is part of the Pacific Northwest Laboratory, P.O. Box 999, Richland, Washington 99352, USA, and funded by the U.S. Department of Energy. The Pacific Northwest Laboratory is a multi-program laboratory operated by Battelle Memorial Institute for the U.S. Department of Energy under contract DE-AC06-76RLO 1830. Contact Karen Schuchardt for further information.

[48] P. J. Hay, J. Chem. Phys. **66**, 4377 (1977).

[49] C. W. J. Bauschlicher, S. R. Langhoff, and L. A. Barnes, J. Chem. Phys. **91**, 2399 (1989).

[50] T. H. Dunning, Jr., J. Chem. Phys. **55**, 716 (1971).

[51] A. Schäfer, C. Huber, and R. Ahlrichs, J. Chem. Phys. **100**, 5829 (1994).

[52] A. Schäfer, H. Horn, and R. Ahlrichs, J. Chem. Phys. **97**, 2571 (1992).

[53] F. Weigend, F. Furche, and R. Ahlrichs, J. Chem. Phys. **119**, 12753 (2003).

[54] T. H. Dunning, Jr., J. Chem. Phys. **90**, 1007 (1989).

[55] R. A. Kendall, T. H. Dunning, and R. J. Harrison, J. Chem. Phys. **96**, 6796 (1992).

[56] D. Papoušek and M. R. Aliev, Molecular Vibrational-Rotational Spectra (Elsevier, Amsterdam, 1982).

[57] J. K. G. Watson, in Vibrational Spectra and Structure, edited by J. R. Durig (Elsevier, Amsterdam, 1997), Vol. 6, p.1.

[58] H. H. Nielsen, Rev. Mod. Phys. **23**, 90 (1951).

[59] D. A. Clabo Jr., W. D. Allen, R. B. Remington, Y. Yamaguchi, and H. F. Schaefer III, Chem. Phys. **123**, 187 (1988).

[60] W. D. Allen, Y. Yamaguchi, A. G. Császár, D. A. Clabo Jr., R. B. Remington, and H. F. Schaefer III, Chem. Phys. **145**, 427 (1990).

[61] INTDIF2004 is an abstract program developed by Wesley D. Allen for use within Mathematica (Wolfram Research Inc., Champaign, Illinois) to perform high-order numerical differentiations of electronic structure data.

[62] R. L. DeKock, M. J. McGuire, P. Piecuch, W. D. Allen, H. F. Schaefer III, K. Kowalski, S. A. Kucharski, M. Musial, A. R. Bonner, S. A. Spronk, D. B. Lawson, and S. L. Laursen, J. Phys. Chem. A. **108**, 2893 (2004).

[63] INTDER2000 is a general program developed by Wesley D. Allen and co-workers which performs various vibrational analyses and higher-order nonlinear transformations among force field representations.

[64] W. D. Allen and A. G. Császár, J. Chem. Phys. **98**, 2983 (1993).

[65] W. D. Allen, A. G. Császár, V. Szalay, and I. M. Mills, Mol. Phys. **89**, 1213 (1996).

[66] See program descriptions in K. Sarka and J. Demaison in Computational Molecular Spectroscopy, edited by P. Jensen and P. R. Bunker (Wiley, Chichester, 2000), pp. 255-303.

[67] ANHARM is a FORTRAN program written for VPT2 analyses by Yukio Yamaguchi and Henry F. Schaefer (Center for Computational Quantum Chemistry, University of Georgia, Athens, GA 30602, USA).

[68] J. F. Stanton, J. Gauss, J. D. Watts, M. Nooijen, N. Oliphant, S. A. Perera, P. G. Szalay, W. J. Lauderdale, S. A. Kucharski, S. R. Gwaltney, S. Beck, A. Balková, D.

E. Bernholdt, K. K. Baeck, P. Rozyczko, H. Sekino, C. Hober, and R. J. Bartlett, Integral packages included are VMOL (J. Almlöf and P.R. Taylor); VPROPS (P. Taylor) ABACUS; (T. Helgaker, H.J. Aa. Jensen, P. Jørgensen, J. Olsen, and P.R. Taylor).

[69] H.-J. Werner, P. J. Knowles, M. Schütz, R. Lindh, P. Celani, T. Korona, G. Rauhut, F. R. Manby, R. D. Amos, A. Bernhardsson, A. Berning, D. L. Cooper, M. J. O. Deegan, A. J. Dobbyn, F. Eckert, C. Hampel, G. Hetzer, A. W. Lloyd, S. J. McNicholas, W. Meyer, M. E. Mura, A. Nicklaß, P. Palmieri, R. Pitzer, U. Schumann, H. Stoll, A. J. Stone, R. Tarroni, and T. Thorsteinsson.

[70] K. Balasubramanian, *Relativistic Effects in Chemistry: Part A, Theory and Techniques* (Wiley, New York, 1997).

[71] K. Balasubramanian, *Relativistic Effects in Chemistry: Part B, Applications* (Wiley, New York, 1997).

[72] R. D. Cowan and D. C. Griffin, J. Opt. Soc. Am. **66**, 1010 (1976).

[73] S. A. Perera and R. J. Bartlett, Chem. Phys. Lett. **252**, 425 (1993).

[74] G. Tarczay, A. G. Császár, W. Klopper, and H. M. Quiney, Mol. Phys. **99**, 1769 (2001).

[75] C. E. Moore, Atomic Energy Levels, Volume 1 (Circular of the National Bureau of Standards 467, Issued June 15, 1949).

[76] L. A. Pugh and K. Narahari Rao, J. Mol. Spectrosc. **47**, 403 (1973).

[77] C. Camy-Peyret, J.-M. Flaud, J.-P. Maillard, and G. Guelachvili, Mol. Phys. **33**, 1641 (1977).

[78] W. S. Benedict, N. Gailar, and E. K. Plyler, J. Chem. Phys. **24**, 1139 (1956).

[79] J. Plíva, V. Špirko, and D. Papoušek, J. Mol. Spectrosc. **23**, 331 (1967).

[80] A. G. Császár and I. M. Mills, Spectrochim. Acta **53A**, 1101 (1997).

[81] MolStruct is an abstract program developed by Wesley D. Allen for use within Mathematica (Wolfram Research Inc., Champaign, Illinois) to perform diverse fits of molecular structures to sets of isotopologic rotational constants.

[82] A. G. Császár, G. Czakó, T. Furtenbacher, J. Tennyson, V. Szalay, S. V. Shirin, N. F. Zobov, and O. L. Polyansky, J. Chem. Phys. **122**, 214305 (2005).

[83] O. L. Polyansky, A. G. Császár, S. V. Shirin, N. F. Zobov, P. Barletta, J. Tennyson, D. W. Schwenke, and P. J. Knowles, Science **299**, 539 (2003).

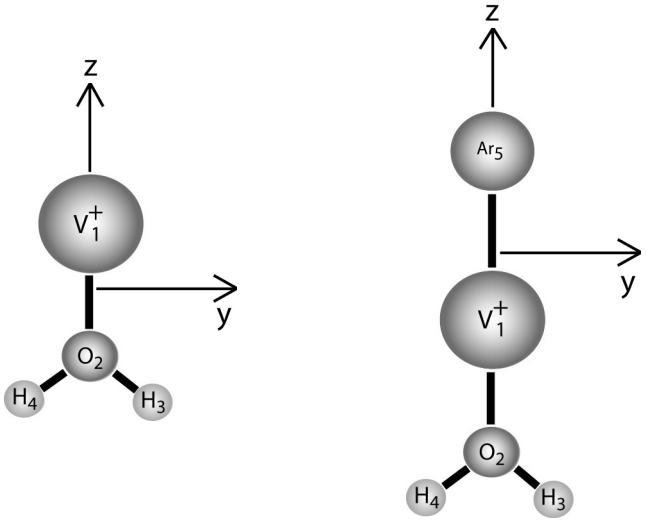

(a) (b)

Figure 3.1: The C_{2v} structures of the (a) $V^+(H_2O)$ and (b) $ArV^+(H_2O)$ complexes.

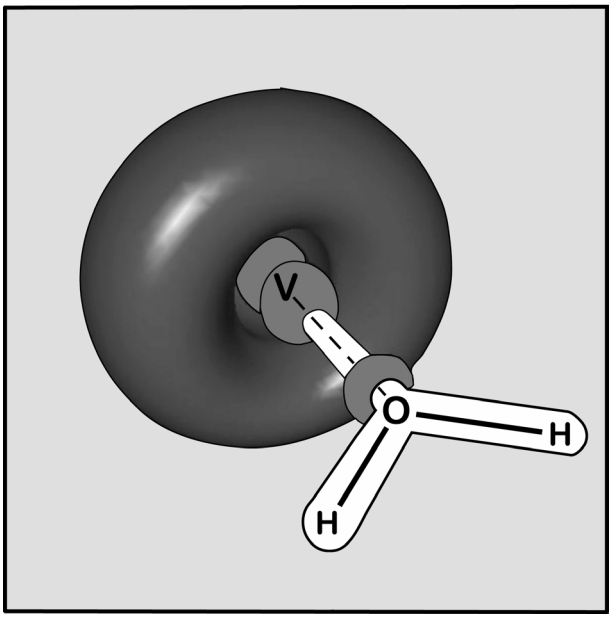

Figure 3.2: The HOMO of the $V^+(H_2O)$ $^5A_1$ ground state.

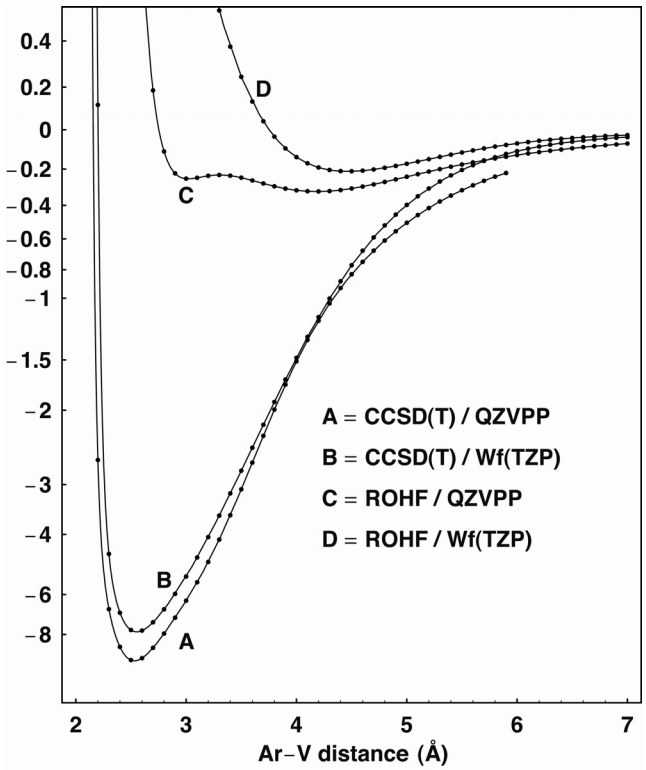

Figure 3.3: Theoretical argon dissociation curves for the $^5A_1$ state of $ArV^+(H_2O)$. In this plot $V^+(H_2O)$ is fixed at its optimum structure for the corresponding level of theory; only the Ar-V distance was changed. Note the nonuniform scale on the energy axis, which is necessary to reveal the shallow ROHF minima.

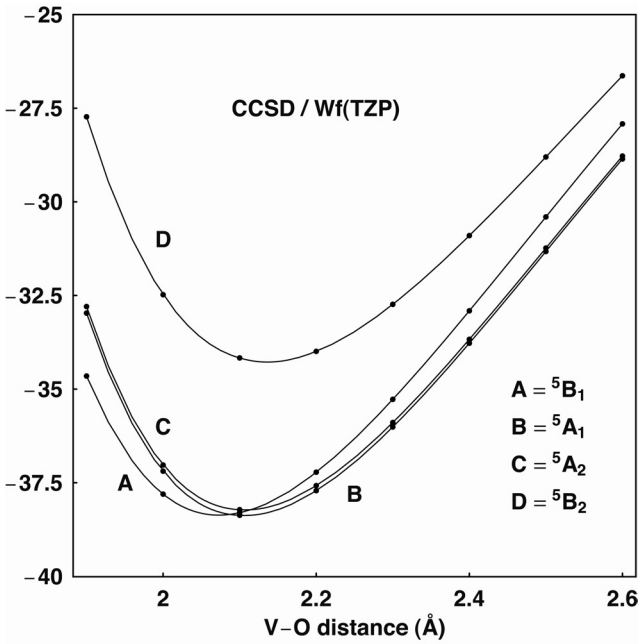

Figure 3.4: Energy versus the V-O distance of four low-lying states of $ArV^+(H_2O)$, relative to dissociation into H_2O plus the $^5A_1$ state of ArV^+, computed at the CCSD / Wf(TZP) level of theory. Constrained optimizations were performed for each plotted V-O distance.

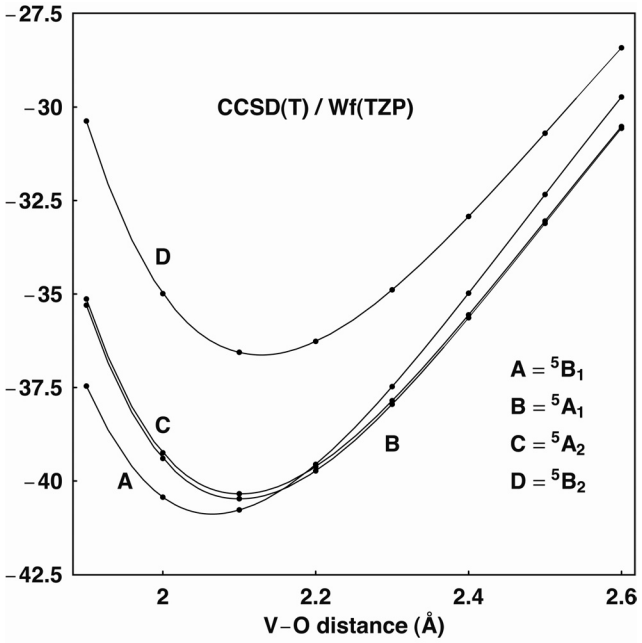

Figure 3.5: Energy versus the V-O distance of four low-lying states of $ArV^+(H_2O)$, relative to dissociation into H_2O plus the $^5A_1$ state of ArV^+, computed at the CCSD(T) / Wf(TZP) level of theory. Constrained optimizations were performed for each plotted V-O distance.

Table 3.1. Dissociation energies for $^5A_1$ state of $V^+(H_2O)$ in kcal mol^{-1}.

Present work	D_e	D_0
ROHF/Wf(TZP)	37.5	35.8
CCSD/Wf(TZP)	38.1	36.4
CCSD(T)/Wf(TZP)	38.5	36.8
ROHF/QZVPP	35.8	34.2
CCSD/QZVPP	37.6	35.8
CCSD(T)/QZVPP	38.0	36.2
Previous theory		
MCPF/Wachters+f TZP[a]	36.4	34.7
MP2/6-311++G**[b]		38.5[m]
CCSD(T)/6-311++G**//MP2/6-311++G**[b]	43.4[m]	
B3LYP/TZVP+G(3df,2p)[c]	38.5	36.62
CCSD(T)/TZVP+G(3df,2p)//B3LYP/TZVP+G(3df,2p)[c, d]	36.7	32.42
B3LYP/B3//B3LYP/B2[e]		38.7
MPW1PW91/6-311+G(d)[f]		35.4
Experiment		
Collision-induced dissociation[g]		36.2±3
Collision-induced dissociation[h]		35.1±4
Photo dissociation spectrum[i]		< 45.4
Collision-induced dissociation[j]		35.8±1.2
mass spectrometry[k]		35.1±1.2

[a] References 31, 32. [b] Reference 34. [c] References 35, 30. [d] B2: 6-31+G* basis for V, 6-31G* basis for O and H; B3: B2 with diffuse *s* and *p* functions added to O. [e] Reference 36. [f] Reference 37. [g] Reference 22. [h] Reference 23. [i] Reference 29. [j] Reference 25. [k] Reference 30. [m] Obtained from attendant supplementary material of Ref. 34; The text of the paper reports $\Delta H^{298} = 41.8$ kcal mol^{-1}.

Table 3.2. Adiabatic excitation energies T_e (T_0) in kcal mol^{-1} within the lowest-lying electronic manifold of $V^+(H_2O)$ and $ArV^+(H_2O)$.

$V^+(H_2O)$	$^5A_1$	$^5A_2$	$^5B_1$	$^5B_2$
Present work				
ROHF/Wf(TZP)	0	0.02 (0.03)	4.30	6.44
CCSD/Wf(TZP)	0	0.19 (0.20)	0.75	4.99
CCSD(T)/Wf(TZP)	0	0.14 (0.16)	0.67	5.45
ROHF/QZVPP	0	0.02 (0.02)	4.27	6.40
CCSD/QZVPP	0	0.25 (0.27)	0.47	4.57
CCSD(T)/QZVPP	0	0.15 (0.16)	0.37	5.09
Previous theory				
MCPF/Wachters+f TZP[a]	0	0.09	6.0	1.5
MP2/6-311++G**[b]	0	0.07	-	-
CCSD(T) 6-311++G**//MP2/6-311++G**[b]	0	0.21	-	-
B3LYP/B3//B3LYP/B2[c,d]	0	(0.5)	(0.2)	(4.7)
$ArV^+(H_2O)$				
Present work				
ROHF/ Wf(TZP)	0	0.02	4.35	6.52
CCSD/ Wf(TZP)	0	0.15	0.01	4.10
CCSD(T)/Wf(TZP)	0.40	0.53	0	4.25
ROHF/QZVPP (min 1)	0	0.02	4.22	6.52
ROHF/QZVPP (min 2)	0	0.04	4.37	7.19
CCSD/QZVPP	0.10	0.27	0	3.98
CCSD(T)/QZVPP	0.49	0.62	0	4.17

[a] References 31, 32.
[b] Reference 34.
[c] Reference 36.
[d] See footnote d for Table 3.1 for basis explanation.

Table 3.3. Optimum geometric parameters (Å, deg) for the lowest-lying $^5A_1$, $^5A_2$, $^5B_1$ and $^5B_2$ states of $V^+(H_2O)$ and for free water.

		r(V-O)	r(O-H)	θ(H-O-H)
$^5A_1$	ROHF/Wf(TZP)	2.1481	0.9513	107.41
	CCSD/Wf(TZP)	2.0878	0.9699	106.93
	CCSD(T)/Wf(TZP)	2.0774	0.9720	106.93
	ROHF/QZVPP	2.1427	0.9465	107.46
	CCSD/QZVPP	2.0626	0.9601	106.73
	CCSD(T)/QZVPP	2.0492	0.9629	106.76
	MCPF/Wachters+f TZP[a]	2.091	-	-
	MP2/6-311++G**[b]	2.069	0.965	106.9
	B3LYP/DZVP[c]	2.109	0.971	107.4
	B3LYP/B3//B3LYP/B2[d]	2.086	-	-
	B3LYP TZVP+G(3df,2p)[e]	2.10	0.966	107.8
$^5A_2$	ROHF/Wf(TZP)	2.1484	0.9513	107.40
	CCSD/Wf(TZP)	2.0876	0.9699	106.81
	CCSD(T)/Wf(TZP)	2.0783	0.9719	106.83
	ROHF/QZVPP	2.1430	0.9465	107.45
	CCSD/QZVPP	2.0611	0.9602	106.58
	CCSD(T)/QZVPP	2.0509	0.9628	106.63
	MCPF/Wachters+f TZP[a]	2.093	-	-
	B3LYP/B3//B3LYP/B2[d]	2.084	-	-
$^5B_1$	ROHF/Wf(TZP)	2.1810	0.9520	107.23
	CCSD/Wf(TZP)	2.0670	0.9707	107.01
	CCSD(T)/Wf(TZP)	2.0430	0.9729	107.23
	ROHF/QZVPP	2.1725	0.9472	107.30
	CCSD/QZVPP	2.0449	0.9609	106.75
	CCSD(T)/QZVPP	2.0193	0.9637	107.05
	MCPF/ Wachters+f TZP[a]	2.051	-	-
	B3LYP/B3//B3LYP/B2[d]	2.056	-	-
$^5B_2$	ROHF/Wf(TZP)	2.2425	0.9516	106.77
	CCSD/Wf(TZP)	2.1276	0.9697	106.28
	CCSD(T)/Wf(TZP)	2.0965	0.9719	106.49
	ROHF/QZVPP	2.2320	0.9469	106.86
	CCSD/QZVPP	2.1005	0.9601	106.03
	CCSD(T)/QZVPP	2.0672	0.9627	106.31
	MCPF/ Wachters+f TZP[a]	2.117	-	-
	B3LYP/B3//B3LYP/B2[d]	2.124	-	-
H_2O	RHF/TZP[f]	-	0.9441	106.41
	CCSD/TZP	-	0.9652	104.27
	CCSD(T)/TZP	-	0.9673	104.02
	RHF/aug-cc-pVQZ[f]	-	0.9398	106.33
	CCSD/aug-cc-pVQZ	-	0.9561	104.62
	CCSD(T)/aug-cc-pVQZ	-	0.9590	104.37
	Exact, empirical[g]	-	0.9578	104.48

[a] References 31, 32. [b] Reference 34. [c] Reference 35. [d] Reference 36. [e] Reference 30. [f] The TZP and aug-cc-pVQZ basis sets for free H_2O respectively correspond to the Wf(TZP) and QZVPP basis sets for $V^+(H_2O)$. [g] Reference 78-80.

Table 3.4. Harmonic vibrational frequencies (in cm^{-1}) for the four lowest-lying states of $V^+(H_2O)$ and for free water.

		$\omega_1(a_1)$ O-H sym stretch	$\omega_2(a_1)$ H_2O scissor	$\omega_3(a_1)$ V-O stretch	$\omega_4(b_1)$ H_2O wag	$\omega_5(b_2)$ O-H asym stretch	$\omega_6(b_2)$ H_2O rock
$^5A_1$	ROHF/Wf(TZP)	4036	1794	364	385	4116	568
	CCSD/Wf(TZP)	3795	1679	407	266	3879	553
	CCSD(T)/Wf(TZP)	3763	1666	419	232	3849	554
	ROHF/QZVPP	4041	1792	368	370	4117	561
	CCSD/QZVPP	3836	1692	428	330	3916	524
	CCSD(T)/QZVPP	3794	1675	449	304	3876	527
$^5A_2$	ROHF/Wf(TZP)	4037	1795	364	386	4116	568
	CCSD/Wf(TZP)	3795	1682	408	265	3878	557
	CCSD(T)/Wf(TZP)	3764	1669	417	235	3849	557
	ROHF/QZVPP	4041	1793	367	371	4117	562
	CCSD/QZVPP	3836	1696	432	328	3915	532
	CCSD(T)/QZVPP	3795	1679	443	306	3877	531
$^5B_1$	ROHF/Wf(TZP)	4026	1789	312	a	a	a
	CCSD/Wf(TZP)	3784	1675	396	a	a	a
	CCSD(T)/Wf(TZP)	3750	1660	426	a	a	a
	ROHF/QZVPP	4030	1786	316	a	a	a
	CCSD/QZVPP	3826	1689	416	a	a	a
	CCSD(T)/QZVPP	3782	1671	451	a	a	a
$^5B_2$	ROHF/Wf(TZP)	4033	1789	291	a	a	a
	CCSD/Wf(TZP)	3801	1677	365	a	a	a
	CCSD(T)/Wf(TZP)	3768	1663	402	a	a	a
	ROHF/QZVPP	4036	1786	295	a	a	a
	CCSD/QZVPP	3841	1690	387	a	a	a
	CCSD(T)/QZVPP	3800	1673	432	a	a	a
H_2O	RHF/TZP[b]	4122	1736			4230	
	CCSD/TZP	3832	1639			3943	
	CCSD(T)/TZP	3800	1629			3913	
	RHF/aug-cc-pVQZ[b]	4128	1747			4229	
	CCSD/aug-cc-pVQZ	3874	1663			3981	
	CCSD(T)/aug-cc-pVQZ	3831	1649			3940	
	Experiment[c]	3832.2	1648.5			3942.5	

[a] Upon distortion along b_1 or b_2 normal modes, $^5B_1$ and $^5B_2$ are no longer the lowest quintet states of the irreps (A' or A'') in C_s symmetry to which they correlate. Therefore, variational collapse of the excited-state $^5B_1$ and $^5B_2$ solutions is a concern for the electronic structure methods applied here, all based on a Hartree-Fock reference wavefunction. Accordingly, ω_4-ω_6 for the $^5B_1$ and $^5B_2$ states are suspect and were not computed. [b] The TZP and aug-cc-pVQZ basis sets for free H_2O respectively correspond to the Wf(TZP) and QZVPP basis sets for $V^+(H_2O)$. [c] Ref. 78-80.

Table 3.5: Optimum geometric parameters (Å, deg) for the lowest-lying $^5A_1$, $^5A_2$, $^5B_1$ and $^5B_2$ states of $ArV^+(H_2O)$.

		r(Ar-V)	r(V-O)	r(O-H)	θ(H-O-H)
$^5A_1$	ROHF/Wf(TZP)	4.4685	2.1477	0.9513	107.43
	CCSD/Wf(TZP)	2.5666	2.1056	0.9691	106.71
	CCSD(T)/Wf(TZP)	2.5503	2.1004	0.9712	106.64
	ROHF/QZVPP (min 1)	3.0198	2.1378	0.9457	107.61
	ROHF/QZVPP (min 2)	4.1857	2.1421	0.9464	107.49
	CCSD/QZVPP	2.5553	2.0762	0.9595	106.44
	CCSD(T)/QZVPP	2.5298	2.0698	0.9622	106.37
$^5A_2$	ROHF/Wf(TZP)	4.4740	2.1481	0.9512	107.41
	CCSD/Wf(TZP)	2.5641	2.1065	0.9691	106.60
	CCSD(T)/Wf(TZP)	2.5486	2.1014	0.9711	106.55
	ROHF/QZVPP (min 1)	3.0298	2.1382	0.9457	107.58
	ROHF/QZVPP (min 2)	4.1968	2.1424	0.9464	107.48
	CCSD/QZVPP	2.5520	2.0768	0.9595	106.32
	CCSD(T)/QZVPP	2.5279	2.0707	0.9622	106.27
$^5B_1$	ROHF/Wf(TZP)	4.7529	2.1800	0.9520	107.25
	CCSD/Wf(TZP)	2.5627	2.0736	0.9701	106.89
	CCSD(T)/Wf(TZP)	2.5492	2.0654	0.9722	106.87
	ROHF/QZVPP (min 1)	2.7897	2.1325	0.9453	107.60
	ROHF/QZVPP (min 2)	4.6273	2.1708	0.9472	107.34
	CCSD/QZVPP	2.5594	2.0482	0.9604	106.62
	CCSD(T)/QZVPP	2.5376	2.0387	0.9632	106.62
$^5B_2$	ROHF/Wf(TZP)	4.8743	2.2423	0.9516	106.78
	CCSD/Wf(TZP)	2.5606	2.1358	0.9692	106.26
	CCSD(T)/Wf(TZP)	2.5472	2.1283	0.9713	106.24
	ROHF/QZVPP (min 1)	2.7748	2.1902	0.9449	106.94
	ROHF/QZVPP (min 2)	4.7948	2.2316	0.9468	106.87
	CCSD/QZVPP	2.5564	2.1041	0.9597	106.00
	CCSD(T)/QZVPP	2.5345	2.0956	0.9624	105.99

Table 3.6: Argon binding energies[a] [$D_e(D_0)$ in kcal mol^{-1}] for the $^5A_1$ and $^5B_1$ states of $ArV^+(H_2O)$.

	$^5A_1$	$^5B_1$
ROHF/Wf(TZP)	0.21(0.17)	−4.14
CCSD/Wf(TZP)	6.89(6.46)	6.87
CCSD(T)/Wf(TZP)	7.91	8.31
ROHF/QZVPP	0.25	−3.97
CCSD/QZVPP	8.01	8.12
CCSD(T)/QZVPP	9.42	9.91 (9.36)[b]

[a] All values are referenced to the ground-state $^5A_1$ $V^+(H_2O)$ + Ar fragments.

[b] Computation of the ZPV effect on the argon binding energy is complicated by difficulties in determining the CCSD(T)/QZVPP b_1 vibrational frequencies of $^5B_1$ $ArV^+(H_2O)$. Here we assumed that the H_2O wagging frequency does not change with Ar tagging and the Ar-V-O out-of-plane linear bend has the same frequency (84 cm^{-1}) as the corresponding in-plane linear bend. This approach provides a reasonable accounting of ZPVE within ca. 0.1 kcal mol^{-1} in the presence of intricate vibronic coupling within the ($^5A_1$, $^5B_1$, $^5A_2$) manifold.

Table 3.7: Harmonic vibrational frequencies (in cm^{-1}) of the $ArV^+(H_2O)$ complex.[a]

		ω_1 (a_1)	ω_2 (a_1)	ω_3 (a_1)	ω_4 (a_1)	ω_5 (b_1)	ω_6 (b_1)	ω_7 (b_2)	ω_8 (b_2)	ω_9 (b_2)
$^5A_1$	ROHF/Wf(TZP)	4037	1794	364	14	383	8	4117	567	8
$^5A_1$	CCSD/Wf(TZP)	3804	1678	395	163	255	67	3888	542	88
$^5B_1$	CCSD(T)/Wf(TZP)	3759	1662	408	168	655[b]	113[b]	3845	536	84
$^5A_1$	ROHF/QZVPP	4052	1789	371	34	345	54	4130	548	58
$^5B_1$	CCSD/QZVPP	3833	1688	424	160	-	-	3911	506	83
$^5B_1$	CCSD(T)/QZVPP	3790	1671	433	168	-	-	3870	606	84

[a] Results are tabulated for the lowest electronic state at each level of theory. ω_1 = O-H symmetric stretch, ω_2 = H_2O scissor, ω_3 = V-O stretch, ω_4 = Ar-V stretch, ω_5 = H_2O wag, ω_6 = Ar-V-O out-of-plane linear bend, ω_7 = O-H antisymmetric stretch, ω_8 = H_2O rock, ω_9 = Ar-V-O in-plane linear bend.

[b] The $^5B_1$ state is the lowest one at the CCSD(T) level, but not at the Hartree-Fock level. For b_1 displacements from C_{2v} symmetry, the $^5B_1$ solution for the Hartree-Fock reference wavefunction can be continuously followed due to the atomic character of the open-shell manifold, but there is no guarantee against variational collapse.

Table 3.8: Summary of CCSD/Wf(TZP) VPT2 anharmonic vibrational analysis of the $^5A_1$ states of $ArV^+(H_2O)$ and $V^+(H_2O)$.[a]

	i	ω_i	Δ_i	ν_i	α_i^A	α_i^B	α_i^C
$ArV^+(H_2O)$							
O-H sym. stretch	1	3804.3	–183.0	3621.3	0.23876	0.0000059	0.0000094
H_2O scissor	2	1678.1	–44.0	1634.1	–0.17072	–0.0000060	0.0000086
V-O stretch	3	395.2	–12.8	382.4	–0.00600	0.0002637	0.0002651
Ar-V stretch	4	162.5	–7.5	155.1	0.00181	0.0005642	0.0005542
H_2O wag	5	255.4	124.6	379.9	1.83244	–0.0000202	–0.0000464
Ar-V-O bend (b_1)	6	66.7	21.7	88.4	0.27989	–0.0000579	–0.0001646
O-H asym. stretch	7	3888.3	–198.0	3690.3	0.13627	0.0000034	0.0000041
H_2O rock	8	542.2	–3.2	539.0	–1.49487	–0.0000101	0.0000116
Ar-V-O bend (b_2)	9	87.5	10.0	97.5	0.07836	–0.0000484	0.0000502
$V^+(H_2O)$							
O-H sym. stretch	1	3794.3	–182.0	3612.3	0.24162	–0.0000878	0.0000031
H_2O scissor	2	1679.3	–43.6	1635.7	–0.17069	–0.0002382	0.0001265
V-O stretch	3	407.3	–11.1	396.2	–0.00674	0.0030815	0.0030579
H_2O wag	4	265.3	120.5	385.8	1.86054	–0.0001442	–0.0007827
O-H asym. stretch	5	3878.5	–197.3	3681.2	0.14051	–0.0000800	–0.0000583
H_2O rock	6	552.7	–3.3	549.4	–1.46988	–0.0001857	0.0003552
H_2O							
O-H sym. stretch	1	3831.7	–176.7	3655.0	0.63733	0.2230477	0.1724306
H_2O scissor	2	1639.3	–43.3	1596.0	–2.56400	–0.1529430	0.1405468
O-H asym. stretch	3	3942.6	–189.8	3752.9	1.12194	0.0948105	0.1396034

[a] Harmonic frequencies (ω_i), total anharmonicities (Δ_i), fundamental frequencies (ν_i), and rovibration interaction constants (α_i^A, α_i^B, α_i^C) for $^5A_1$ state of $^{40}Ar^{51}V^+(H_2{}^{16}O)$, $^{51}V^+(H_2{}^{16}O)$, and $H_2{}^{16}O$ in cm^{-1}. No strong anharmonic resonances required exclusion. The $\omega_6 - \omega_9$ Coriolis resonance was removed in computing the α_i constants of $ArV^+(H_2O)$.

Table 3.9: Wf(TZP) coupled-cluster quartic force fields (sector I) of the $^5A_1$ state of $V^+(H_2O)$ and $ArV^+(H_2O)$.[a,b]

	$V^+(H_2O)$ CCSD(T)	$V^+(H_2O)$ CCSD	$ArV^+(H_2O)$ CCSD		$V^+(H_2O)$ CCSD(T)	$V^+(H_2O)$ CCSD	$ArV^+(H_2O)$ CCSD
F_{11}	1.38257	1.30439	1.21753	F_{3221}	0.040	0.043	0.024
F_{21}	0.10250	0.09950	0.08476	F_{3222}	1.036	1.019	1.017
F_{22}	8.07729	8.21424	8.25502	F_{3311}	–0.022	–0.019	–0.020
F_{31}	–0.00836	–0.00616	–0.00560	F_{3321}	0.111	0.104	0.109
F_{32}	0.23855	0.24176	0.25244	F_{3322}	0.437	0.418	0.443
F_{33}	0.72534	0.73371	0.73232	F_{3331}	–0.070	–0.084	–0.071
F_{44}	0.01772	0.02307	0.02266	F_{3332}	1.080	1.058	1.080
F_{55}	8.14121	8.26656	8.31063	F_{3333}	–0.219	–0.259	–0.261
F_{65}	0.04116	0.03946	0.03826	F_{4411}	0.151	0.139	0.076
F_{66}	0.15109	0.14983	0.14242	F_{4421}	0.116	0.113	0.102
				F_{4422}	–0.175	–0.172	–0.152
F_{111}	–7.234	–7.029	–6.537	F_{4431}	–0.019	–0.033	–0.002
F_{211}	–0.286	–0.245	–0.236	F_{4432}	0.068	0.067	0.043
F_{221}	–0.013	–0.023	–0.027	F_{4433}	–0.097	–0.089	–0.081
F_{222}	–39.329	–39.819	–40.022	F_{4444}	0.488	0.462	0.387
F_{311}	0.148	0.148	0.142	F_{5511}	–0.418	–0.389	–0.412
F_{321}	0.107	0.107	0.100	F_{5521}	–0.048	–0.095	–0.093
F_{322}	–0.608	–0.608	–0.606	F_{5522}	169.795	172.201	172.956
F_{331}	–0.050	–0.053	–0.047	F_{5531}	–0.036	–0.010	–0.032
F_{332}	–0.451	–0.443	–0.443	F_{5532}	–0.797	–0.792	–0.798
F_{333}	–0.579	–0.585	–0.594	F_{5533}	–0.990	–1.003	–0.989
F_{441}	–0.067	–0.059	–0.058	F_{5544}	0.072	0.043	0.036
F_{442}	–0.120	–0.112	–0.102	F_{5555}	171.199	173.628	174.406
F_{443}	0.106	0.101	0.089	F_{6511}	0.157	0.145	0.155
F_{551}	0.130	0.119	0.118	F_{6521}	–0.058	0.035	0.044
F_{552}	–39.357	–39.865	–40.061	F_{6522}	–0.091	–0.111	–0.105
F_{553}	0.331	0.334	0.343	F_{6531}	–0.038	–0.080	–0.064
F_{651}	–0.078	–0.078	–0.075	F_{6532}	0.075	0.044	0.027
F_{652}	0.063	0.060	0.060	F_{6533}	0.011	0.002	0.003
F_{653}	–0.030	–0.030	–0.031	F_{6544}	0.029	0.014	0.016
F_{661}	–0.077	–0.085	–0.077	F_{6555}	–0.187	–0.171	–0.166
F_{662}	–0.047	–0.043	–0.040	F_{6611}	–0.059	–0.083	–0.066
F_{663}	0.105	0.106	0.100	F_{6621}	0.082	0.081	0.075
				F_{6622}	–0.153	–0.157	–0.139
F_{1111}	31.355	29.896	28.050	F_{6631}	–0.007	–0.018	–0.010
F_{2111}	1.061	1.033	1.023	F_{6632}	0.003	0.011	0.012
F_{2211}	–0.279	–0.286	–0.297	F_{6633}	–0.059	–0.051	–0.056
F_{2221}	–0.266	–0.238	–0.214	F_{6644}	0.224	0.219	0.213
F_{2222}	168.111	170.453	171.244	F_{6655}	–0.063	–0.073	–0.059
F_{3111}	–0.372	–0.352	–0.372	F_{6665}	0.023	0.021	0.021
F_{3211}	–0.145	–0.133	–0.133	F_{6666}	–0.120	–0.111	–0.119

[a] Sector I comprises only the symmetry-adapted internal coordinates S_1-S_6 of the text, i.e., those coordinates common to both the untagged $V^+(H_2O)$ and tagged $ArV^+(H_2O)$ ions.
[b] Units consistent with energy in aJ, distances in Å, and angles in rad.

Table 3.10: CCSD/Wf(TZP) quartic force field (sector II) of the $^5A_1$ state of $ArV^+(H_2O)$.[a,b]

F_{71}	0.03660	F_{991}	–0.062	F_{8411}	10.508	F_{9622}	–0.002
F_{72}	–0.00579	F_{992}	0.003	F_{8421}	0.378	F_{9631}	0.002
F_{73}	–0.00605	F_{993}	0.009	F_{8422}	–0.064	F_{9632}	–0.002
F_{77}	0.39828	F_{997}	–0.085	F_{8431}	0.036	F_{9633}	–0.011
F_{84}	0.01342			F_{8432}	–0.030	F_{9644}	0.027
F_{88}	0.04995	F_{7111}	0.243	F_{8433}	–0.017	F_{9655}	0.001
F_{95}	0.00877	F_{7211}	–0.028	F_{8444}	0.005	F_{9665}	0.002
F_{96}	0.00994	F_{7221}	–0.013	F_{8554}	–0.070	F_{9666}	–0.021
F_{99}	0.07914	F_{7222}	0.040	F_{8654}	–0.008	F_{9751}	0.059
		F_{7311}	–0.015	F_{8664}	0.017	F_{9752}	0.058
F_{711}	–0.088	F_{7321}	–0.024	F_{8741}	0.004	F_{9753}	–0.023
F_{721}	0.012	F_{7322}	0.003	F_{8742}	0.120	F_{9761}	0.009
F_{722}	0.007	F_{7331}	–0.004	F_{8743}	0.013	F_{9762}	0.013
F_{731}	0.010	F_{7332}	–0.009	F_{8774}	–0.014	F_{9763}	–0.012
F_{732}	–0.008	F_{7333}	0.004	F_{8811}	–0.001	F_{9775}	–0.007
F_{733}	0.000	F_{7441}	0.005	F_{8821}	–0.922	F_{9776}	–0.002
F_{744}	–0.004	F_{7442}	–0.015	F_{8822}	0.209	F_{9854}	0.029
F_{755}	–0.001	F_{7443}	0.015	F_{8831}	–0.072	F_{9864}	–0.013
F_{765}	0.000	F_{7551}	–0.012	F_{8832}	0.074	F_{9885}	0.010
F_{766}	0.005	F_{7552}	–0.019	F_{8833}	–0.014	F_{9886}	–0.050
F_{771}	–0.059	F_{7553}	0.010	F_{8844}	–0.013	F_{9911}	–0.048
F_{772}	–0.001	F_{7651}	0.042	F_{8855}	0.144	F_{9921}	–0.011
F_{773}	0.008	F_{7652}	0.071	F_{8865}	–0.020	F_{9922}	–0.022
F_{777}	–2.494	F_{7661}	–0.024	F_{8866}	–0.009	F_{9931}	0.010
F_{841}	–0.042	F_{7662}	–0.007	F_{8871}	–0.036	F_{9932}	0.013
F_{842}	0.023	F_{7663}	–0.005	F_{8872}	–0.235	F_{9933}	–0.007
F_{843}	–0.008	F_{7711}	0.003	F_{8873}	0.019	F_{9944}	0.072
F_{874}	–0.015	F_{7721}	0.162	F_{8877}	–0.129	F_{9955}	–0.018
F_{881}	0.019	F_{7722}	–0.017	F_{8884}	–0.011	F_{9965}	–0.009
F_{882}	–0.028	F_{7731}	–0.036	F_{8888}	–0.155	F_{9966}	–0.009
F_{883}	–0.004	F_{7732}	–0.019	F_{9511}	0.002	F_{9971}	0.127
F_{887}	–0.028	F_{7733}	0.010	F_{9521}	0.050	F_{9972}	0.008
F_{951}	–0.011	F_{7744}	0.005	F_{9522}	–0.003	F_{9973}	–0.014
F_{952}	0.010	F_{7755}	0.001	F_{9531}	–0.019	F_{9977}	–0.020
F_{953}	–0.002	F_{7765}	–0.046	F_{9532}	–0.039	F_{9984}	0.066
F_{961}	–0.001	F_{7766}	–0.009	F_{9533}	0.005	F_{9988}	–0.242
F_{962}	–0.002	F_{7771}	–0.002	F_{9544}	–0.006	F_{9995}	–0.011
F_{963}	0.007	F_{7772}	0.195	F_{9555}	0.004	F_{9996}	–0.031
F_{975}	–0.010	F_{7773}	0.017	F_{9611}	0.013	F_{9999}	0.066
F_{976}	–0.011	F_{7777}	–0.020	F_{9621}	0.012		

[a] Sector II includes diagonal and off-diagonal blocks involving the symmetry-adapted internal coordinates S_7-S_9 of the text, i.e., the additional modes resulting from argon tagging.
[b] Units consistent with energy in aJ, distances in Å, and angles in rad.

Table 3.11: Wf(TZP) coupled cluster quartic force fields[a] of free H_2O.

	CCSD	CCSD(T)		CCSD	CCSD(T)
F_{11}	8.3500	8.2095	F_{1111}	175.9	173.4
F_{21}	0.3603	0.3618	F_{2111}	0.505	0.499
F_{22}	0.7048	0.6998	F_{2211}	0.644	0.670
F_{33}	8.5580	8.4313	F_{2221}	1.664	1.739
			F_{2222}	0.025	0.112
F_{111}	–41.31	–40.83	F_{3311}	176.9	174.4
F_{211}	–0.720	–0.730	F_{3321}	–1.154	–1.173
F_{221}	–0.430	–0.449	F_{3322}	–0.910	–0.908
F_{222}	–0.724	–0.717	F_{3333}	178.40	175.81
F_{331}	–41.13	–40.61			
F_{332}	0.3963	0.3893			

[a] Units consistent with energy in aJ, distances in Å, and angles in rad. In symmetry-adapted internal coordinates $S_1 = 2^{-1/2}\left(r_{OH} + r'_{OH}\right)$, $S_2 = \theta_{HOH}$, and $S_3 = 2^{-1/2}\left(r_{OH} - r'_{OH}\right)$.

CHAPTER 4

MOLECULAR STRUCTURES OF THE TWO MOST STABLE CONFORMERS OF FREE GLYCINE[*]

[*] V. Kasalová, W. D. Allen, E. Czinki, A. G. Császár, H. F. Schaefer III. In preparation.

4.1 ABSTRACT

The equilibrium molecular structures of the two lowest-energy conformers of glycine, Gly-**Ip** and Gly-**IIn**, have been characterized by high-level *ab initio* electronic structure computations, including all-electron cc-pVTZ CCSD(T) geometry optimizations and 6-31G* MP2 quartic force fields, the latter to account for anharmonic zero-point vibrational effects to isotopologic rotational constants. Based on experimentally measured vibrationally averaged effective rotational constant sets of several isotopologues and our *ab initio* data for structural constraints and zero-point vibrational shifts, least-squares structural refinements were performed to determine improved Born–Oppenheimer equilibrium structures of Gly-**Ip** and Gly-**IIn**. Without the *ab initio* constraints even the extensive set of empirical rotational constants available for five and ten isotopologues of Gly-**Ip** and Gly-**IIn**, respectively, cannot satisfactorily fix their molecular structure. Excellent agreement between theory and experiment is found for the rotational constants of both conformers, the rms residual of the final fits being 7.8 and 51.6 kHz for Gly-**Ip** and Gly-**IIn**, respectively. The barrier to planarity separating Gly-**IIp** and Gly-**IIn** has been determined to be 20.5 cm^{-1}. The equilibrium torsional angle τ(NCCO) of Gly-**IIn**, characterizing the deviation of its heavy-atom framework from planarity, is 11º.

4.2 INTRODUCTION

Glycine (Gly) is the simplest naturally occuring amino acid, and thus one of the most fundamental molecules of biological interest. Gly is considered by many a prototypical amino acid in structural studies of peptides and proteins. Detection of glycine in interstellar space,[1] which most likely will involve its lowest-energy conformer Gly-**Ip**

(Figure 4.1), is relevant to theories about the origin of molecules vital to life on Earth. Therefore, the molecular structures of the conformers of Gly, a neutral species in the gas phase, have been the focus of extensive experimental[2-6] and computational[7-14] studies. For a more complete list of work prior to 1992, see Ref. 7.

There is consensus in the qualitative structural features of the two most stable conformers of glycine (Figure 4.1), **I** and **II**. The notation employed in Figure 4.1 and throughout this paper follows that introduced in Ref. 7, whereby **p** stands for a conformer (or conformation) having C_s point-group symmetry, **n** stands for a conformer having C_1 point-group symmetry, and in general Roman numerals, from **I** through **VIII**, indicate the relative stabilities of the conformers. Consequently, the two most stable conformers of Gly are **Ip** and **IIn**,[7] having substantially different atomic arrangements.

Early on, around 1978, there was some confusion about the relative energies of the most stable conformers of glycine.[2,6,14] Theory, even at the low levels applicable in those days,[14] proved to be vital in the correct interpretation of the experimental microwave (MW) results and in proving that Gly-**Ip** is the global minimum on the potential energy surface (PES) of neutral glycine. For Gly-**II** it remained unclear whether its equilibrium structure was planar or not. The determination of an extensive set of rotational constants of several isotopologues of Gly-**IIn**[5] was aided by the substantial dipole moments of this conformer. The empirical rotational constants of Gly-**II** indicated that the effective structure is planar, because the amino hydrogens were indistinguishable in the monodeuterated [OH, NDH] and [OD, NDH] spectra obtained. Electronic structure theory at most levels suggested[7] that the true equilibrium structure is non-planar, though the energy difference between Gly-**IIp** and Gly-**IIn** was predicted to be only on the order of 20 cm^{-1}. Despite the extensive

experimental and theoretical data, the question of the (non-)planarity of Gly-**II** was not definitely settled. Our current study proves, using extensive *ab initio* computations, that the equilibrium structure of Gly-**II** is indeed non-planar.

None of the studies performed up to now were able to obtain satisfactory Born–Oppenheimer *equilibrium* structures, r_e^{BO}, of Gly-**Ip** and Gly-**IIn**, quantities allowing direct comparison among disparate molecules. Furthermore, neither the gas electron diffraction (GED),[4] as detailed before,[5,8] nor the MW[5] and millimeterwave (MMW)[6] experimental studies yielded an accurate vibrationally averaged molecular structure of Gly-**Ip**. Application of the computational strategy of equilibrium structure determination of this study, outlined below, offers no difficulties for Gly-**Ip**, and the resulting r_e^{BO} structure should be highly reliable. For Gly-**IIn** both the substitution (r_s) and the least-squares structures have been determined based on effective ground-state rotational constants of 12 isotopologues.[5] The r_s structure seemed to be suspect[5] due to "the small *b*-axis coordinates associated with both the nitrogen and carbonyl carbon atoms." The least-squares structural fit indicated[5] that *in the ground vibrational state* Gly-**IIn** has C_s point-group symmetry. Nevertheless, no attempt was made in Ref. 5 to derive the *equilibrium* structure of Gly-**IIn**, for which all dependable *ab initio* computations, including those of the present study, indicate a non-planar atomic arrangement. Therefore, based on our recently successful determination of the r_e^{BO} structure for the considerably larger and even less rigid amino acid, L-proline,[15] here we report results of a similar study on two conformers of neutral glycine.

4.3 THEORETICAL METHODS

The computational strategy employed in this work, and recommended for similar studies to obtain highly reliable equilibrium structures, can be summarized as follows. First, accurate values of r_e^{BO} are determined at advanced levels of electronic structure theory, in the present case at the all-electron cc-pVTZ CCSD(T) level (see below). For small molecules where the accuracy of the computations can be checked more or less readily, this level of theory, due in small part to fortuitious error cancellation, is known[16] to yield equilibrium structures with expected errors in bond lengths and bond angles not exceeding 0.005 Å and 0.5°, respectively. Second, vibrational corrections between equilibrium and ground-state rotational constants are determined, in the present case at the all-electron 6-31G* MP2 level, through computation of a full cubic force field and the use of vibrational second-order perturbation theory (VPT2).[17-21] A weakness of this simple approach is that no special consideration is given to large-amplitude motion(s). Third, the experimental ground-state rotational constants of all the isotopologues[3,5] are corrected to yield empirically-based equilibrium rotational. Fourth, guided weighted least-squares refinements are performed with various *ab initio* structural constraints to determine the r_e^{BO} parameters in best agreement with the available corrected experimental equilibrium rotational constants. In particular, for Gly-**IIn** we decided to check carefully whether the experimental rotational constants can support an r_e^{BO} of C_1 point-group symmetry.

4.3.1 Electronic Structure Computations

Several correlated levels of electronic structure theory have been used previously in order to determine equilibrium structures of certain conformers of glycine. In Ref. 7 geometry optimizations for all conformers of Gly were performed at the 6-311++G** MP2 level, known to yield reasonably accurate equilibrium Born–Oppenheimer structures and rotational constants. In Ref. 10 the highest-level optimizations were performed at the DZP CCSD level. The Born–Oppenheimer equilibrium structures of Gly-**Ip**, Gly-**IIp**, and Gly-**IIn** have been reoptimized in this study using the cc-pVTZ[22] basis set at the all-electron (AE) CCSD(T) level,[23-25] where CCSD(T) stands for coupled-cluster theory with all single and double excitations and a perturbative estimate of connected triple excitations. The geometry optimizations were performed with the program packages MOLPRO[26] and ACESII.[27]

The barrier to planarity of Gly-**IIn** was reported to be about 20 cm^{-1} in previous work.[7] With such a minuscule barrier, we deemed it important to compute a definitive value for the **IIn** → **IIp** barrier, indeed, to prove conclusively that this conformation is non-planar. A focal-point analysis[28-32] of this quantity was executed, with a detailed layout of the related focal-point increments presented in Table 4.1. For the extrapolation of the Hartree–Fock energies, an exponential formula,[33,34]

$$E_X^{\mathrm{HF}} = E_\infty^{\mathrm{HF}} + ae^{-bX} \tag{4.1}$$

was used, while for the extrapolation of the MP2 and CCSD electron correlation energies (ε), a two-parameter polynomial formula[35]

$$\varepsilon_X^{\mathrm{CC}} = \varepsilon_\infty^{\mathrm{CC}} + bX^{-3} \tag{4.2}$$

was employed. The aug-cc-pV*X*Z (X = D, T, Q, 5) basis sets[22,36-40] were used in the extrapolations. Core correlation was determined at the cc-pCVTZ[22,40] CCSD(T) level of theory.

In order to account for zero-point vibrational effects in the experimental rotational constants, anharmonic force field expansions of the vibrational potentials were computed for Gly-**Ip** and Gly-**IIn** at the all-electron 6-31G* MP2 level in normal coordinates, employing the code ACESII[27,41-43] The anharmonic force fields include all force constants of type F_{ij}, F_{ijk}, and F_{ijkk} for all degrees of freedom. The force fields were computed at the respective equilibrium structures in order to avoid the non-zero force dilemma.[44] In determining the total vibrational contributions to ground-state rotational constants, Coriolis resonances need not be considered because all resonance denominators cancel in the summation over normal modes. For the Gly-**IIp** transition state, in-house programs were used to compute anharmonic force constants. The program INTDIF2004[45,46] was employed to determine the required displacements as well as compute the force constants in internal coordinates. The transformation of the force constants from internal to normal coordinates and the computation of spectroscopic constants were performed using the programs INTDER2000[47-49] and ANHARM,[50,51] respectively.

4.3.2 Structural Refinements

With the aid of our fully optimized all-electron cc-pVTZ CCSD(T) structures, we undertook a weighted least-squares refinement (LSR) to determine improved equilibrium

structural parameters for Gly-**Ip** and Gly-**IIn**. We exclusively employed a *Mathematica* program MolStruct[15,52] during this study for LSR.

Upon constraining diverse sets of internal coordinates to their cc-pVTZ CCSD(T) equilibrium values and then performing LSR on the rest, we were always able to achieve facile convergence in the fit for Gly-**Ip**. The situation was more difficult for the Gly-**IIn** LSR, but after careful selection of structural constraints we were able to achieve a convergence with a root-mean-square (rms) error of only 51.6 kHz even for this conformer. For the planar conformation Gly-**IIp**, we were not able to achieve a small rms error. More detailed description of the weighted least-squares refinement procedures and results for Gly-**Ip**, Gly-**IIp**, and Gly-**IIn** are given in section 4.4.

4.4 RESULTS AND DISCUSSION

Due to sizable vibrational averaging effects, the directly computed *ab initio* equilibrium Born–Oppenheimer rotational constants (A_e, B_e, and C_e) may deviate substantially from the experimentally measured ground-state ones (A_0, B_0, and C_0). To wit, the all-electron 6-31G* MP2 and cc-pVTZ CCSD(T) equilibrium rotational constants of Gly-**Ip** and Gly-**IIn** (Table 4.2) display differences as large as 113 MHz from the experimental rotational constants. The corrections for vibrational averaging computed from the all-electron 6-31G* MP2 anharmonic force field, amounting to 0.7–1.1 % of the equilibrium rotational constants for the parent isotopologue, reduce the deviations from experiment by an order of magnitude, in accord with the usually observed,[15,17,18,53-55] good accuracy of theoretical rotation-vibration interaction (α_i) constants.

The computed differences between the vibrationally-averaged rotational constants of the parent isotopologue and those of the substituted ones of Gly-**Ip**, as reported in Table 4.3, reproduce remarkably well the experimentally measured differences. The situation is not so clear for Gly-**IIn** (Table 4.4). McGlone et al.[5] reported 12 sets of effective rotational constants for Gly-**IIn**. For ten of these the agreement is about as good for Gly-**II** as for Gly-**Ip**. However, for the substitutions [OH,NDH] and [OD,NDH] relatively large discrepancies are observed between the computed and measured rotational constant shifts. These disparities are a consequence of the inability to measure the rotational constants corresponding to the individual isotopomers NDH/NHD. The effective, average rotational constants determined by McGlone et al.[5] correspond to neither isotopomer of this C_1-symmetry conformer but to an average. Consequently, the 'observed' rotational constants of [OH,NDH] and [OD,NDH] were not employed in the final structural fits here. When the inclusion of these rotational constants data in the set experimental observables was attempted,unacceptably large fitting errors resulted.

4.4.1 Least-SquareS Refinement for Gly-**Ip**

Although the isotopologic rotational constant data for Gly-**Ip** are extensive, they are clearly insufficient to give a well-defined a structure without the imposition of constraints. There are 15 structural degrees of freedom for planar Gly-**Ip**, and 15 empirical rotational constants in the data set.

Having all-electron cc-pVTZ CCSD(T) optimum structural parameters, we are in a position to impose realistic and reliable constraints on the structural refinement of Gly-**Ip**. With all parameters fixed, the variables that are best determined from the input

rotational constants are identified on the basis of the least-squares Hessian. Candidates for constraint release are relaxed one by one, and new determinants of the least-squares Hessian are evaluated. Using this automatic procedure to predict the parameters to be optimized, we found that it is best to start the fitting procedure with the four heavy-atom distances relaxed while keeping the rest of the internal coordinates fixed at their cc-pVTZ CCSD(T) optimum values. Somewhat to our surprise, the corrected empirical rotational constants can be fit quite well this way, the weighted rms error is 0.2157 MHz and no residual is over 2 MHz. The corresponding results are listed under Fit 1 in Table 4.6.

The structure of Gly-**Ip** can be improved by performing additional fits with further relaxation of constraints. More variables are selected and released using the procedure outlined above. In the end, only four structural constraints are required, as given in Table 4.5. Of these constraints, r(OH) and θ(COH) are not well defined by the data, which is not surprising since no O–D substitution information is available for the hydroxyl group. Similarly, no rotational constants are available for the NHD and ND_2 substitutions; therefore θ(NH_2 scissor) and θ(NH_2 wag) are not defined well by the data and need to be constrained as well. The r(NH) bond length was released because it led to a small decrease in the rms error.

Results from the final structural refinement for Gly-**Ip** are presented in Table 4.6 as Fit 2. Deviations between the fitted semitheoretical and the all-electron cc-pVTZ CCSD(T) r_e^{BO} structures of Gly-**Ip** are comfortably small. For bond lengths, the largest difference is 0.006 Å for the N–H bond, which is due to the limited data available to fit this variable, as noted above. The value of θ(C–C–O) in Fit 2 differs form the cc-pVTZ CCSD(T) value by 0.5º, while deviations for the other angles are considerably smaller.

This verifies the generally accepted predictive power of structure optimizations at high levels of electronic structure theory.

There are significant discrepancies between the r_α^0 parameters derived from gas-phase electron diffraction (GED) data[4] and our fitted parameters (Table 4.6). Considerable problems with this GED investigation have been addressed previously by Császár[7,8] and are not elaborated here further.

4.4.2 Barrier to Planarity of Gly-**IIn**

Prior to the structural refinement of the second lowest-lying conformer of glycine, Gly-**IIn**, we determined the energy difference between Gly-**IIp** and Gly-**IIn** using the technique of focal-point analysis (FPA).[28-32] The FPA valence-only increments are listed in Table 4.1. Because the basis set extrapolations are converged well (within 2 cm^{-1}), the error bars for the barrier to planarity are determined from the less converged extrapolation of the correlation effects (5.0 cm^{-1}). The results of Table 4.1 show definitively that at equilibrium Gly-**II** is non-planar. After including core-correlation effects (–2.07 cm^{-1}), our best estimate for the barrier to planarity is 20.5 ± 5.0 cm^{-1}. This small barrier readily supports the observed planar ground-state structure of Gly-**II**.

4.4.3 Least-Squares Refinement for Gly-**IIn**

As a starting point, we attempted to reproduce the structural parameters from a least-squares fit reported by McGlone and co-workers,[5] by performing an unconstrained LSR of a planar structure with no vibrational corrections to the rotational constants included. All 12 isotopologues were used in the fit, and the fit is designated as Fit A in

Table 4.7. The parameters r_0(C–N), r_0(C=O), r_0(C–O), r_0(O–H), r_0(C–H av), θ_0(C–O–H), and θ_0(C–C–O) are identical to the number of digits reported in Ref. 5. Among the other structural parameters, the largest differences are 0.04 Å and 1.2º for the r_0(C–C) bond length and the θ_0(CH_2 scissor) angle, respectively. These deviations are still well within the uncertainities of the two sets of data, and small differencies are due to different fitting procedures. It must be emphasized that the rms error for Fit A is substantial, 0.724 MHz. The uncertainties for the structural parameters for Fit A are significant as well, being up to 0.03 Å for bond lengths and up to 3.3º for most angles, with the uncertainty of the γ(NH_2 wag) of 33º. When isotopologues for the [OH,NDH] and [OD,NDH] substitutions are excluded from the fit, which results in Fit B of Table 4.7, the rms error decreases to 0.438 MHz. This involves a significant decrease in the uncertainities of the individual structural parameters, with standard errors in Fit B less than half of those of Fit A. Due to the significant error reduction, the [OH,NDH] and [OD,NDH] isotopologues were excluded in all least-squares refinements to follow.

For all subsequent fits, we used the all-electron 6-31G* MP2 vibrational corrections with the empirical rotational constants to obtain the equilibrium r_e^{BO} structure of Gly-**II**. It is important to note the significant difference in the zero-point vibrational (ZPV) corrections for Gly-**IIp** and Gly-**IIn** (Tables 4.9 and 4.10). The ZPV corrections differ by 16-43 MHz, 8-16 MHz, and 7-15 MHz for the rotational constants *A*, *B*, and *C*, respectively. If the [OH,NDH] and [OD,NDH] isotopologues are excluded from the comparision, the range for the discrepances decreases, but the differences remain large (20-32 MHz for *A*, 9-11 MHz for *B* and *C*).

Because the experimental rotational constants correspond to a vibrationally averaged planar structure,[3,5] we attempted to perform a LSR on planar Gly-**IIp**. Gly-**IIp** cc-pVTZ CCSD(T) equilibrium geometry and Gly-**IIp** 6-31G* MP2 vibrational corrections were employed in conjunction with the set of the empirical rotational constants available for Gly-**II**. This LSR proved to be very difficult, and no reasonable fits could be obtained.

Gly-**IIn** has C_1 point-group symmetry and thus considerably more structural parameters than Gly-**Ip**, 24 vs. 15. To determine candidates for constraint release, the same procedure based on determinants of the least-squares Hessian was used as for Gly-**Ip**. Releasing variables one by one, we obtained the preliminary fit designated as Fit 1 in Table 4.7. The standard errors for the parameters in Fit 1 are reduced compared those in Fit A and Fit B, and the rms error decreased to 0.303 MHz. The variables for Fit 1 differ from the all-electron cc-pVTZ CCSD(T) structural parameters by at most 0.004 Å for bond lengths and 1.7º for angles, with the exception of r(O–H), where the difference is a substantial 0.019 Å.

The uncertainities and rms deviations can be further reduced by releasing two more parameters, γ(NH_2 wag) and $\Delta\theta$(NH_2 rock). The release of γ(NH_2 wag) and $\Delta\theta$(NH_2 rock) yields a fit designated as Fit 2 in Table 4.7. The uncertainities of Fit 2 are less than 0.002 Å for bond lengths and 1º for bond angles. The uncertainities are larger for the torsional and out-of-plane angles, but still less than 1.5º. This represents a huge improvement in the uncertainities for the out-of-plane NH_2 wag, which were 33º and 13º in Fits A and B, respectively. Fit 2 provides the smallest uncertainities from all LSR procedures of Gly-**IIn**, and the rms error (52.9 kHz) is drastically smaller than those of Fits A, B, and 1.

Next, we released the γ(COOH oop). The resulting fit is designated as Fit 3 in Table 4.7. The rms error of Fit 3 is 51.6 kHz and the uncertainities increased slightly for Fit 3 as compared to Fit 2. Fit 3 provides the value of γ(COOH oop), 0.12º ± 2.86º. No other parameters are determined well enough by the experimental data in order to be released, and Fit 3 is our final fit for Gly-**IIn**. The all-electron cc-pVTZ CCSD(T) constraints involved in Fit 3 are listed in Table 4.5. Because the experimental data do not distinguish between the NHD and CHD monodeuterated substitutions, the differences Δr(NH) = r(N3H9) – r(N3H10) and Δr(CH) = r(C2H7) – r(C2H8) could not be determined from the experimental data and therefore have been constrained.

As can be seen from the results in Table 4.7, deviations between the fitted semitheoretical bond lengths of Fit 3 and the all-electron cc-pVTZ CCSD(T) r_e^{BO} bond lengths are smaller than (or equal to) 0.005 Å, except for r(O–H), where the deviation is 0.015 Å. For the angles, the situation is somewhat more complicated. The deviations for bond angles are all smaller than 0.8º, except for $\Delta\theta$(CH_2 wag) and $\Delta\theta$(NH_2 rock), where the deviations are substantially larger, 2.4º and 7.6º, respectively. The torsional and out-of-plane angles deviate by at most 1.6º and 4º, respectively.

4.5 CONCLUSIONS

It has been established that while the lowest-energy conformer of neutral glycine, Gly-**Ip**, has a planar equilibrium structure, the second lowest-energy conformer, Gly-**IIn**, has a non-planar equilibrium structure. A definitive estimate, 20.5 ± 5.0 cm^{-1}, has been obtained through the focal-point approach for the barrier to planarity of Gly-**IIn.**

Ulitimate representations of the equilibrium structures of the two lowest-energy conformers of free glycine have been obtained. They are based on all-electron cc-pVTZ CCSD(T) structure optimizations, all-electron 6-31G* MP2 vibration-rotation interaction constants to correct the experimentally observed rotational constants, and a weighted constrained least-squares refinement procedure adjusting selected structural parameters. The final fits resulted in rms errors of only 7.8 and 51.6 kHz for Gly-**Ip** and Gly-**IIn**, respectively. Clearly, the experimentally observed rotational constants corresponding to a planar ground-state structure are compatible with a non-planar equilibrium structure for Gly-**IIn**.

4.6 ACKNOWLEDGEMENTS

Work performed in the U.S.A. and in Hungary has been supported by the U.S. National Science Foundation (NSF-CHE01-36186) and by the Hungarian Scientific Research Fund, OTKA T047185, respectively. Collaboration between the two research groups has received support from an NSF-MTA-OTKA collaboration grant (INT-0312355). This research was performed in part using the Molecular Science Computing Facility (MSCF) in the William R. Wiley Environmental Molecular Sciences Laboratory, a national scientific user facility sponsored by the U.S. Department of Energy's Office of Biological and Environmental Research and located at the Pacific Northwest National Laboratory, operated for the Department of Energy by Battelle.

4.7 REFERENCES

[1] F. Combes, Nguyen-Q-Rien, and G. Wlodarczak, Astron. Astrophys. **308**, 618 (1996).

[2] R. D. Brown, P. D. Godfrey, S. J. W. V., and M. P. Bassez, J. Chem. Soc. Chem. Commun. (13), 547 (1978).

[3] P. D. Godfrey and R. D. Brown, J. Am. Chem. Soc. **117**, 2019 (1995).

[4] K. Iijima, K. Tanaka, and S. Onuma, J. Mol. Struct. **246**, 257 (1991).

[5] S. J. McGlone, P. S. Elmes, R. D. Brown, and P. D. Godfrey, J. Mol. Struct. **485-486**, 225 (1999).

[6] R. D. Suenram and F. J. Lovas, J. Mol. Spectrosc. **72**, 372 (1978).

[7] A. G. Császár, J. Am. Chem. Soc. **114**, 9568 (1992).

[8] A. G. Császár, J. Mol. Struct. **346**, 141 (1995).

[9] A. G. Császár and A. Perczel, Progr. Biophys. Mol. Biol. **71**, 243 (1999).

[10] C.-H. Hu, M. Shen, and H. F. Schaefer, J. Am. Chem. Soc. **115**, 2923 (1993).

[11] H. L. Sellers and L. Schäfer, J. Am. Chem. Soc. **100**, 7728 (1978).

[12] S. G. Stepanian, I. D. Reva, E. D. Radchenko, M. T. S. Rosado, M. L. T. S. Duarte, R. Fausto, and L. Adamowicz, J. Phys. Chem. A **102**, 1041 (1998).

[13] S. Vishveshwara and J. A. Pople, J. Am. Chem. Soc. **99**, 2422 (1977).

[14] L. Schäfer, H. L. Sellers, F. J. Lovas, and R. D. Suenram, J. Am. Chem. Soc. **102**, 6566 (1980).

[15] W. D. Allen, E. Czinki, and A. G. Császár, Chem. Eur. J. **10**, 4512 (2004).

[16] A. Halkier, P. Jørgensen, J. Gauss, and T. Helgaker, Chem. Phys. Lett. **274**, 235 (1997).

[17] W. D. Allen, Y. Yamaguchi, A. G. Császár, D. A. Clabo, R. B. Remington, and H. F. Schaefer III, Chem. Phys. **145**, 427 (1990).

[18] D. A. Clabo, W. D. Allen, R. B. Remington, Y. Yamaguchi, and H. F. Schaefer III, Chem. Phys. **123**, 187 (1988).

[19] H. H. Nielsen, Rev. Mod. Phys. **23**, 90 (1951).

[20] D. Papoušek and M. R. Aliev, Molecular Vibrational-Rotational Spectra (Elsevier, Amsterdam, 1982).

[21] J. K. G. Watson, in Vibrational Spectra and Structure, edited by J. R. Durig (Elsevier, Amsterdam, 1997), Vol. 6, p.1.

[22] T. H. Dunning Jr., J. Chem. Phys. **90**, 1007 (1989).

[23] C. Hampel, K. Peterson, and H.-J. Werner, Chem. Phys. Lett. **190**, 1 (1992).

[24] G. D. Purvis III and R. J. Bartlett, J. Chem. Phys. **76**, 1910 (1982).

[25] K. Raghavachari, G. W. Trucks, J. A. Pople, and M. Head-Gordon, Chem. Phys. Lett. **157**, 479 (1989).

[26] H.-J. Werner, P. J. Knowles, M. Schütz, R. Lindh, P. Celani, T. Korona, G. Rauhut, F. R. Manby, R. D. Amos, A. Bernhardsson, A. Berning, D. L. Cooper, M. J. O. Deegan, A. J. Dobbyn, F. Eckert, C. Hampel, G. Hetzer, A. W. Lloyd, S. J. McNicholas, W. Meyer, M. E. Mura, A. Nicklaß, P. Palmieri, R. Pitzer, U. Schumann, H. Stoll, A. J. Stone, R. Tarroni, and T. Thorsteinsson.

[27] J. F. Stanton, J. Gauss, J. D. Watts, M. Nooijen, N. Oliphant, S. A. Perera, P. G. Szalay, W. J. Lauderdale, S. A. Kucharski, S. R. Gwaltney, S. Beck, A. Balková, D. E. Bernholdt, K. K. Baeck, P. Rozyczko, H. Sekino, C. Hober, and R. J. Bartlett, Integral packages included are VMOL (J. Almlöf and P.R. Taylor); VPROPS (P. Taylor) ABACUS; (T. Helgaker, H.J. Aa. Jensen, P. Jørgensen, J. Olsen, and P.R. Taylor).

[28] W. D. Allen, A. L. L. East, and A. G. Császár, in *Structures and Conformations of Non-Rigid Molecules*, edited by J. Laane, M. Dakkouri, B. van der Vecken, and H. Oberhammer (Kluwer, Dordrecht, 1993), p. 343.

[29] A. G. Császár, W. D. Allen, and H. F. Schaefer III, J. Phys. Chem. **108**, 9751 (1998).

[30] A. G. Császár, G. Tarczay, M. L. Leininger, O. L. Polyansky, J. Tennyson, and W. D. Allen, in *Spectroscopy from Space*, edited by J. Demaison ajd K. Sarka (Kluwer, Dordrecht, 2001), p. 317.

[31] A. L. L. East and W. D. Allen, J. Chem. Phys. **99**, 4638 (1993).

[32] J. M. Gonzales, C. Pak, R. S. Cox, W. D. Allen, H. F. Schaefer III, G. Tarczay, and A. G. Császár, Chem.-Eur. J. **9**, 2173 (2003).

[33] D. Feller, J. Chem. Phys. **96**, 6104 (1992).

[34] D. Feller, J. Chem. Phys. **98**, 7059 (1993).

[35] T. Helgaker, W. Klopper, H. Koch, and J. Noga, J. Chem. Phys. **106**, 9639 (1997).

[36] R. A. Kendall, T. H. Dunning, and R. J. Harrison, J. Chem. Phys. **96**, 6796 (1992).

[37] A. K. Wilson, T. van Mourik, and T. H. Dunning, J. Mol. Struct. **388**, 339 (1996).

[38] D. E. Woon and T. H. Dunning, J. Chem. Phys. **98**, 1358 (1993).

[39] D. E. Woon and T. H. Dunning, J. Chem. Phys. **100**, 2975 (1994).

[40] D. E. Woon and T. H. Dunning, J. Chem. Phys. **103**, 4572 (1995).

[41] W. Schneider and W. Thiel, Chem. Phys. Lett. **157**, 367 (1989).

[42] J. F. Stanton and J. Gauss, Int. Rev. Phys. Chem. **19**, 61 (2000).

[43] J. F. Stanton, C. Lopreore, and J. Gauss, J. Chem. Phys. **108**, 7190 (1998).

[44] W. D. Allen and A. G. Császár, J. Chem. Phys. **98**, 2983 (1993).

[45] INTDIF2004 is an abstract program developed by Wesley D. Allen for use within Mathematica (Wolfram Research Inc., Champaign, Illinois) to perform high-order numerical differentiations of electronic structure data.

[46] R. L. DeKock, M. J. McGuire, P. Piecuch, W. D. Allen, H. F. Schaefer III, K. Kowalski, S. A. Kucharski, M. Musial, A. R. Bonner, S. A. Spronk, D. B. Lawson, and S. L. Laursen, J. Phys. Chem. A. **108**, 2893 (2004).

[47] INTDER2000 is a general program developed by Wesley D. Allen and co-workers which performs various vibrational analyses and higher-order nonlinear transformations among force field representations.

[48] W. D. Allen and A. G. Császár, J. Chem. Phys. **98**, 2983 (1993).

[49] W. D. Allen, A. G. Császár, V. Szalay, and I. M. Mills, Mol. Phys. **89**, 1213 (1996).

[50] See program descriptions in K. Sarka and J. Demaison in Computational Molecular Spectroscopy, edited by P. Jensen and P. R. Bunker (Wiley, Chichester, 2000), pp. 255-303.

[51] ANHARM is a FORTRAN program written for VPT2 analyses by Yukio Yamaguchi and Henry F. Schaefer (Center for Computational Quantum Chemistry, University of Georgia, Athens, GA 30602, USA).

[52] MolStruct is an abstract program developed by Wesley D. Allen for use within Mathematica (Wolfram Research Inc., Champaign, Illinois) to perform diverse fits of molecular structures to sets of isotopologic rotational constants.

[53] A. L. L. East, W. D. Allen, and S. J. Klippenstein, J. Chem. Phys. **102**, 8506 (1995).

[54] A. L. L. East, C. S. Johnson, and W. D. Allen, J. Chem. Phys. **98**, 1299 (1993).

[55] W. Thiel, G. Scusseria, H. F. Schaefer III, and W. D. Allen, J. Chem. Phys. **89**, 4965 (1988).

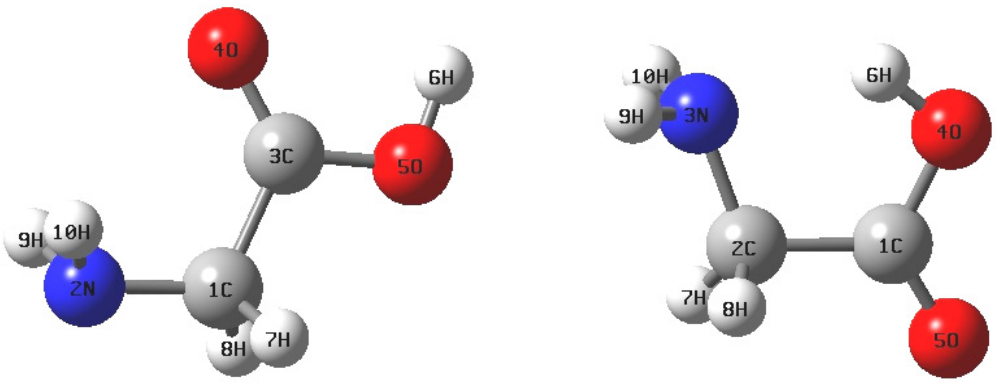

Gly-**Ip** Gly-**IIn**

Figure 4.1: Structure of the two lowest-energy conformers of neutral glycine.

Table 4.1. Layout of the focal-point increments of valence energy differences (cm^{-1}) between Gly-**IIn** and Gly-**IIp**.[a,b,c]

Basis	E(RHF)	δ[MP2]	δ[CCSD]	δ[CCSD(T)]	ΔE_e[CCSD(T)]
aug-cc-pVDZ	64.12	–55.06	16.29	–9.84	15.51
aug-cc-pVTZ	61.22	–41.31	14.19	–8.62	25.47
aug-cc-pVQZ	61.99	–42.42	14.37	[–8.62]	[25.32]
aug-cc-pV5Z	61.84	–44.04	14.78	[–8.62]	[23.97]
CBS[c]	[61.68]	[–45.74]	[15.22]	[–8.62]	[22.54]

[a] The fixed reference structures employed for all the focal-point computations have been optimized at the all-electron cc-pVTZ CCSD(T) level.
[b] The symbol δ denotes the increment in the relative energy (ΔE_e) with respect to the preceding level of theory, as given by the competing higher-order correlation series [HF→MP2→CCSD→CCSD(T)]. The higher-order correlation increments listed in brackets are taken for the purpose of extrapolation from corresponding entries for smaller basis sets, thus yielding the net ΔE_e values also appearing in the brackets.
[c] CBS = complete basis set limit. Based on X=(3, 4, 5) aug-cc-pVXZ HF and X=(4, 5) aug-cc-pVXZ MP2 and CCSD energy points. See text for extrapolation formulas. Additivity was assumed for the CCSD(T) energy increments.

Table 4.2. Equilibrium, B_e, and effective, B_0, rotational constants in MHz for the parent isotopologues of Gly-**Ip**, Gly-**IIp**, and Gly-**IIn**.

Gly-**Ip**	$A_e[A_0]$	$B_e[B_0]$	$C_e[C_0]$
6-311++G** MP2[a]	10279.0	3877.0	2908.1
6-31G* MP2 (AE)	10228.1 [10149.4]	3893.5 [3862.2]	2912.8 [2890.5]
cc-pVTZ CCSD(T)(AE)[b]	10407.5 [10328.8][c]	3914.0 [3882.7][c]	2937.5 [2915.2][c]
Expt.[d]	[10341.521(89)]	[3876.1785(12)]	[2912.3509(10)]
Gly-**IIp**			
6-311++G** MP2[a]	10175.1	4076.3	3010.9
6-31G* MP2 (AE)	10119.5 [10023.7]	4071.9 [4049.4]	3003.7 [2982.6]
cc-pVTZ CCSD(T) (AE)[b]	10255.0 [10159.2][c]	4097.0 [4074.5][c]	3028.0 [3006.9][c]
Gly-**IIn**			
6-311++G** MP2[a]	10127.5	4085.3	3024.8
6-31G* MP2 (AE)	10022.9 [9957.2]	4093.3 [4059.4]	3031.3 [2998.9]
cc-pVTZ CCSD(T) (AE)[b]	10182.8 [10117.1][c]	4112.6 [4078.7][c]	3045.3 [3012.9][c]
Expt.[d]	[10129.86(34)]	[4071.497(11)]	[3007.485(11)]

[a] Ref. 7.
[b] Zero-point vibrational contributions to the rotational constants were determined from 6-31G* MP2(AE) vibration-rotation interaction constants.
[c] The cc-pVTZ CCSD(T) A_0, B_0, and C_0 values were determined using cc-pVTZ CCSD(T) equilibrium A_e, B_e, and C_e rotational constants and the 6-31G* MP2 vibrational corrections.
[d] Effective ground-state values, Ref. 3.

Table 4.3. Theoretical and experimental isotopic shifts of the vibrationally averaged rotational constants of isotopologues of Gly-**Ip**.[a]

	Parent	^{13}C(3)	^{13}C(1)	C(1)-d$_2$	^{15}N	ε[b]
A_0/MHz	10149.4 [10341.5]	–0.6 [–0.6]	–112.8 [–114.4]	–999.2 [–1023.1]	–0.1 [–0.1]	6.4
B_0/MHz	3862.2 [3876.2]	–7.1 [–7.0]	–17.0 [–17.1]	–77.5 [–76.9]	–113.5 [–113.7]	0.3
C_0/MHz	2890.5 [2912.4]	–4.0 [–4.0]	–18.8 [–18.6]	–80.2 [–80.0]	–64.0 [–64.7]	0.3

[a] Values obtained at the 6-31G* MP2 (AE) level of theory. Shifts in the rotational constants of the isotopologues are given relative to the absolute values listed for the parent. Measured effective quantities from Ref. 3 are given, for the ease of visualization, in brackets. All theoretical rotational constants include 6-31G* MP2 (AE) zero-point vibrational corrections (see Table 4.2). See Figure 4.1 for numbering of the atoms. Points of significant disparity between theory and experiment are printed in bold face.

[b] Mean absolute difference between theoretical and experimental isotopic shifts.

Table 4.4. Theoretical and experimental isotopic shifts of the vibrationally averaged rotational constants of isotopologues of Gly-**IIn**.[a]

	Parent	^{15}N	^{13}C(2)	^{13}C(1)	C=^{18}O	H-^{18}O	OD, NH_2	CD_2	OH, NHD[b]	OH, ND_2	OD, NHD[c]	OD, ND_2
A_0	9957.2 [10129.9]	–1.9 [–0.7]	–133.1 [–133.7]	0.5 [0.8]	–126.0 [–129.2]	–599.7 [–609.8]	–381.0 [–397.7]	–1031.5 [–1049.3]	**–202.4** **[–131.1]**	–269.4 [–265.9]	**–569.2** **[–520.1]**	–633.5 [–645.1]
B_0	4059.4 [4071.5]	–108.5 [–109.6]	–16.6 [–16.4]	–11.6 [–11.7]	–175.2 [–173.6]	–13.4 [–14.3]	–9.9 [–9.0]	–83.8 [–82.5]	**–181.2** **[–203.2]**	–380.3 [–385.8]	**–189.2** **[–210.2]**	–386.4 [–391.4]
C_0	2998.9 [3007.5]	–59.6 [–60.3]	–20.6 [–20.7]	–6.3 [–6.3]	–107.2 [–106.6]	–63.8 [–63.8]	–40.3 [–40.7]	–89.6 [–89.9]	**–82.1** **[–101.1]**	–191.5 [–194.8]	**–119.6** **[–138.7]**	–226.0 [–229.5]

[a] Values obtained at the 6-31G* MP2 (AE) level of theory. See Figure 4.1 for numbering of the atoms. The units assumed for the vibrationally averaged rotational constants and are MHz. Shifts are given for the isotopically substituted species relative to the absolute values listed for the parent molecule. The MP2(AE)/6-31G* values are listed first with measured effective quantities from Ref. 3,5 in brackets. All theoretical rotational constants include MP2(AE)/6-31G* zero-point vibrational corrections. Points of significant disparity are printed in bold face for easier visualization. Mean absolute difference between theoretical and experimental isotopic shifts for the rotational constants are 7.2 MHz, 1.8 MHz, 1.0 MHz (A_0,B_0,C_0); the statistics exclude the outlying data for the (OH,NDH) and (OD,NDH) isotopologues.

[b] The theoretical differences corresponding to H9D10 substitued isotopologue are listed in the table, while the same values are for D9H10 substitued isotopologue are: –57.3 MHz, –221.5 MHz, –118.5 MHz (A_0,B_0,C_0).

[c] The theoretical differences corresponding to D6,H9D10 substitued isotopologue are listed in the table, while the same values are for D9H10 substitued isotopologue are: –436.6 MHz, –228.9 MHz, –155.4 MHz (A_0,B_0,C_0).

Table 4.5. Structural constraints employed in the final structural fits for Gly-**Ip** and Gly-**IIn**. Units for distances (r) are Å.

Gly-**Ip**	Gly-**IIn**	
1. r(O–H) = 0.9660	1. Δr(CH) = –0.000189	5. γ(COOHoop)[a] = –0.0221°
2. θ(COH) = 106.04°	2. Δr(NH) = –0.00170	6. τ(HNCC av)[a] = 5.43°
3. θ(NH_2 scissor) = 104.98°	3. $\Delta\theta$(CH_2 rock)[a] = 0.116°	7. $\Delta\theta$(NH_2 rock) = 0.00635°
4. θ(NH_2 wag) = 57.67°	4. $\Delta\theta$(CH_2 twist)[a] = 0.0642°	8. γ(NH_2 wag) = 0.917°

[a] $\Delta\theta$(CH_2 rock) = θ(7,2,3) + θ(7,2,1) – θ(8,2,3) – θ(8,2,1); $\Delta\theta$(CH_2 twist) = θ(7,2,3) –θ(7,2,1) – θ(8,2,3) + θ(8,2,1); γ(COOHoop) = γ(2,1,4,5); τ(HNCC av) = τ(9,3,2,1) + τ(10,3,2,1). See Figure 4.1 for atom numbering.

Table 4.6. Structural parameters of Gly-**Ip**.[a]

	Expt.[b]	cc-pVTZ CCSD(T)	r_e(Fit 1)[c]	r_e(Fit 2)[d] Final
r(C–N)	1.466	1.446	1.448(4)	1.441(1)
r(C–C)	1.529	1.511	1.514(2)	1.511(1)
r(C=O)	1.204	1.204	1.203(1)	1.207(2)
r(C–O)	1.354	1.349	1.347(4)	1.353(1)
r(C–H)	1.081	1.088	–	1.091
r(N–H)	1.001	1.012	–	1.006
θ(C–C–O)	111.5	111.4	–	111.9(1)
θ(O–C–O)	123.5	123.1	–	123.2(1)
θ(C–C–N)	113.0	115.2	–	115.4(1)
θ(CH_2 scissor)	–	105.9	–	105.9
θ(CH_2 wag)	–	5.1	–	5.4(1)
rms resid./MHz			0.2157	0.0078

[a] Units are Å for distances (r) and degrees for bond angles (θ). Standard errors of the weighted least-squares fit are given in parentheses. The weights in the fits to the experimental rotational constants are set to the reciprocal uncertainties. [b] Ref. 4. For uncertainties of the r_α^0 parameters determined see the original publication.

[c] Fit 1 releases r(C–N), r(C–C), r(C=O), and r(C–O) only.

[d] Fit 2 imposes all constraints listed in Table 4.5.

Table 4.7. Structural parameters of Gly-**IIn**.[a]

	Expt.[b]	Expt.[c]	cc-pVTZ CCSD(T)	r_0(Fit A)[d]	r_0(Fit B)[e]	r_e(Fit 1)[f]	r_e(Fit 2)[f]	r_e(Fit 3)[f] Final
r(C–C)	1.545	1.52(3)	1.524	1.538(16)	1.540(7)	1.522(6)	1.525(1)	1.524(2)
r(C–N)	1.459	1.46(3)	1.463	1.461(30)	1.460(12)	1.466(6)	1.462(2)	1.462(2)
r(C=O)	1.228	1.21(2)	1.201	1.210(16)	1.210(6)	1.197(5)	1.201(1)	1.202(2)
r(C–O)	1.291	1.33(4)	1.337	1.329(22)	1.326(9)	1.340(7)	1.333(1)	1.333(2)
r(O–H)	0.993	0.98(2)	0.977	0.976(17)	0.999(8)	0.996(7)	0.991(1)	0.992(2)
r(C–H av)	1.098	1.10(2)	1.087	1.099(7)	1.100(3)	1.084(3)	1.084(1)	1.084(1)
r(N–H av)	1.000	1.01(2)	1.009	1.004(20)	1.003(8)	1.013(2)	1.012(2)	1.014(3)
θ(C–O–H)	104.8	105(1)	104.4	104.8(9)	104.8(4)	104.9(3)	105.2(1)	105.2(1)
θ(C–C–O)	116.1	115(2)	113.8	115.0(11)	114.9(4)	114.0(4)	114.2(1)	114.3(1)
θ(O–C–O)	–	–	123.5	123.8(17)	124.0(7)	122.9(6)	123.4(1)	123.3(2)
θ(C–C–N)	110.6	112.2	111.2	111.4(12)	111.4(5)	111.3(3)	111.3(2)	111.4(2)
θ(CH_2 scissor)	107.4	107(2)	107.3	108.2(10)	108.3(4)	106.4(4)	106.6(2)	106.7(2)
$\Delta\theta$(CH_2 wag)[g]	–	–	10.4	10.9(33)	10.8(13)	8.7(10)	7.9(2)	8.0(4)
θ(NH_2 scissor)	112.5	110(3)	107.2	111.2(33)	110.9(13)	105.9(5)	107.0(7)	107.0(11)
τ(NCCO)	–	–	12.8	–	–	12.3(15)	12.1(13)	11.2(19)
τ(CCOH)	–	–	–2.3	–	–	–2.9(37)	–3.4(15)	–2.5(19)
γ(NH_2 wag)	–	–	52.5	43.7(331)	43.7(127)	–	48.4(15)	48.5(23)
$\Delta\theta$(NH_2 rock)[g]	–	–	0.4	–	–	–	7.2(10)	8.0(17)
γ(COOHoop)	–	–	–1.3	–	–	–	–	0.12(286)
rms resid./MHz				0.7241	0.4375	0.3027	0.0529	0.0516

[a] Units are Å for distances (r) and degrees for bond (θ), torsional(τ), and out-of-plane (γ) angles. Standard errors of the weighted least-squares fit are given in parentheses. The weights in the fits to the experimental rotational constants are set to the reciprocal uncertainties. [b] Substitutuion structure from ref. 5. [c] Structure from an unconstrained least-square fit from ref. 5. [d] Planar r_0 structure with all 12 isotopologues included in the fit; no constraints other then to define planarity were imposed. [e] Planar r_0 structure with [OH,NDH] and [OD,NDH] isotopologues excluded from the fit no; constraints other then to define planarity were imposed. [f] Non-planar r_e structure with [OH,NDH] and [OD,NDH] isotopologues excluded from the fits; Fits 1 and 2 impose all constraints listed in Table 4.5 and, in addition, [γ(NH_2 wag), θ(NH_2 rock), γ(COOHoop)] and [γ(COOHoop)], respectively. Fit 3 imposes all constraints listed in Table 4.5. [g] $\Delta\theta$(CH_2 wag) = θ(7,2,3) – θ(7,2,1) + θ(8,2,3) – θ(8,2,1); $\Delta\theta$(NH_2 rock) = θ(2,3,9) – θ(2,3,10).

Table 4.8. Zero-point vibrational corrections [MHz] to rotational constants of Gly-**Ip** isotopologues, obtained at the all-electron 6-31G* MP2 level.

	Parent	^{13}C(3)	^{13}C(1)	C(1)-d$_2$	^{15}N
A_e–A_0	78.6664	77.7954	76.7296	69.8361	78.7599
B_e–B_0	31.3045	30.9463	30.9460	31.2061	30.1316
C_e–C_0	22.3266	22.0562	21.9234	21.4796	21.7094

Table 4.9. Zero-point vibrational corrections [MHz] to rotational constants of Gly-**IIp** isotopologues, obtained at the all-electron 6-31G* MP2 level.

	Parent	^{15}N	^{13}C(2)	^{13}C(1)	C=^{18}O	H-^{18}O	OD, NH$_2$	CD$_2$	OH, NHD	OH, ND$_2$	OD, NHD	OD, ND$_2$
A_e–A_0	95.8780	95.7490	93.9864	95.0241	95.4515	87.0190	92.2094	84.6182	93.9694	89.4073	89.8096	85.1806
B_e–B_0	22.4651	21.8110	22.2517	22.1399	20.8484	22.5357	22.8746	22.1722	20.2851	19.4400	20.6700	19.8001
C_e–C_0	21.1105	20.5616	20.8509	20.8366	19.9750	20.6712	21.0697	20.3642	19.4327	18.9012	19.3623	18.8221

Table 4.10. Zero-point vibrational corrections [MHz] to rotational constants of Gly-**IIn** isotopologues, obtained at the all-electron 6-31G* MP2 level.

	Parent	^{15}N	^{13}C(2)	^{13}C(1)	C=^{18}O	H-^{18}O	OD, NH$_2$	CD$_2$	OH, NHD[a]	OH, ND$_2$	OD, NHD[b]	OD, ND$_2$
A_e–A_0	65.7335	64.9656	65.0110	64.8521	63.5978	60.9008	60.0665	64.7879	51.1431	63.7664	46.8018	57.9030
B_e–B_0	33.8726	32.9609	33.2005	33.5784	32.0476	33.6383	33.6830	31.3485	35.9204	30.6976	35.5099	30.4396
C_e–C_0	32.3584	31.6125	31.9531	32.0786	30.8104	31.4488	31.3846	30.4493	34.1491	28.9958	33.0496	28.1437

[a] The ZPV corrections corresponding to H9D10 substitued isotopologue are listed in the table, while the same values are for D9H10 substitued isotopologue are: 78.0537, 28.3915, 26.9572 (A_e–A_0, B_e–B_0, C_e–C_0).

[b] The ZPV corrections corresponding to D6,H9D10 substitued isotopologue are listed in the table, while the same values are for D9H10 substitued isotopologue are: 70.7722, 28.3453, 26.2281 (A_e–A_0, B_e–B_0, C_e–C_0).

CHAPTER 5

CONCLUSIONS

It was shown how various theoretical methods can be used to study molecular structures. The methods include density functional theory and coupled-cluster theory.

In Chapter 1, density functional theory was used to predict molecular structures of the di-arsenic fluorides As_2F_n (n=1-8) and their anions. Due to large number of electrons and many degrees of freedom for n>2, these systems are inaccessible to highly correlated methods such as coupled cluster. The structures obtained for As_2F_n (n=1-8) provide a very good starting point for possible future experimental studies. These experimental studies are encouraged due to the large electron affinity exhibited by the As_2F_n with large number of fluorines (n).

In Chapter 2, the $V^+(H_2O)$ and $ArV^+(H_2O)$ complexes were studied with high level *ab initio* methods. Because of the discrepancy between the experimental vibrationally averaged (r_0) structure and the theoretically predicted equlibrium structure (r_e), coupled cluster methods were necessary to compute highly precise structures. Quartic force fields were used to obtain vibrational correction to equilibrium rotational constants and, consequently, to evaluate the theoretical vibrationally averaged (r_0) structure. The theoretically computed θ_e(H-O-H) angle of 106.8º and 106.4º for $V^+(H_2O)$ and $ArV^+(H_2O)$, respectively, increases by 2-3º when vibrational effects are included, explaninig partially the previous discrepancy between experiment and theory.

In Chapter 3, the three lowest lying conformers of glycine were studied. The goal was to obtain the most precise r_e structures possible using high level *ab initio* data in conjunction with experimental rotational constants for various isotopologs. Structural refinement fits were performed and extremely precise equilibrium structures were obtained for the global minimum Gly-I and the second lowest lying conformer Gly-IIn.

At the end I would like to say that it is very important to know beforehand what the goal of a theoretical study is and choose the method accordingly. If molecular structures are needed with, for example, a few degree accuracy for the bond angles, density functional theory is a good choice. If higher precision is needed, coupled-cluster methods are appropriate. For cases where a final and definite structure is desired, high-level *ab initio* data needs to be combined with highly accurate experimental data to achieve the goal.

APPENDIX

SUPPLEMENTARY MATERIAL FOR CHAPTER 3

Table S1: CCSD(T)/Wf(TZP) quartic force field of the $^5B_1$ state of $ArV^+(H_2O)$.[a,b]

Sector I [c]		Sector I		Sector II [d]	
F_{11}	1.28148	F_{3221}	–0.006	F_{71}	0.00790
F_{21}	0.12514	F_{3222}	1.074	F_{72}	–0.00271
F_{22}	8.06499	F_{3311}	–0.077	F_{73}	–0.00093
F_{31}	0.00160	F_{3321}	0.151	F_{77}	0.43263
F_{32}	0.24355	F_{3322}	0.452	F_{84}	*–0.16689*
F_{33}	0.72155	F_{3331}	–0.038	F_{88}	*0.41023*
F_{44}	0.11056	F_{3332}	1.075	F_{95}	0.01092
F_{55}	8.12412	F_{3333}	–0.238	F_{96}	0.00820
F_{65}	0.04063	F_{4411}	*50.521*	F_{99}	0.06988
F_{66}	0.13971	F_{4421}	*–9.211*		
		F_{4422}	*1.952*	F_{711}	–0.118
F_{111}	–6.862	F_{4431}	*–1.815*	F_{721}	0.009
F_{211}	–0.376	F_{4432}	*0.372*	F_{722}	0.003
F_{221}	–0.013	F_{4433}	–0.067	F_{731}	0.015
F_{222}	–39.283	F_{4444}	*3.160*	F_{732}	–0.002
F_{311}	0.109	F_{5511}	–0.558	F_{733}	–0.002
F_{321}	0.104	F_{5521}	0.031	F_{744}	*0.290*
F_{322}	–0.589	F_{5522}	169.412	F_{755}	–0.001
F_{331}	–0.034	F_{5531}	–0.085	F_{765}	–0.004
F_{332}	–0.459	F_{5532}	–0.774	F_{766}	0.007
F_{333}	–0.589	F_{5533}	–0.986	F_{771}	–0.051
F_{441}	*1.244*	F_{5544}	0.197	F_{772}	0.005
F_{442}	–0.294	F_{5555}	170.859	F_{773}	0.007
F_{443}	*–0.009*	F_{6511}	0.179	F_{777}	–2.569
F_{551}	0.153	F_{6521}	–0.010	F_{841}	*–3.573*
F_{552}	–39.316	F_{6522}	–0.098	F_{842}	*0.506*
F_{553}	0.345	F_{6531}	–0.041	F_{843}	*0.196*
F_{651}	-0.076	F_{6532}	0.043	F_{874}	*–0.454*
F_{652}	0.052	F_{6533}	0.021	F_{881}	*9.496*
F_{653}	–0.025	F_{6544}	–0.039	F_{882}	*–1.209*
F_{661}	–0.070	F_{6555}	–0.194	F_{883}	*–0.525*
F_{662}	–0.041	F_{6611}	–0.020	F_{887}	*0.506*
F_{663}	0.093	F_{6621}	0.097	F_{951}	–0.021
		F_{6622}	–0.146	F_{952}	0.016
F_{1111}	29.938	F_{6631}	–0.004	F_{953}	–0.003
F_{2111}	1.461	F_{6632}	0.000	F_{961}	–0.015
F_{2211}	–0.384	F_{6633}	–0.069	F_{962}	0.004
F_{2221}	–0.224	F_{6644}	0.109	F_{963}	0.008
F_{2222}	167.785	F_{6655}	–0.043	F_{975}	–0.013
F_{3111}	–0.269	F_{6665}	0.038	F_{976}	0.002
F_{3211}	–0.134	F_{6666}	–0.134	F_{991}	–0.083

Table S1 cont.: CCSD(T)/Wf(TZP) quartic force field of the $^5B_1$ state of $ArV^+(H_2O)$

Sector II		Sector II		Sector II	
F_{992}	0.010	F_{8411}	*–123.942*	F_{9621}	–0.003
F_{993}	0.013	F_{8421}	*18.461*	F_{9622}	–0.013
F_{997}	–0.043	F_{8422}	*–4.263*	F_{9631}	–0.010
		F_{8431}	*6.932*	F_{9632}	0.011
F_{7111}	0.386	F_{8432}	*–0.950*	F_{9633}	–0.007
F_{7211}	–0.044	F_{8433}	–0.060	F_{9644}	*–0.423*
F_{7221}	–0.007	F_{8444}	*–3.460*	F_{9655}	0.007
F_{7222}	0.016	F_{8554}	–0.174	F_{9665}	0.005
F_{7311}	–0.044	F_{8654}	*0.157*	F_{9666}	–0.020
F_{7321}	0.016	F_{8664}	*0.318*	F_{9751}	–0.012
F_{7322}	0.006	F_{8741}	*–24.862*	F_{9752}	–0.057
F_{7331}	0.003	F_{8742}	*2.308*	F_{9753}	0.015
F_{7332}	–0.009	F_{8743}	*0.565*	F_{9761}	*0.118*
F_{7333}	0.002	F_{8774}	*–2.980*	F_{9762}	–0.025
F_{7441}	*10.297*	F_{8811}	*347.116*	F_{9763}	–0.009
F_{7442}	*–1.469*	F_{8821}	*–56.194*	F_{9775}	0.009
F_{7443}	*–0.349*	F_{8822}	*10.248*	F_{9776}	*–0.048*
F_{7551}	0.009	F_{8831}	*–15.360*	F_{9854}	–0.095
F_{7552}	0.000	F_{8832}	*2.825*	F_{9864}	*0.510*
F_{7553}	–0.002	F_{8833}	0.289	F_{9885}	–0.029
F_{7651}	–0.028	F_{8844}	*–1.643*	F_{9886}	–0.128
F_{7652}	0.012	F_{8855}	0.266	F_{9911}	0.229
F_{7661}	0.059	F_{8865}	*–0.567*	F_{9921}	–0.025
F_{7662}	–0.021	F_{8866}	*–0.932*	F_{9922}	–0.015
F_{7663}	0.005	F_{8871}	*38.268*	F_{9931}	–0.014
F_{7711}	*0.069*	F_{8872}	*–5.072*	F_{9932}	0.017
F_{7721}	*0.015*	F_{8873}	–0.276	F_{9933}	0.000
F_{7722}	0.008	F_{8877}	*5.260*	F_{9944}	*–0.918*
F_{7731}	*0.003*	F_{8884}	*30.092*	F_{9955}	–0.011
F_{7732}	0.009	F_{8888}	*–150.410*	F_{9965}	–0.010
F_{7733}	0.001	F_{9511}	*0.057*	F_{9966}	–0.026
F_{7744}	*2.116*	F_{9521}	–0.093	F_{9971}	0.258
F_{7755}	*0.018*	F_{9522}	*0.046*	F_{9972}	–0.026
F_{7765}	0.000	F_{9531}	0.028	F_{9973}	–0.040
F_{7766}	–0.013	F_{9532}	0.005	F_{9977}	–0.179
F_{7771}	*0.245*	F_{9533}	0.008	F_{9984}	*1.330*
F_{7772}	0.047	F_{9544}	*0.080*	F_{9988}	–0.642
F_{7773}	–0.021	F_{9555}	–0.005	F_{9995}	–0.011
F_{7777}	*10.616*	F_{9611}	*0.181*	F_{9996}	–0.083
				F_{9999}	–0.057

[a] Sector I comprises only the symmetry-adapted internal coordinates S_1-S_6 of the text, i.e., those coordinates common to both the untagged $V^+(H_2O)$ and tagged $ArV^+(H_2O)$ ions.

[b] Sector II includes diagonal and off-diagonal blocks involving the symmetry-adapted internal coordinates S_7-S_9 of the text, i.e., the additional modes resulting from argon tagging.

[c] Units consistent with energy in aJ, distances in Å, and angles in rad.

[d] Anomalous force constants, i.e. force constants differing from the corresponding CCSD/Wf(TZP) $ArV^+(H_2O)$ force constants of the $^5A_1$ electronic state by more than one order of magnitude, are italicized.

Table S2: Summary of CCSD/Wf(TZP) VPT2 anharmonic vibrational analysis of the $^5A_1$ states of $^{40}Ar^{51}V^+(D_2O)$, $^{51}V^+(D_2O)$, and D_2O.[a]

	i	ω_i	Δ_i	ν_i	α_i^A	α_i^B	α_i^C
$^{40}Ar^{51}V^+(D_2O)$							
O-H sym. stretch	1	2743.0	–94.7	2648.3	0.09864	0.0000150	0.0000205
H_2O scissor	2	1232.5	–24.3	1208.3	–0.06801	–0.0000119	0.0000050
V-O stretch	3	379.4	–11.2	368.2	–0.00295	0.0002513	0.0002737
Ar-V stretch	4	161.4	–7.4	154.1	0.00088	0.0005051	0.0004928
H_2O wag	5	192.1	76.5	268.6	0.57691	–0.0000843	–0.0001134
Ar-V-O lin. bend (b_1)	6	65.4	10.8	76.2	0.10149	–0.0000543	–0.0001490
O-H antisym. stretch	7	2851.1	–108.2	2742.9	0.04502	0.0000205	0.0000204
H_2O rock	8	405.6	–3.7	401.9	–0.49165	–0.0000207	–0.0000162
Ar-V-O lin. bend (b_2)	9	83.4	3.2	86.6	0.00999	–0.0000524	0.0000385
$^{51}V^+(D_2O)$							
O-H sym. stretch	1	2735.7	–93.7	2642.0	0.09954	0.0000874	0.0002018
H_2O scissor	2	1233.8	–24.0	1209.7	–0.06793	–0.0002624	0.0001039
V-O stretch	3	390.3	–9.9	380.5	–0.00336	0.0025134	0.0023893
H_2O wag	4	203.2	68.4	271.6	0.60264	–0.0007833	–0.0013685
O-H antisym. stretch	5	2844.2	–107.6	2736.6	0.04670	0.0002098	0.0002032
H_2O rock	6	411.3	–3.4	407.9	–0.49020	–0.0004444	0.0001828
D_2O							
O-H sym. stretch	1	2762.5	–91.8	2670.7	0.20234	0.0942451	0.0666358
H_2O scissor	2	1199.6	–22.9	1176.7	–1.02067	–0.0619885	0.0533747
O-H antisym. stretch	3	2888.5	–102.8	2785.7	0.49633	0.0286014	0.0500181

[a] All values in cm^{-1}. See footnote a of Table 8 for definitions.

Table S3: Summary of CCSD/Wf(TZP) VPT2 anharmonic vibrational analysis of the $^5A_1$ states of $^{40}Ar^{51}V^+(H_2{}^{18}O)$, $^{51}V^+(H_2{}^{18}O)$, and $H_2{}^{18}O$.[a]

	i	ω_i	Δ_i	ν_i	α_i^A	α_i^B	α_i^C
$^{40}Ar^{51}V^+(H_2{}^{18}O)$							
O-H sym. stretch	1	3796.2	–182.3	3613.9	0.23423	0.0000032	0.0000063
H_2O scissor	2	1670.7	–43.5	1627.2	–0.16830	–0.0000044	0.0000091
V-O stretch	3	381.0	–11.8	369.2	–0.00569	0.0002593	0.0002601
Ar-V stretch	4	161.4	–7.4	154.1	0.00177	0.0005232	0.0005143
H_2O wag	5	253.5	121.6	375.1	1.85193	–0.0000081	–0.0000323
Ar-V-O lin. bend (b_1)	6	65.4	21.7	87.1	0.27902	–0.0000591	–0.0001586
O-H antisym. stretch	7	3872.1	–196.0	3676.1	0.13737	–0.0000001	0.0000005
H_2O rock	8	538.7	–2.8	535.9	–1.50864	–0.0000067	0.0000137
Ar-V-O lin. bend (b_2)	9	86.1	10.1	96.2	0.08878	–0.0000476	0.0000438
$^{51}V^+(H_2{}^{18}O)$							
O-H sym. Stretch	1	3786.3	–181.4	3604.9	0.23713	–0.0001096	–0.0000313
H_2O scissor	2	1671.9	–43.2	1628.7	–0.16830	–0.0001962	0.0001230
V-O stretch	3	392.1	–10.3	381.8	–0.00646	0.0027728	0.0027496
H_2O wag	4	262.8	118.7	381.6	1.88025	–0.0000045	–0.0005705
O-H antisym. stretch	5	3862.3	–195.4	3667.0	0.14156	–0.0001183	–0.0000973
H_2O rock	6	549.4	–3.0	546.4	–1.48095	–0.0001232	0.0003553
$H_2{}^{18}O$							
O-H sym. Stretch	1	3823.6	–176.0	3647.6	0.64255	0.2181194	0.1720821
H_2O scissor	2	1632.5	–43.0	1589.5	–2.52778	–0.1504092	0.1390226
O-H antisym. stretch	3	3926.6	–188.0	3738.6	1.09217	0.0964880	0.1381235

[a] All values in cm^{-1}. See footnote a of Table 8 for definitions.

Table S4: Summary of CCSD/Wf(TZP) VPT2 anharmonic vibrational analysis of the $^5A_1$ states of $^{40}Ar^{50}V^+(H_2O)$ and $^{50}V^+(H_2O)$.[a]

	i	ω_i	Δ_i	ν_i	α_i^A	α_i^B	α_i^C
$^{40}Ar^{50}V^+(H_2O)$							
O-H sym. stretch	1	3804.3	–183.0	3621.3	0.23876	0.0000059	0.0000094
H_2O scissor	2	1678.1	–44.0	1634.1	–0.17072	–0.0000061	0.0000086
V-O stretch	3	396.3	–12.9	383.5	–0.00601	0.0002669	0.0002684
Ar-V stretch	4	162.9	–7.5	155.4	0.00181	0.0005650	0.0005551
H_2O wag	5	255.4	124.6	380.0	1.83120	–0.0000203	–0.0000465
Ar-V-O lin. bend (b_1)	6	67.0	21.7	88.7	0.28011	–0.0000595	–0.0001659
O-H antisym. stretch	7	3888.3	–198.0	3690.3	0.13627	0.0000034	0.0000041
H_2O rock	8	542.3	–3.2	539.1	–1.49479	–0.0000100	0.0000118
Ar-V-O lin. bend (b_2)	9	87.9	9.9	97.9	0.07836	–0.0000489	0.0000495
$^{50}V^+(H_2O)$							
O-H sym. Stretch	1	3794.3	–182.0	3612.3	0.24162	–0.0000880	0.0000039
H_2O scissor	2	1679.3	–43.6	1635.7	–0.17069	–0.0002407	0.0001278
V-O stretch	3	408.4	–11.2	397.2	–0.00676	0.0031054	0.0030819
H_2O wag	4	265.3	120.5	385.8	1.86047	–0.0001442	–0.0007892
O-H antisym. stretch	5	3878.5	–197.3	3681.2	0.14051	–0.0000800	–0.0000581
H_2O rock	6	552.8	–3.3	549.4	–1.46990	–0.0001895	0.0003562

[a] All values in cm^{-1}. See footnote a of Table 8 for definitions.

Table S5: Summary of CCSD/Wf(TZP) VPT2 anharmonic vibrational analysis of the $^5A_1$ states of $^{36}Ar^{51}V^+(H_2O)$.[a]

	i	ω_i	Δ_i	ν_i	α_i^A	α_i^B	α_i^C
$^{36}Ar^{51}V^+(H_2O)$							
O-H sym. stretch	1	3804.3	–183.0	3621.3	0.23876	0.0000060	0.0000099
H_2O scissor	2	1678.1	–44.0	1634.1	–0.17072	–0.0000070	0.0000093
V-O stretch	3	395.2	–12.7	382.5	–0.00600	0.0002842	0.0002857
Ar-V stretch	4	168.1	–8.0	160.1	0.00187	0.0006067	0.0005958
H_2O wag	5	255.4	124.3	379.7	1.83079	–0.0000217	–0.0000507
Ar-V-O lin. bend (b_1)	6	67.2	21.7	88.9	0.27806	–0.0000598	–0.0001776
O-H antisym. stretch	7	3888.3	–198.0	3690.3	0.13627	0.0000034	0.0000042
H_2O rock	8	542.2	–3.2	539.0	–1.49486	–0.0000110	0.0000132
Ar-V-O lin. bend (b_2)	9	88.2	9.9	98.1	0.08048	–0.0000537	0.0000549

[a] All values in cm^{-1}. See footnote a of Table 8 for definitions.

Table S6: Summary of CCSD(T)/Wf(TZP) VPT2 anharmonic vibrational analysis of the $^5A_1$ state of $V^+(H_2O)$ and water.[a]

	i	ω_i	Δ_i	ν_i	α_i^A	α_i^B	α_i^C
$V^+(H_2O)$							
O-H sym. stretch	1	3762.4	–186.7	3575.7	0.24454	–0.0000901	0.0000043
H_2O scissor	2	1666.2	–45.1	1621.1	–0.16997	–0.0002618	0.0001123
V-O stretch	3	419.3	–10.6	408.8	–0.00589	0.0029125	0.0028973
H_2O wag	4	232.1	165.3	397.5	1.91563	–0.0001111	–0.0008405
O-H antisym. stretch	5	3848.9	–201.5	3647.4	0.14289	–0.0000756	–0.0000527
H_2O rock	6	554.1	–0.7	553.3	–1.37430	–0.0002871	0.0002614
H_2O							
O-H sym. stretch	1	3799.8	–180.0	3619.9	0.64543	0.2256051	0.1749056
H_2O scissor	2	1629.2	–42.9	1586.3	–2.51660	–0.1549302	0.1416081
O-H antisym. stretch	3	3912.9	–192.8	3720.1	1.12561	0.0951280	0.1413769

[a] Harmonic frequencies (ω_i), total anharmonicities (Δ_i), fundamental frequencies (ν_i), and rovibration interaction constants (α_i^A, α_i^B, α_i^C) for $^5A_1$ state of $^{51}V^+(H_2{}^{16}O)$ and $H_2{}^{16}O$ in cm^{-1}. No strong anharmonic resonances required exclusion.